TKK Dissertations 87
Espoo 2007

THE AXIAL LOAD-DISPLACEMENT BEHAVIOR OF STEEL STRANDS USED IN ROCK REINFORCEMENT

Doctoral Dissertation

Ilkka Satola

Helsinki University of Technology
Department of Civil and Environmental Engineering
Rock Engineering

TKK Dissertations 87
Espoo 2007

THE AXIAL LOAD-DISPLACEMENT BEHAVIOR OF STEEL STRANDS USED IN ROCK REINFORCEMENT

Doctoral Dissertation

Ilkka Satola

Dissertation for the degree of Doctor of Science in Technology to be presented with due permission of the Department of Civil and Environmental Engineering for public examination and debate in Auditorium V1 at Helsinki University of Technology (Espoo, Finland) on the 22nd of October, 2007, at 12 noon.

Helsinki University of Technology
Department of Civil and Environmental Engineering
Rock Engineering

Teknillinen korkeakoulu
Rakennus- ja ympäristötekniikan osasto
Kalliorakentaminen

Distribution:
Helsinki University of Technology
Department of Civil and Environmental Engineering
Rock Engineering
P.O. Box 6200 (Vuorimiehentie 2)
FI - 02015 TKK
FINLAND
URL: http://www.tkk.fi/Yksikot/Rakennus/Kallio/
Tel. +358-9-451 2803
Fax +358-9-451 2812
E-mail: ilkka.satola@tkk.fi

ISBN 978-951-22-8972-1
ISBN 978-951-22-8973-8 (PDF)
ISSN 1795-2239
ISSN 1795-4584 (PDF)
URL: http://lib.tkk.fi/Diss/2007/isbn9789512289738/

TKK-DISS-2347

Picaset Oy
Helsinki 2007

ABSTRACT OF DOCTORAL DISSERTATION	HELSINKI UNIVERSITY OF TECHNOLOGY P.O. BOX 1000, FI-02015 TKK http://www.tkk.fi

Author Ilkka Sakari Satola

Name of the dissertation
THE AXIAL LOAD-DISPLACEMENT BEHAVIOR OF STEEL STRANDS USED IN ROCK REINFORCEMENT

Manuscript submitted 23.04.2007	Manuscript revised 03.09.2007
Date of the defence 22.10.2007	
☒ Monograph	☐ Article dissertation (summary + original articles)

Department Civil and Environmental Engineering
Laboratory Rock Engineering
Field of research Rock reinforcement
Opponent(s) Prof. Håkan Stille, Royal Institute of Technology, Division of Soil and Rock Mechanics, Sweden
Supervisor Prof. Pekka Särkkä
Instructor

Abstract

The aim of this thesis was to test and evaluate the load-displacement behavior of different types of grouted steel strands and rebar applicable to rock reinforcement. The main interest was focused on the effect of the epoxy and zinc coatings on the axial load-displacement behavior of the strand.

The bolt types tested were standard steel strand, galvanized steel strand, epoxy-coated steel strand, bulbed strand and rebar. New equipment for the axial laboratory pull test was designed and constructed for this study. The test apparatus enabled testing of different bolt types with embedment lengths from 250 mm up to 2000 mm. The loading rate used in the tests was 10 kN/min. The test apparatus worked as desired and was easy to operate.

The results showed that untwisting mechanism dominates the axial behavior of the steel strands. The roughness of the surface of the steel strands had a remarkable effect on the untwisting of the steel strands and thus on the axial behavior as well.

Rebar had a significantly higher bond strength, breaking load and maximum load, allowing shorter displacement values corresponding to the loads than any of the tested strands. The strands allowed larger displacement than rebar, especially the plain steel strand. The axial behavior of the bulbed strand was very close to that of the rebar, however.

On the basis of the results, corrosion protection on the surface of the steel strand significantly increased the bond strength and the stiffness of the grouted steel strand and decreased the displacement in proportion to the load under axial loading. The results showed that the maximum load-carrying capacity of galvanized steel strand and epoxy-coated steel strand increased linearly as the embedment length increased from 250 mm to 1000 mm. The critical embedment length of these bolt types was between 750 and 1000 mm.

The effect of the debonding material was found to be based both on the thickness of the debonding layer and the ability to decrease the friction between the strand and the grout. By thickening the layer, the pull-out resistance is decreasing leading lower pull-out loads for the strand.

Keywords Rock reinforcement, steel strand, rebar, epoxy-coated steel strand, galvanized steel strand, pull-out tests

ISBN (printed) 978-951-22-8972-1	ISSN (printed) 1795-2239
ISBN (pdf) 978-951-22-8973-8	ISSN (pdf) 1795-4584
Language English	Number of pages 120 p.

Publisher Rock Engineering, Helsinki University of Technology

Print distribution Rock Engineering, Helsinki University of Technology

☒ The dissertation can be read at http://lib.tkk.fi/Diss/2007/isbn9789512289738/

VÄITÖSKIRJAN TIIVISTELMÄ	TEKNILLINEN KORKEAKOULU PL 1000, 02015 TKK http://www.tkk.fi

Tekijä Ilkka Sakari Satola

Väitöskirjan nimi
THE AXIAL LOAD-DISPLACEMENT BEHAVIOR OF STEEL STRANDS USED IN ROCK REINFORCEMENT

Käsikirjoituksen päivämäärä 23.04.2007	Korjatun käsikirjoituksen päivämäärä 03.09.2007

Väitöstilaisuuden ajankohta 22.10.2007

☒ Monografia	☐ Yhdistelmäväitöskirja (yhteenveto + erillisartikkelit)

Osasto	Rakennus. ja ympäristötekniikan osasto
Laboratorio	Kalliorakentaminen
Tutkimusala	Kallion lujitus
Vastaväittäjä(t)	Prof. Håkan Stille, KTH, Maa- ja kalliomekaniikka, Tukholma, Ruotsi
Työn valvoja	Prof. Pekka Särkkä
Työn ohjaaja	

Tiivistelmä

Työn tavoitteena oli selvittää kallion lujituksessa käytettävien juotettujen jännepunosten ja harjateräksen voima-siirtymä käyttäytymistä. Tutkimuksessa keskityttiin erityisesti selvittämään, miten punoksen pinnalla oleva epoksipinnoite ja sinkkipinnoite vaikuttavat jännepunoksen aksiaaliseen käyttäytymiseen. Tutkitut pulttityypit olivat jännepunos, kuumasinkitty jännepunos, epoksipäällysteinen jännepunos, bulb – punos ja harjateräs. Testipulttien ulosvetokokeita varten kehitettiin ja rakennettiin uusi testauslaitteisto, jolla pystyttiin testaamaan pultteja laboratorio-olosuhteissa eripituisilla tartuntapituuksilla 250 mm:stä 2000 mm:iin saakka. Testin aikana vetovoimaa kasvatettiin tasaisesti, kunnes pultti katkesi tai juotoksen ja pultin välinen tartunta petti. Laitteisto toimi suunnitellulla tavalla ja oli helppokäyttöinen.

Tulokset osoittivat, että kuormitettaessa sementtijuotettua jännepunosta aksiaalisesti, punokseen varastoituvalla muodonmuutosenergialla ja punoksen rakenteesta johtuvalla punoksen kiertymisellä on oleellinen vaikutus aksiaaliseen voima - siirtymä käyttäytymiseen, erityisesti lyhyillä tartuntapituuksilla. Mikäli punoksen kiertymistä ei ole estetty, jännepunos liukuu kiertymällä irti laastista. Jännepunoksen pinnan karheuden todettiin niin ikään vaikuttavan merkitsevästi punoksen kiertymiseen ja sitä kautta edelleen aksiaaliseen käyttäytymiseen. Harjateräksellä oli selvästi korkeammat tartuntalujuuden, murtovoiman ja maksimivoiman arvot, ja lyhyemmät kuormitusta vastaavat siirtymän arvot kuin testatuilla punostyypeillä. Punokset, ja erityisesti käsittelemätön jännepunos, sallivat suuremmat siirtymät kuin harjateräs. Bulb–punoksen aksiaalinen käyttäytyminen oli kuitenkin hyvin lähellä harjaterästä.

Tulosten perusteella korroosiosuojaus jännepunoksen pinnalla lisäsi teräksen ja juotoslaastin välistä kitkaa ja tartuntapinta-alaa, ja näin ollen kasvatti merkittävästi tartuntalujuutta ja juotetun punoksen jäykkyyttä, ja vastaavasti pienensi siirtymiä suhteessa aksiaaliseen kuormitukseen. Kuumasinkityn ja epoksipinnoitettujen punosten maksimaalinen ulosvetovoima kasvoi lineaarisesti tartuntapituuden kasvaessa 250 mm:stä 1000 mm:iin. Edellä mainittujen punosten kriittinen tartuntapituus oli tulosten perusteella 750 mm:n ja 1000 mm:n välillä.

Tartuntaa heikentävien aineiden vaikutuksen todettiin perustuvan sekä punoksen pinnalla olevan aineen paksuuteen että sen kykyyn vähentää punoksen ja laastin välistä kitkaa. Kerroksen paksuutta lisäämällä punoksen ulosvetoa vastustavaa voimaa voidaan pienentää.

Asiasanat kallion lujitus, jännepunos, harjateräs, kuumasinkitty jännepunos, epoksipäällysteinen jännepunos, ulosvetokokeet

ISBN (painettu) 978-951-22-8972-1	ISSN (painettu) 1795-2239
ISBN (pdf) 978-951-22-8973-8	ISSN (pdf) 1795-4584
Kieli Englanti	Sivumäärä 120 s.

Julkaisija Kalliorakentaminen, Teknillinen korkeakoulu

Painetun väitöskirjan jakelu Kalliorakentaminen, Teknillinen korkeakoulu

☒ Luettavissa verkossa osoitteessa http://lib.tkk.fi/Diss/2007/isbn9789512289738/

PREFACE

The research work presented in this thesis was carried out in the Laboratory of Rock Engineering at the Helsinki University of Technology from autumn 1999 to March 2003.

I am very grateful to my supervisor Professor Pekka Särkkä for believing in my ability, his encouragement and allowing me to work independently, but with guidance and support whenever needed throughout this project.

I would like to thank Professor Charlie C. Li from The Norwegian University of Science and Technology, Norway and PhD Pasi Tolppanen from Pöyry Infra Ltd., Finland for acting as my pre-examiners of dissertation.

I would also like to thank Dr. Alan Thompson and Professor Ernesto Villaescusa from the Western Australian Schoool of Mines, Australia and Dr. Will Bawden from the University of Toronto, Canada for providing valuable comments and help concerning rock bolt testing and test apparatus along the way.

I would like to express my special thanks to Matti Hakala for his valuable support in simulation work using an axi-symmetric finite difference method model (FLAC 3.3) and fruitful discussions during this project.

I would like to acknowledge the Technology Development Centre, Sandvik Tamrock Ltd, The Geotechnical Division of the City of Helsinki, The Rescue Department of the City of Helsinki, YIT Corporation, Lemcon Ltd, Posiva Ltd, Outokumpu Mining Ltd, Gridpoint Finland Ltd, Dywidag Systems International, Miranet Ltd and Finnish Tunnelling Association for funding and supporting this research.

Special thanks are due to the staff of Sandvik Tamrock Ltd. for development and construction of the double pipe test equipment. I also wish to thank my colleagues and the staff at the Laboratory of Rock Engineering for their support and help.

Finally, I would like to sincerely thank my dear wife Päivi and our lovely children Sebastian and Wilhelmiina for their love and support which gave wind to my sail in times of need.

This thesis is dedicated to my father (1944 – 1998) and to my mother (1942 – 2002).

Helsinki, October 2007

Ilkka Satola

CONTENTS

1 INTRODUCTION 14

1.1 BACKGROUND 14
1.2 AIM OF THE THESIS 15
1.3 SCOPE OF THE THESIS 15
1.4 THESIS OUTLINE 16
1.5 CONTRIBUTION 17

2 REVIEW OF THE AXIAL BEHAVIOR OF CABLE BOLTS 18

2.1 CABLE BOLT REINFORCEMENT 18
2.2 LOAD TRANSFER MECHANISMS 18
2.3 BOND STRENGTH 19
2.3.1 Properties of grout 20
2.3.2 Borehole diameter 21
2.3.3 Stiffness of the confinement 22
2.3.4 Stress change 22
2.3.5 Properties of a cable bolt 23
2.3.6 Interface separation 23
2.3.7 Rotation 24
2.4 AXIAL BEHAVIOR AND MODES OF FAILURE OF CABLE BOLTS 24
2.5 AXIAL TESTS OF CABLE BOLTS 29
2.5.1 Test configurations of axial tests of cable bolts 29
2.5.2 Literature on previous pull tests of cable bolts 32

3 AXIAL LABORATORY TESTS 37

3.1 TEST EQUIPMENT 37
3.2 BOLT TYPES TESTED 41
3.3 GROUTING 43
3.3.1 Grouting and installation of the test bolts 43
3.3.2 Quality control of the grout 44
3.4 TEST SAMPLE PREPARATION 45
3.5 TEST PROCEDURE 48
3.6 ANALYSES OF THE TEST DATA 48
3.7 LONG EMBEDMENT LENGTH 51
3.7.1 Aim of the tests 51
3.7.2 Test bolt types 51
3.7.3 Results 51
3.7.4 Discussion 53
3.8 SHORT EMBEDMENT LENGTHS 55
3.8.1 Aim of the tests 55
3.8.2 Test bolt types 55
3.8.3 Test results 56
3.8.4 Discussion 61
3.9 BOLTS WITH PLATES AND UNEQUAL EMBEDMENT LENGTHS 63
3.9.1 Aim of the tests 63
3.9.2 Test bolt types 63
3.9.3 Test results 64
3.9.4 Discussion 66
3.10 UNGROUTED STEEL STRAND 69
3.11 EFFECT OF DEBONDING MATERIAL ON BOND STRENGTH (LICENTIATE THESIS) 70

3.11.1 General 70
3.11.2 Aim of the tests 71
3.11.3 Test sample preparation 71
3.11.4 Grouting and installation of the test steel strands 72
3.11.5 Pull-out tests 72
3.11.6 Test procedure 73
3.11.7 Test results 73
3.11.8 Discussion 74
3.12 INTERPRETATION OF THE TEST RESULTS 75

4 FINAL DISCUSSION 77

4.1 EFFECT OF CORROSION PROTECTION 77
4.2 EFFECT OF THE EMBEDMENT LENGTH 78
4.3 EFFECT OF THE DEBONDING MATERIAL 81
4.4 EFFECT OF UNTWISTING MECHANISM 82

5 CONCLUSIONS 83

6 RECOMMENDATIONS FOR FURTHER STUDIES 86

LIST OF SYMBOLS AND ABBREVIATIONS

Roman letters

A_1	Contact area of the embedded cable
C	Torsional rigidity of the strand
C_S	Circumference of the strand
d_i	Inside diameter of the steel pipe
d_o	Outside diameter of the steel pipe
D	Diameter of the strand
D1	Displacement value at measuring point 1
D2	Displacement value at measuring point 2
D3	Displacement value at measuring point 3
$D_{(204\ kN)}$	Because of the structure of the steel strand, the yield load cannot be uniquely determined. Instead of the yield load, the 0.2 limit defined in the Finnish standard (SFS 3173) is used as a reference value. According to the strength qualification for strand for prestressed structures, the 0.2 limit ($R_{p\ 0.2}$) is 1470 N/mm^2, corresponding to a load of 204 kN (SFS 1265)
E	Young's modulus
E.L.	Embedment length
E.L. 1	Embedment length 1
E.L. 2	Embedment length 2
F_a	Axial force corresponding to the failure mechanisms
$F_{(bond)}$	Pull-out load when the first bond failure is detected along the full embedment length on one of the embedment sections
$F_{(2nd\ bond)}$	Pull-out load which occurs in the other embedment section after the first bond failure ($F_{(bond)}$) has already occurred
$F_{(10\ mm)}$	Pull-out load at the displacement (D1) of 10 mm
$F_{(break)}$	Pull-out load when bolt failure occurs
$F_{(max)}$	Maximum pull-out load during the test
i	Dilation angle
K_r	Radial stiffness of the steel pipe
L_e	Embedment length of the bolt

L_f	Initial free length (the length exists between the test and anchor sections)
L_s	Length over which shear failure occurs
l	Pitch length of the strand
N	Number of outer wires of the strand
p_1	Radial pressure at the inner radius of the cement annulus
u_a	Axial displacement of the exit point
UBS	Ultimate bond strength determined by using the true contact area (bond area) of the test bolt and the maximum pull-out load $F_{(max)}$. Defined as N/mm^2
UCS	Uniaxial compressive strength
V_i	Values of the galvanized steel strand or epoxy-coated steel strand
V_{ref}	Value of the steel strand
w:c	Water-cement ratio
Q	Component of the pull-out force required to untwist the free length of cable

Greek letters

θ	Rotation angle of the strand
v	Poisson's ratio
ϕ_{gs}	Sliding angle of friction between grout and steel
α	Angle of the pitch
ϕ_g	Internal angle of friction for the grout

1 INTRODUCTION

1.1 Background

Cable bolting has been used successfully in reinforcing the stopes in Finnish mines since 1971. The most commonly used cable bolt material is a seven-wire steel strand. Interest in expanding the use of cable bolting to civil rock engineering is increasing due to the many benefits of the cable bolting method and the material properties of steel strand. However, the use of cable bolts as a permanent reinforcement structure in rock construction has not been approved by the authorities in Finland to date. This is the main reason for the very limited use of cable bolts in rock constructions. Uncertainty regarding their sensitivity to corrosion has been one of the main problems to be resolved before cable bolts can be accepted for use in long-term reinforcement. Another important issue to be determined is the mechanical applicability of cable bolts in rock reinforcement for civil rock engineering and long-term reinforcement purposes.

A research project entitled “Corrosion-protected cable bolts in long-term reinforcement” was carried out at the Helsinki University of Technology in 1999 – 2002 (Satola & Hakala 2001a). The object of the project was to study the applicability of corrosion-protected cable bolts in long-term reinforcement. The project was divided into two parts. The first part concentrated on determining the mechanical behavior of different steel strand modifications. The axial load-displacement behavior of the fully grouted test bolts was tested by double pipe pull tests with different embedment lengths and the different test configurations.

The mechanical behavior of rock reinforcement element is affected by many important factors such as like shear loading, tensile loading and a combination of both, the creep of the bolt material and the contact between the bolt and grout and corrosion issues. However, the subject of this thesis is focused only on the axial load-displacement behavior of the different steel strands tested in the present research.

To the knowledge of the author, very limited information was available regarding the axial load-displacement behavior of corrosion-protected steel strands for rock reinforcement purposes at the time that this research was initiated. Secondly, axial tests

of the steel strands and rebars used in this research have not been performed previously under equal conditions in the same host material with identical test system.

1.2 Aim of the thesis

The scope of the thesis was to test and evaluate the axial load-displacement behavior of different types of steel strands applicable for rock reinforcement purposes. This was performed by conducting strictly controlled axial laboratory pull tests on full-scale standard steel strands, modified steel strands and corrosion-protected steel strands under axial loading. Rebar was tested as a reference test bolt of the bolt type most commonly used in civil rock engineering.

Of special interest was to determine the effect of the corrosion protection material (hot-dip galvanization or epoxy coating) on the load-displacement behavior of the steel strand.

It was also considered important to contribute to the understanding of the axial behavior of standard steel strand related to the untwisting mechanism of steel strand observed by previous researchers (Hyett et al. 1992b).

In addition, test results obtained from the licentiate thesis by the author were added in this thesis (Satola 1999a). The aim of the tests was to determine the effect of the different debonding material on the axial load-displacement behavior of the steel strand.

1.3 Scope of the thesis

A total of about 70 axial laboratory pull-out tests were performed, including different set-ups for the tests and different embedment lengths used.

This study focused on the axial behavior of cement-grouted test bolts. Resin or any other grout material was not in the scope of the study. In addition, no aggregates were used in the grout because they are not used in mechanized cable bolting.

In practice, rock reinforcement elements are usually subjected to axial loading, shear loading and a combination of both. It is also well known that shear loading reduces cable bolt capacity and plays an important role in the mechanical behavior of the rock bolt (Hyett et al. 1992b). However, only the axial behavior of the steel strands was within the scope of this study because it usually dominates the behavior of the rock reinforcement element and was considered more important to be studied. The axial test is also the most common way to study the behavior of rock bolts, and thus the results can be compared with the results obtained by the other researchers.

1.4 Thesis outline

Chapter 1: Introduction, describes the background, the aim and the scope of the thesis and the contribution it makes to the understanding of axial load-displacement behavior of steel strands in rock reinforcement.

Chapter 2: Describes the cable bolt performance in practice, the factors affecting the bond strength as well as the failure mechanisms of the grouted cable bolts. This chapter presents the methods used to test cable bolts. A literature review of work and research done by previous researchers on the subject of the thesis is also given in this chapter.

Chapter 3: Deals with axial laboratory tests carried out on test bolts. The interpretation of the results is given in this chapter.

Chapter 4: Presents the final discussion on the test results.

Chapter 5: Conclusion.

Chapter 6: Recommendations for further studies are given in this chapter.

Each of the chapters has individual discussions and the final discussion is given in the Chapter 4.

1.5 Contribution

A new modification of the axial double pipe test apparatus was designed and constructed. This modification enables testing of rock bolts and cable bolts with embedment lengths from 250 mm up to 2000 mm. The loading range is from 0 kN to 350 kN. Displacements of the test bolt can be measured at three different points.

The effect of the different debonding materials on the axial behavior of fully grouted steel strand was determined.

The effects of the epoxy coating and galvanizing on the axial behavior of the steel strand were determined.

The axial behavior of steel strand, epoxy-coated steel strand, galvanized steel strand, bulbed strand and rebar was tested and evaluated under equal conditions in the same host material using an identical test system for the purpose of the rock reinforcement.

2 REVIEW OF THE AXIAL BEHAVIOR OF CABLE BOLTS

2.1 Cable bolt reinforcement

Rock reinforcement and rock support are specific techniques within the general category of rock improvement methods. Rock improvement includes all techniques that seek to increase the strength or decrease the deformability characteristics of a rock mass (Windsor & Thompson 1993).

It is important to understand the difference between different reinforcement and support techniques. Windsor and Thompson (1993) defined support as including all methods that essentially provide surface restraint to the rock mass by the installation of structural elements on the excavation boundary. By way of contrast, reinforcement is considered to include methods that modify the interior behavior of the rock mass by the installation of structural elements within the rock mass. In the case of rock reinforcement the prime objective is to improve the shear and tensile strength of the rock mass adjacent to the surface and underground excavations.

Cable-bolt reinforcement can perform a combination of reinforcement and holding functions. As reinforcement, the cables are effective in preventing separation and slip along planes of weakness or blocks in the rock mass. Cable bolts can also provide support by retaining elements, keeping the failed rock or free rock blocks in place (Hutchinson & Diederichs 1996).

The basic in situ types of cable bolting loading are: axial or tensile, shear and a combination of axial and shear. These types can occur individually or in combination. In practice the displacements at discontinuities are combined and much more complex consisting of translation and rotation in a three-dimensional manner (Windsor & Thompson 1993).

2.2 Load transfer mechanisms

The grout column surrounding the cable bolts builds up the anchorage medium and is necessary for the load transfer mechanisms between the cable bolt and the rock mass.

The load distribution in the fully grouted cable bolt can be divided into two parts: pick-up length and anchor length. In the pick-up length, the bolt takes up the load from the rock mass and reinforces the rock mass. The load is transferred from the rock mass to the cable bolt via the shear resistance at the interface between the cable bolt and the grout. As the rock slips with respect to the cable, shear stresses accumulate along the length of the cable due to the addition of incremental rock loads, the tension in the steel strand increases from zero at the face to a maximum at some point into the borehole. Beyond this point, in the anchor length, the shear stresses act in the opposite direction, as the cable tends to slip down with respect to the rock. In this region, the loads accumulated in the bottom portion of the cable are transferred back to the rock mass and the cable tension drops back to zero at the upper end of the grouted strand (Hutchinson & Diederichs 1996).

2.3 Bond strength

The bond strength of a cable bolt is defined as the resistance to slip at the interface between the cable and grout along a unit length or a unit surface area of cable. (Hutchinson & Diederichs 1996). Simply put, the bond means the gripping ability of a grout column with an embedded length of a cable bolt to resist forces tending to pull the strand longitudinally (Moosavi 2002).

When the cable bolt is being pulled out, it provides resistance by the following mechanisms: chemical adhesion, friction and mechanical interlocking between the cable bolt and the grout (Stillborg 1984).

The effect of the chemical adhesion between the steel and the grout is temporary because the chemical adhesion is destroyed after less than one-fifth of a millimeter of relative slip by the cable bolt (Fuller & Cox 1975). The importance of adhesion in bond strength is also considered minor because the axially directed shear stresses induced near the steel/grout interface at low load levels quickly exceed the shear strength of the grout. Therefore, even if a significant adhesive bond between the grout and reinforcement existed, failure would tend to occur in the grout. Secondly, the optimum adhesion relies on the surface conditions of the strand and in practice, it is very difficult to keep the surface of the strand clean (Windsor & Thompson 1993; Hyett et al. 1992b).

As the cable is loaded and begins to slip at the cable/grout interface, a wave of localized adhesion failure propagates down the cable away from the loading point. After the adhesion is removed from the interface, the cable slips with respect to the grout annulus. A geometric mismatch occurs between the cable flutes and the corresponding grout ridges if the rotation of the cable bolt is prevented. This mismatch increases with increasing relative slip. Since the grout ridges must ride up and over the cable wires, the grout compresses in the confined borehole and thus generates a normal pressure at the grout/steel interface. Friction (pressure-dependent shear strength) thus develops along this interface providing resistance to further slippage. This interaction is called dilation. Dilation is limited in the extreme by the absolute scale (height) of the grout ridges. In reality, dilation pressures develop to the point where these ridges crush, reducing the maximum dilation to less than 0.1 mm for plain strand cable. Dilation is dependent on grout stiffness, rock stiffness around the borehole and grout strength (Hutchinson & Diederichs 1996).

If the plates are attached to the cable bolt, the dependence on the bond strength is reduced. The load is generated immediately, and if the anchor is designed with a higher capacity than the strand, the full tensile capacity of the cable bolt will be made available (Hutchinson & Diederichs 1996).

2.3.1 Properties of grout

The water-cement ratio (w:c) is the most important factor affecting the physical and mechanical properties of cement grout:

$$w:c = \frac{m_w}{m_c}, \tag{1}$$

where m_w is the mass of water and m_c is the mass of anhydrous cement powder used in the same mix.

The optimum water-cement ratio of the grout varies from 0.35 to 0.4 (Hyett et al. 1992a). Decreasing the water-cement ratio of the grout decreases its sedimentation and porosity and, thus increases the strength of the grout. Increased strength results in

increased maximum dilation pressure, which in turn results in an increase in ultimate bond strength. However, decreasing the water-cement ratio from a value of 0.3 would make pumping very difficult or even impossible because of the increased viscosity of the grout. A very low water-cement ratio also decreases the mixing efficiency of the grout and there might also be a problem with complete saturation and hydration of the cement particles due to the less excess water being available (Hutchinson & Diederichs 1996).

Increasing the water-cement ratio from a value of 0.4 assists pumping but then the grout is so thin, that it does not stay in the up holes and it may flow into open joints intersecting the boreholes. A high water-cement ratio also reduces the compressive and tensile strengths of the grout and increases micro-voids, water bleeding and cement particle sedimentation (Goris 1991).

Bleeding of the grout occurs when the particles of cement settle down to the bottom and water flows up to the top of the grout column. The section of the cable bolt which is within the water filled upper section of the borehole will have less load carrying capacity than designed and the effective embedment length of the cable bolt will be reduced from the design length (Hutchinson & Diederichs 1996).

Any steel-cement composite is characterized by a “transition zone” at the interface between the two, wherein the microstructure of the cement paste is considerably different from that of the cement paste away from the interface. In this region, the cement paste is much more porous due to bleeding and entrapment of water along the surface of the steel, and irregular packing of the cement grains within a zone. The adhesional bond between the steel and the cement is not continuous, but instead comprises a series of point contacts, resulting in a relatively weak and compliant bond (Hyett et al. 1992b).

2.3.2 Borehole diameter

The borehole diameter has minimal effect on the bond strength and pull-out behavior of the cable bolt (Stillborg 1984; Hutchinson & Diederichs 1996). The pull tests performed on rebars with diameter of 18.2 mm indicated that the use of different borehole

diameters, between 27 mm and 75 mm, had no influence on the bolt behavior in practice (Stjern 1995).

2.3.3 Stiffness of the confinement

The radial stiffness of the confinement due to grout stiffness and the stiffness of the rock mass around the borehole has a remarkable effect on bond strength (Moosavi 1997; Hutchinson & Diederichs 1996). The structure of the rock mass and joints around the borehole affects the stiffness of the rock mass surrounding the borehole (Hutchinson & Diederichs 1996).

The effect of the radial stiffness of the rock mass around the borehole is most evident for high-strength grouts (0.30 and 0.40, UCS > 65 MPa) (Hyett et al. 1992b). Rock stiffness has a remarkable influence on bond strength when the modulus of the rock surrounding the borehole is close to or less than the modulus of the grout. In that case the probable failure mechanism is radial fracturing and lateral displacement of the grout wedges.

In very stiff rocks, the grout modulus and strength are the critical parameters determining bond strength (Hutchinson & Diederichs 1996).

If the water-cement ratio of the grout is 0.45 - 0.50 and thus the strength of the grout low, then the bond strength of the strand is almost independent of the radial stiffness of the rock mass (Hyett et al. 1992b).

2.3.4 Stress change

The rock stiffness around the borehole can change during the service life of a cable bolt due to stress changes, blasting- and mining-induced stresses. Stress change in the surrounding rock mass after the installation of a cable bolt can profoundly affect the bond strength of the cable. In short, increase of stress cause an increase in bond strength while decrease of stress can reduce the strength (Kaiser et al. 1992; Maloney et al. 1992; Hyett et al. 1995a).

In the case of mine-induced stress changes, two effects can occur: first, destressing of the ground can cause a decrease in the stiffness of the confining rock mass as it relaxes; second, mining-induced stress changes within the rock mass can cause a change in the radial stress acting across the cable/grout interface, and hence change the frictional resistance which controls the cable capacity. Both stress-induced fracturing and mining-induced destressing will reduce expected cable capacities, while a stress increase will maintain or increase them (Hyett et al. 1992b).

2.3.5 Properties of a cable bolt

The surface properties, the diameter and the geometry of a cable bolt are the main properties of a cable bolt that affect the bond strength. A dirty, greasy or rusty cable bolt surface decreases the bond strength. However, it has been stated that light rust on the cable surface improved the bond strength, although, rusting of the cable bolt surface is not recommended (Goris 1990a). Interface friction is dependent on the surface of the cable bolt. The effective friction coefficient between the steel strand wire surface and the grout is approximately 0.4, corresponding to an average friction angle of 21º to 23º (Hyett et al. 1995b).

In epoxy-coated steel strands, silica grit is embedded in the outer surface of the coating to improve bond strength between the strand and the grout (Goris 1990b).

Cables with a modified geometry (bulbed strand, birdcage, nut cage etc.) have an increased geometric mismatch between the strand and the grout and, thus increased bond strength. This will be discussed in more detail later in the text.

2.3.6 Interface separation

Interface separation can occur mainly due to grout shrinkage and cable radial strain. Grout shrinkage can cause the grout to pull away from the cable bolt before any cable loading occurs. This gap must be closed before any dilation pressure can be generated (Hutchinson & Diederichs 1996). This gap results in a reduction in dilation pressure and thus reduced bond strength. To minimize grout shrinkage, high water-cement ratios,

high temperature and low humidity conditions in the grouting should be avoided. Shrinkage can be minimized also by using additives in the grout.

The reduction of an effective diameter in the cable bolt occurs when the cable bolt is loaded axially. This reduction can cause interface separation and reduced bond strength (Hutchinson & Diederichs 1996). The amount of the reduction of the diameter is affected by the load in the bolt, the pretension of the bolt and the distance to the loading point.

2.3.7 Rotation

When rotation of the strand is permitted, the strand will tend to take the path of least resistance as it slips past the grout interface. Rather than pushing the grout ridges up and out of the way, the strand will tend to "corkscrew" out of the grout column resulting in reduced dilation, interface pressure and pullout resistance (Hutchinson & Diederichs 1996).

2.4 Axial behavior and modes of failure of cable bolts

It is generally accepted that the interface between the grout and the steel strand controls the behavior and failure mechanism of a cable bolt (Fuller & Cox 1975; Goris 1990a; Hyett et al. 1992b; Windsor 1992).

There are three possible mechanisms of bond failure (Hyett et al. 1995b; Moosavi 1997):
(1) Untwisting (rotational slip)
(2) Shear failure of the cement flutes and
(3) Dilational slip of the cable accommodated by radial splitting

The importance of the untwisting mechanism in the axial behavior of plain cables was not properly highlighted until it was emphasized in work by Hyett and others (Hyett et al. 1992b; Hyett et al. 1995b). Instead of shearing the cement flutes or dilational slip during pull-out, the cable rather untwist out of the grout column provided that the strand

is free to rotate. The untwisting mechanism is explained by the helical geometry and low torsional rigidity of a plain strand (Moosavi 1997).

The composite nature of a strand means that its lateral contraction under an axial load is greater than that of solid wires and bars. This is because the peripheral wires, in an attempt to straighten out under a load, rotate in the lay direction, effectively packing the wires closer together and reducing the overall strand diameter. Compact strand has a lower lateral contraction than plain strand (Windsor 2004). In situ, in grout and under axial loads, uncompacted strand laterally contracts away from the grout interface, effectively reducing the adhesion, mechanical interlock and friction components. This may cause the propagation of a debonding front along the element/grout interface, which invalidates a linear extrapolation of load transfer characteristics from shorter to longer lengths. The effects of excessive contraction under an initial load can greatly affect the constitutive relationship in bond failure (Windsor 2004).

This untwisting behavior was shown in the results of laboratory double embedment pull tests by Hyett (1995b; 1992b) and Moosavi (1997). The observation of tested samples showed that along most of test section, bond failure occurred by untwisting and shearing of the grout flutes occurred only on the small section (75 mm) near the exit point of the cable (Hyett et al. 1995b).

For untwisting failure, the torque (T) generated along the length of cable between the test and anchor sections can be defined by the following equation:

$$T = \frac{C\theta}{(u_a + L_f)} = \frac{2\pi C u_a}{l(u_a + L_f)}, \tag{2}$$

where C is the torsional rigidity of the strand, θ is the twist of the strand, u_a is the axial displacement of the exit point, L_f is the initial free length (the length of unbonded strand between the test section and the anchor section) and l is the pitch length of the strand (Hyett et al. 1995b).

The axial force F_a corresponding to the three failure mechanisms mentioned above can be calculated from the following equations (Hyett et al. 1995b):

for dilational slip, after splitting of the cement annulus

$$F_a = A_1 p_1 \tan(\phi_{gs} + i), \tag{3}$$

for non-dilational untwisting

$$F_a = \frac{A_i p_i \tan \phi_{gs}}{\sin \alpha} + Q, \tag{4}$$

and for shear failure of the cement flutes

$$F_a = A_1(\tau_0 + p_i \tan \phi_g), \tag{5}$$

where A_1 is the contact area of the embedded cable, p_1 is the radial pressure at the inner radius of the cement annulus, ϕ_{gs} is the sliding angle of friction between grout and steel (10.3º in Kaiser et al. 1992), i is the dilation angle, α is the angle of the pitch, ϕ_g is the internal angle friction for grout, changing from 20º to 27º depending on the water-cement ratio (Hyett et al. 1992a) and τ_0 is the grout cohesion which is also dependent on grout quality. Q is the component of the pull-out force required to untwist the free length of cable:

$$Q = \frac{4\pi^2 C u_a}{l^2(u_a + L_f)}, \tag{6}$$

Since the dilation angles are so small (i < 0.2º), the pull-out force component related to dilational slip may be ignored and the axial pull-out force may be written approximately as (Hyett et al. 1995a):

$$F_a = \frac{L_s}{L_e} A_1 \left(\tau_0 + p_i \tan\phi_g\right) + \left(1 - \frac{L_s}{L_e}\right) \frac{A_i p_i \tan\phi_{gs}}{\sin\alpha} + Q\,, \tag{7}$$

where L_s is the length over which shear failure occurs, L_e is the embedment length of the bolt. The last term Q should be added for cases in which any length of the test section fails through untwisting.

Evidence of untwisting has been observed in many cases from mines, where rock had stripped off the cables and the cables had showed no sign of failure in the cable or even no signs of a load being taken (Moosavi 1997). This observation was supported by Hyett et al. (1992b) who demonstrated in their paper that the yield strength of a cable bolt could be mobilized only in special cases, where combination of a long embedment length of cable and high radial confinement exists.

Hyett et al. (1995b) studied the axial load-displacement behavior of a plain cable bolt in double embedment tests and presented a failure process, which was divided into four distinct stages:

Stage 1 (u_a < 1 mm): The essentially linear response that characterizes the initial stage of a cable pull-out test is related to the axial stiffness of the cable, the elastic properties of the grout and the properties of the interface between the two. The initial stiffness is sensitive to the confining pressure, as is the onset of non-linearity in the load-displacement plot. Both of these observations confirm that the bond, even during this initial stage, is related to frictional-mechanical rather than adhesional resistance.

Stage 2 (u_a < 1 mm). Near the fixed end of the test section, where the bond will begin to break first and untwisting is restricted, only limited slip can occur at the grout/cable interface unless either (i) radial fracturing of the grout annulus splits it into distinct wedges, which can then be radially displaced to allow dilational slip, or (ii) shear failure through the cement flutes occurs. The initiation and stable propagation of one or both of these mechanisms is responsible for the reduction of axial stiffness and defines the onset and the extent of stage 2.

Stage 2 – stage 3 transition (splitting of the cement annulus, u_a = 1 mm). A pronounced change in stiffness, often accompanied by a drop in capacity, and an audible emission from the specimen, occurs after 1 – 2 mm of axial displacement. It is thought that this corresponds to splitting of the cement annulus.

After the cement annulus is fully split, the stored elastic strain energy in the annulus due to shrinkage must be released, and the individual grout wedges will have a tendency to extend in the radial direction and contract in the tangential direction, prematurely opening the radial fractures. This effect can explain the high bond strengths for higher water-cement ratio grouts during the early stages of the pull test (u_a < 10 mm).

Stage 3 (u_a = 1-50 mm). Research has established that stage 3 is the most critical part of the cable bolt bond failures process, and that the associated failure mechanism is highly sensitive to the radial confinement.

Note that for tests in which a significant free length exists, or for a loosely wound cable with low torsional rigidity C, less torque will develop for a given u_a and the cable will be able to untwist even at the exit point. Hence, less shearing of the grout flutes and less dilation will result in less work hardening during stage 3 (i.e. a nearly perfect plastic response and consequently, lower bond strengths: similarly, for loosely wound cables with a low C).

Stage 4 (u_a > 50 mm). The ultimate capacity and maximum radial dilation are usually attained after 40 or 50 mm of axial displacement.

The axial behavior of modified cable bolts is very different from the behavior of the conventional cable bolts (plain strand), because the presence of the deformed structure (i.e. bulbs) filled with grout greatly increase the geometric mismatch between the cable and the grout, which together with the radial stiffness of the borehole wall, generates higher shear stresses along the cable, resulting in a higher bond strength and shorter critical embedment lengths (consistently less than 0.3 m required to break the strand during pull-out). The flared elements of the modified strand serve as concentrated dilation and load transfer sites along the cable bolt. The modified strands are, in general,

considerably stiffer in pullout than plain strand, generating and transferring much smaller degrees of cable-grout slip to the load (Hutchinson & Diederichs 1996). This property is desirable to reinforce fractured ground and to limit displacements.

The untwisting mechanism observed in the case of conventional cable bolts is prevented by the deformed structure of the modified cable bolts.

2.5 Axial tests of cable bolts

2.5.1 Test configurations of axial tests of cable bolts

The purpose of rock bolt testing is to define their mechanical response to the loading conditions that are likely to arise when they are in service, and to enable the most appropriate device to be chosen for the predicted rock mass response (Windsor 1992). It has to be pointed out that the laboratory axial tests are mostly intended for a comparison of different variables between test bolts. The results obtained from the tests are relative, and comparison can be made only with the results obtained from tests performed in an identical way. None of the laboratory tests can simulate the exact interaction between a rock bolt and the rock mass. The most commonly used tests are pull-out tests because they are simple to perform in the laboratory.

One of the main problems when comparing the pull-test results of different researchers is that the tests are carried out in different ways. This is mainly due to the lack of test standards or universally approved codes of practice. This has led to the differences in grouting techniques, embedment lengths, test configurations and testing procedures, which naturally affect the results and make it difficult to compare and combine the results of different studies. To achieve comparable results for different test bolts, it is necessary to test them in exactly the same way.

The important data being collected are load levels applied to the test bolt and the displacements corresponding to the load levels.

There are two basic configurations performing axial testing of cable bolts in the laboratory: unconstrained tests and non-rotating tests (Hutchinson & Diederichs 1996) (Figure 1).

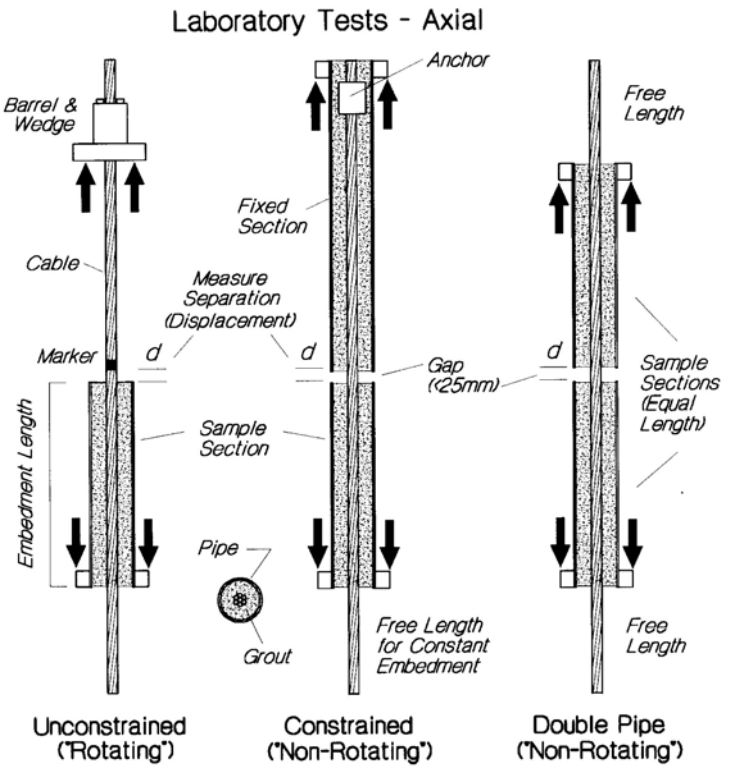

Figure 1. Different configurations for axial pull-out tests performed in the laboratory (Hutchinson & Diederichs 1996).

Unconstrained tests

In an unconstrained test (single embedment axial test, rotating test), the steel strand is allowed to rotate during pull-out. The steel strand is grouted into a rigid pipe or some other confining material, and one end of the strand is left free for gripping and pulling. The section inside the pulling device (hydraulic jack) is unembedded and thus free to lengthen which affects the behavior of the strand. These tests give lower pull-out loads than non-rotating tests.

Stillborg (1984) and Ito et al. (2001) performed rotating tests using concrete blocks as the confining material. Rotating tests in the laboratory have been also been performed by Benmokrane & Chekired (1992) and Benmokrane et al. (1992) who tested cable

bolts grouted inside concrete cylinders. Kaiser et al. (1992) investigated the effect of stress change on the bond strength of fully grouted cables and tested smooth bar grouted inside the granite cylinder in a Hoek triaxial cell. Rotating tests where steel pipes have been used as a confining material have been conducted by the author (Satola 1999a,b).

As in the laboratory, rotating tests can be done in the field as well. In unconstrained tests, the test bolt is covered except for the test section, by plastic tubing for debonding. The test bolt is then grouted into the borehole. By debonding, the exact length of the test section (embedment length) can be ensured. An example of a rotating test in the field is the work done by Maloney et al. (1992). They studied the effect of mining-induced stress changes caused by stope mining on the support capacity of the cable bolt.

Bawden et al. (1992) devised a field-testing procedure for constrained field tests.

As Moosavi stated (1997), the rotating test with a long free length of cable is only suitable for "ground anchoring" situations, while the non-rotating test arrangement with a very short free length (usually equal to the joint aperture) should be used for cable bolt reinforcing applications.

Non-rotating tests

Constrained tests and double pipe tests (double embedment axial tests) are both non-rotating tests where rotation is prevented during pull-out, forcing the steel strand to shear through the grout flutes which results in higher load capacities. In constrained tests, the fixed section of pipe is considerably longer than the test section and/or the slip is prevented by placing a swaged or welded anchor on the steel strand within the grouted test section. In the double pipe test, both sample and test sections are designed to slip equally (Hutchinson & Diederichs 1996). The author would like to point out that in the double pipe tests described in this thesis, it was found that the strand did not rotate between the pipes (joint opening point), but untwisting behavior was detected for almost the full length of the tested cable bolts. Shearing of the flutes occurred only along about 100-mm sections of the joint opening point in both directions inside the grout columns.

In these types of tests, the response of the reinforcing element at the interface between the two halves of the test specimen more closely represents the performance of a similar reinforcing element crossing a dilating discontinuity (Windsor & Thompson 1993).

The first non-rotational "split-pipe pull" test system was developed by Fuller and Cox (1975). They used mild steel tubes as a confining material and grouted test bolts inside two mild steel tubes separated by a washer. Since then the same principle of the split-pipe test has been used widely (Goris 1990a,b; Hyett et al. 1992b; Hassani et al. 1992; Villaescusa et al. 1992; Villaescusa & Wright 1999).

Stillborg (1990) conducted non-rotational pull tests with a special testing system where cable bolts installed in concrete blocks were tested. The same principle of using concrete blocks as the host material was performed by Hassani et al. (1992) and Stjern (1995).

Pull tests conducted in situ in a rock mass have been performed by Bawden et al. (1992).

Hyett et al. (1992b) modified even further the split-pipe test configuration developed by Fuller and Cox (1975). In the modified pull test, the stiffness of the confining material could be changed using different confining tubes (PVC, steel, aluminum) to simulate rock mass conditions. Results from tests conducted with this system were compared to those obtained from a conventional test procedure and no significant differences were found according to Hyett et al. (1992b).

These modified test systems has been used by Hyett et al. (1995a), Moosavi et al. (1996) and Moosavi (1997, 2002).

2.5.2 Literature on previous pull tests of cable bolts

Fuller and Cox (1975) performed double embedment pull tests on grouted steel strands and single wires. They found that the load transfer between the tendon and the grout was critically dependent on both the shape and the surface properties of the strand.

Of particular interest to this study is work conducted by Goris (1990a,b) on fully grouted epoxy-coated cable bolts and conventional cable bolts. This is the only reference where pull tests on grouted epoxy-coated cable bolts have been reported at the time of writing this thesis. Goris performed constrained pull tests and to prevent slippage of the end of the cable embedded in the upper pipe, a barrel and wedge steel anchor was attached to the cable prior to making the pull-test sample (Goris 1990a). In preventing slippage of the strand, the axial behavior of the strand was also affected, because rotation of the strand was prevented as well and the resistance to pull-out was caused by a compressive force applied against the grout column by the steel button. The author would like to point out that, if a barrel and wedge steel anchor is not used in rock reinforcement, one has to be careful implementing the results of the tests where they have been used. For the same reason the results obtained by Goris (1990a,b) are different from those obtained from the tests described in this thesis.

Based on his results, Goris stated that, when using two cables in a single hole, the load-carrying capacity can be more than twice that of single cables. In addition, the average maximum loads for double cable samples can be achieved at shorter displacement lengths than with single cables.

The laboratory tests on epoxy-coated cables performed by Goris (1990b) indicated that the average shear strength for the epoxy-coated cables was approximately 31% higher than the shear strength for conventional cables. Both the conventional and epoxy-coated cables showed similar load-displacement behavior in that they reached the maximum load within the first 50.8 mm (2 inches) of displacement and then maintained a very high residual load-carrying capacity. However, the epoxy-coated cables showed a higher average load-carrying capacity.

Stillborg (1984) studied the effect of embedded length, cable surface properties, curing conditions and grouts with and without additives, on the mechanical behavior of a grouted 15.2-mm seven-wire steel strand. He conducted both short (less than 7xD) and long embedment lengths (between 10xD and 25xD) in his laboratory pull-out tests. In tests with short embedment lengths the rotation of the strand was allowed during pull-out, but in the tests with long embedment lengths the rotation of the strand was prevented.

In his tests Stillborg showed that the cable surface properties, the curing conditions as well as the type of grout, significantly affect the pull-out behavior of the cable. He also showed that the anchorage capacity is reduced with an increased water-cement ratio. Stillborg also demonstrated that Poisson's ratio of seven-wire strand was as low as 0.02.

Later in his research, Stillborg (1990) presented results from a special testing system where cable bolts installed in concrete blocks were tested. The test arrangement was designed to simulate the load-deformation characteristics of a rock bolt subjected to tensile loading across a joint, which opens normal to the joint plane as a result of rock deformation. High-strength reinforced concrete was used for the two 1.5-m concrete blocks simulating two 1.5-m blocks of rock separated by a joint. The boreholes for the rock bolts were all drilled using a percussive technique in order to create borehole surfaces with a roughness comparable to those obtained in metamorphic and igneous rock types. The length of the boreholes and the subsequently installed rock bolts were 3 m. Stillborg tested a wide variety of different test bolts: expansion shell anchor, post-grouted expansion shell anchor, cement grouted rebar (diameter 20 mm), resin grouted rebar (diameter 32 mm), resin grouted fiberglass rock bolt, plain twin steel strand cable bolt, birdcage twin steel strand cable bolt, Split set, standard Swellex, yielding standard Swellex, super Swellex and yielding super Swellex.

Hyett et al. (1992b) investigated what the most important factors affecting the capacity of the cable bolts are both in the laboratory and in the field. They used different radial confinement: aluminum, PVC and steel pipes, in their split pipe (double embedment) laboratory pull tests to determine the effect of confinement on the bond strength of fully grouted cable bolts. It required that the conventional test procedure was modified so that the grout column and confining pipe were pushed rather than pulled off the cable. The results showed that the radial confinement acting on the outer surface of the cement annulus had a strong effect on the capacity of the cable bolts. The results indicated that the capacity is also primarily affected by the embedment length and the properties of grout (water-cement ratio).

Test results of different short embedment lengths indicated that the capacity of the cable bolt increases with embedment length but not in direct proportionality (Hyett et al.

1992b). The failure was found to be non-simultaneous in nature, with one section having failed while another is approaching peak capacity (Hyett et al. 1992b).

The results of the pull tests with different radial confinement showed that, as the degree of radial confinement increased, the failure mechanism changed from radial fracturing and lateral displacement of the grout annulus under low confinement to shearing of the cement flutes and pull-out along a cylindrical frictional surface under high confinement (Hyett et al. 1992b).

Hyett et al. (1995b) performed pull tests on steel strand in a special test arrangement where they used a modified Hoek cell to maintain the confining pressure at the outside of the cement annulus. The results indicated that radial dilations decreased with confining pressure. Low dilations were attributed by the occurrence of an untwisting mechanism along most of the test section. This mechanism was stated to be due to the helical form and low torsional rigidity of seven-wire steel strand.

Hyett et al. (1995a) conducted laboratory pull tests using a modified push test apparatus in order to evaluate the Garford bulb anchor for cable bolt reinforcement. The results indicated that the bond strength of the Garford bulb anchor was significantly higher than that of standard seven-wire strand especially in the tests at low radial confinement and high water-cement ratio grout.

Of particular interest to this study is work performed by Villaescusa et al. (1992) because the pull tests described in this thesis were conducted very similarly to and with the same test arrangement as in the tests performed by Villaescusa. They tested full-scale cable bolts and rock bolts with embedment lengths of 0.5 and 1.0 m and used steel pipes with a high radial stiffness as the confining material. In pull tests they studied the load-displacement behavior of grouted single strand, twin strand, birdcage strand and rebar (diameter 20 mm) prior to tensile failure or slippage of the steel, and determined the bond strength between steel and grout. The effects of different embedment lengths and water-cement ratios were analyzed. The results indicated that the critical embedment length for single and twin strand cables was highly dependent on the grout density.

Moosavi (1997) studied the mechanics of bond failure in both conventional and modified geometry cable bolts. The results confirmed that the cable bond strength is due more to frictional than to adhesional resistance for conventional cable bolts. His observation was also that shearing occurred only on the short section (about 75 mm) of the strand and untwisting was the major mode of failure along the rest of the strand. This behavior was again explained by the helical form of the strand and its low torsional rigidity.

Pull tests on Garford bulb strand showed that the dominant failure mode was shearing of the grout flutes. This was due to the very different behavior of bulb strand because it does not rotate during a pull test because of its deformed structure that restricts the rotation (Moosavi 1997). The main difference in behavior between the conventional and modified cable bolts is caused by the higher radial dilation generated in the modified cables due to the deformed structure (Moosavi et al. 1996).

Stjern (1995) investigated the behavior of different rock bolts in field pull tests and double embedment pull tests in the laboratory. The results showed that different hole diameters (28, 45 and 75 mm) did not have an effect on the load-deformation characteristics of fully grouted rebars. The pull tests on different configurations of twin combination cables showed that the two cables must have similar stiffness for the complete cable bolt to obtain a strength equal to the sum of both cables. The results also showed that the conventional cable bolts rotated rather than sheared off the grout flutes.

3 AXIAL LABORATORY TESTS

The test equipment, preparation of the tests bolts, quality control of the grout and the test procedure are presented in more detail in a research report (Satola & Hakala 2001a) and in referee conference papers (Satola & Hakala 2001b; Satola 2001; Satola & Aromaa 2003, 2004).

3.1 Test equipment

Following the basic principle of an axial laboratory test (Windsor & Thompson 1993), the test system was designed to simulate as closely as possible the performance of rock bolts crossing a dilating discontinuity.

A new configuration for the double pipe test system was designed and constructed on the basis of the fundamental principles of double pipe testing (Satola & Hakala 2001a). The long embedment lengths used in pull-out tests resulted in placing the test machine in a horizontal position because of the free space it required. One of the main proposals was to use a hollow ram hydraulic jack (hereinafter hydraulic jack) as the loading device and RHS steel pipe (RHS = Rectangular Hollow Sections) as the test frame.

The purpose of using steel pipes to demonstrate boreholes was to provide a uniform and identical radial confinement in every test. Also, handling and storing the test samples was easy when using steel pipes. The author was well aware of the main drawback of using steel pipes. Goris (1990a) reported that the main drawback of this kind of test system is that the load-displacement curve for the cable bolt sample was not likely to be exactly what support systems experience in a large rock mass because the stress-strain behavior of pipe is different from that of rock. However, the relative behavior of one laboratory test sample compared with another should approximate the behavior of cable bolts in rock (Goris 1990b).

The double pipe test machine was developed and constructed in cooperation with the Helsinki University of Technology, Sandvik Tamrock Ltd and Gridpoint Finland Ltd. The test equipment was dimensioned for a maximum load of 350 kN, which influenced

the selection of the materials and sizes of the RHS steel pipe, wedges, and the steel pipes where the test bolts were grouted inside (Figure 2).

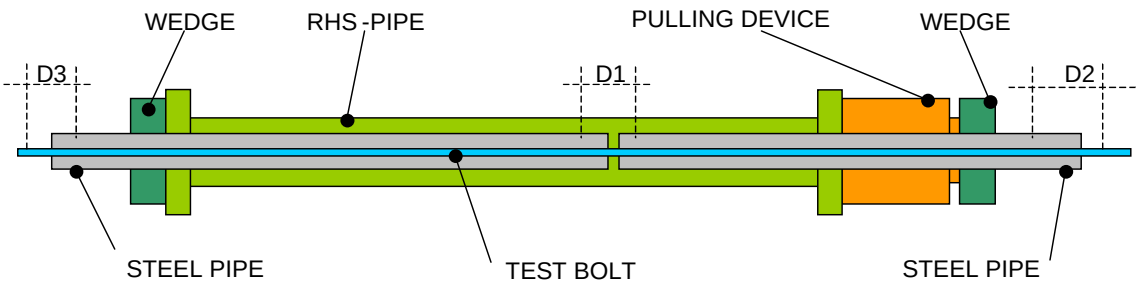

Figure 2. Double pipe test system. Grouted test bolt in double pipe test machine. Displacement measuring points (D1, D2 and D3). Schematic drawing. (Satola & Hakala 2001a).

In this double pipe test configuration, the pressure and flow of the oil from the hydraulic pump causes the cylinder of the hydraulic jack to move. The cylinder pushes against the barrel generating a load that transfers to the steel pipe via the wall and the bottom of the groove on the steel pipe. The load is transferred from the steel pipe to the grout and then to the test bolt inside the grout. The load is developed in the bolt and is transferred along the bolt to the other side of the discontinuity (to the grout column inside another steel pipe). This side works as an anchor section of the test bolt because this steel pipe is connected to the RHS testing pipe and is thus forced to stay in place. The load is transferred in the opposite direction on this side, from the bolt to the grout and then to the steel pipe and via the groove to the barrel and finally to the RHS testing pipe.

The deformation and load transfer in the double pipe test system during pull testing was simulated using an axi-symmetric finite difference method model (FLAC 3.3) (Satola & Hakala 2001a). Modeling was utilized to determine the effect of the connection points on the steel pipes in the test machine (Appendix D). It was found that the best places were as far as possible from the discontinuity point (gap) on the outer edge of the pipe.

The final test system consisted of a pulling device, an electric hydraulic pump, an RHS testing pipe, a wedge system for the connection of test steel pipes, measuring instruments, and a portable PC for data collection (Figure 3).

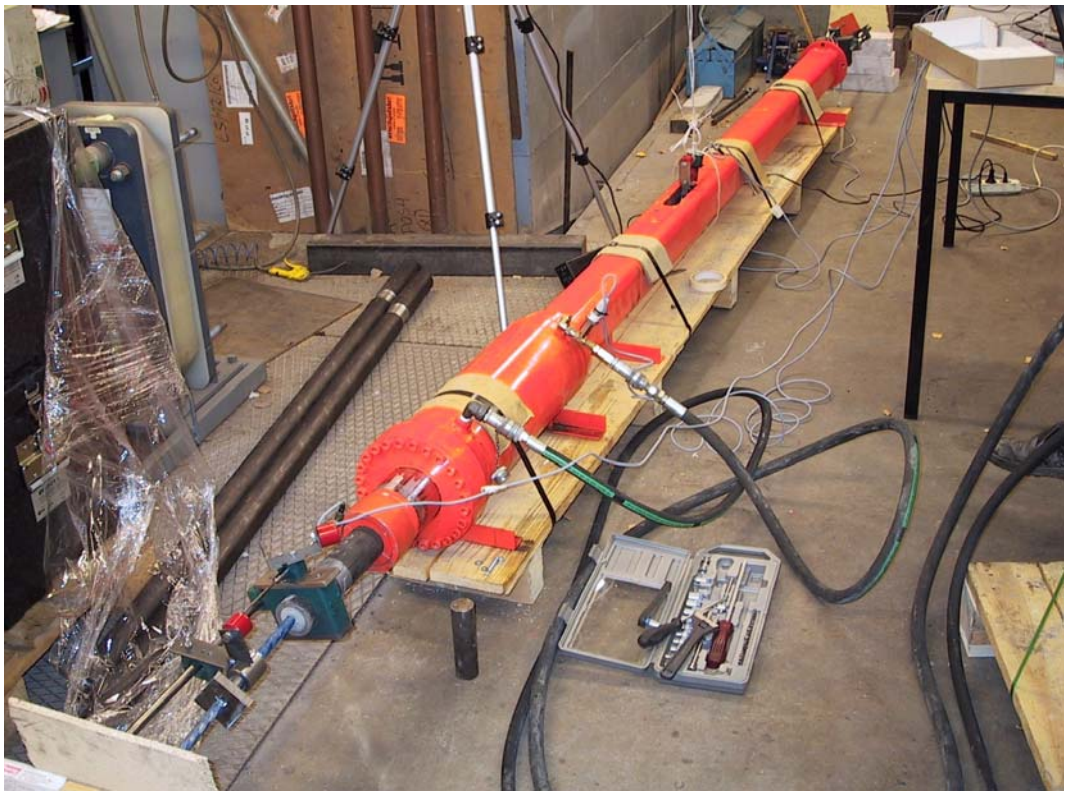

Figure 3. Double pipe axial testing machine (Satola & Hakala 2001a).

The pulling device consisted of a hydraulic jack where the pressure was obtained from an electrically driven hydraulic pump. The double pipe test machine was designed for a maximum capacity of 350 kN, but the pulling device was actually capable of an even higher load capacity. The maximum stroke of the hydraulic jack was 300 mm. The inside diameter of the cylinder of the hydraulic jack was just enough for the steel pipe with an outside diameter of 63 mm.

The idea of the RHS testing pipe was to connect one of the pipes and to keep it in position while the other pipe was pulled by the hydraulic jack and thus the pipes were separated from each other. It was also safe to carry out the pull tests inside the RHS testing pipe when any particles possibly flowing from the grout or any other damage caused by test bolt failure occurs inside the RHS testing pipe. There was a small hole on the RHS testing pipe where the gap was located between the steel pipes for connection of the displacement transducer and for visual observation.

The measuring instruments consisted of:

- Three inductive displacement transducers (HBM WA/100)
- An absolute pressure transducer (HBM P8AP)
- An amplifier system (HBM Spider8) with Spider8 Control measurement technology software package
- A PC for data collection

Three inductive displacement transducers measured the displacements of the test bolts. The displacements were measured not only from the middle (D1), the most important place, but also from both ends of the bolt (D2 & D3) (Figure 2). Displacement transducer D1 measured the displacement between steel pipes, while D2 and D3 measured the displacement between the ends of the steel pipe and the test bolt. Transducers D2 and D3 were used to sense when the entire length of the test bolt embedded in the steel pipe began to slip, thereby indicating that the bond had broken along the entire length of this section of the test bolt. The locations of the connection of displacement transducers were selected so that none of them was in contact with double pipe test machine and thus they were not affected by the deformation of the double pipe test machine itself.

The displacement transducers measure the displacement by the movement of the plunger inside. The displacement transducers D2 and D3 were connected to the steel pipe while the end of the plunger was connected to the magnet that was connected to the test bolt. Because of the steel strands tendency to rotate in pull tests, a special system was designed for connecting the magnet to the test strand. The magnet holder was connected to a normal two-component wedge, which allows the inner wedges to rotate with the strand. The outer part of the wedge, the barrel, was only able to move axially with the inner wedges because rotation was prevented. This system held the magnet in the correct position with the plunger (Figure 4). The magnets were found very practicable in connecting the transducers. When bolt failure occurs, a lot of energy is released resulting in a very rapid movement of the broken parts of the test bolt, which can break the displacement transducer if the connection is too rigid. Using a magnet, the transducer became detached from the magnet and survived without breaking. The influence of the magnet on the displacement results was tested and none was found.

The double pipe test machine was pre-tested with a number of pull tests before the main test program started. Many details were improved and all necessary changes were made to the test configuration on the basis of the pre-tests until the test machine worked as desired.

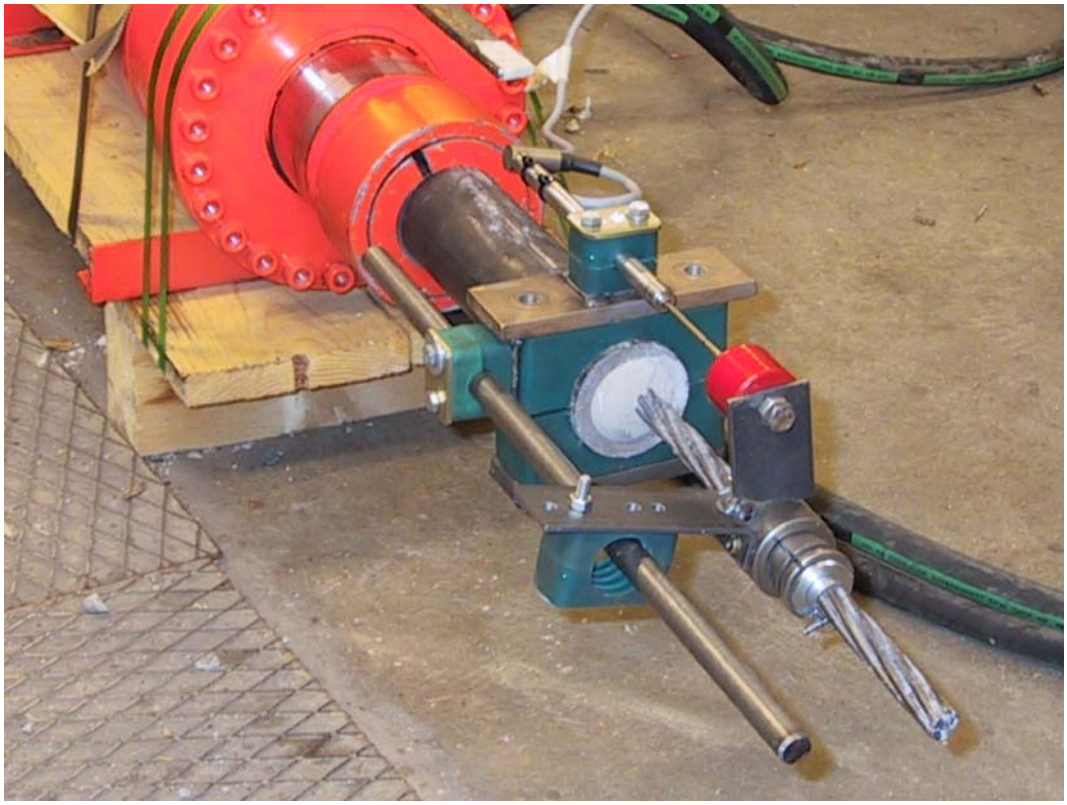

Figure 4. The connection of the displacement transducer to the test strand (Satola & Hakala 2001a).

3.2 Bolt types tested

A total of six different bolt types were tested in different test configurations: rebar, hot-dip galvanized rebar, standard steel strand, hot-dip galvanized steel strand, epoxy-coated steel strand, and bulbed strand (Table 1, Figures 5-7). All the strands were seven-wired steel strand. The rebar was tested as a reference test bolt of the bolt type most commonly used in rock construction in Finland. The galvanized steel strand and the epoxy-coated steel strand were selected for testing because of their corrosion protection ability.

Table 1. Test bolt types and the properties of the test bolts.

Bolt type	**Diameter**	**Average coating thickness**	**Minimum breaking strength**	**Minimum breaking load**
	(mm)	**(µm)**	**(N/mm^2)**	**(kN)**
Rebar	25		550[1]	270[1]
Galvanized rebar	25.3	155[2] (zinc)	550[3]	270[3]
Steel strand	15.2		1801	254[4]
Galvanized steel strand	15.7[4,5]	68[2] (zinc)	1860[4]	260[4]
Epoxy-coated steel strand	16.8[6,5]	800[6] (epoxy)	1860	250[7]
Bulbed strand	15.2 / 28.0			~240[7]

[1] SFS 1215, [2] research report of State Technical Research Centre (2002), [3] assumed to be the same as that of the rebar, [4] information from manufacturer, [5] the diameter of the strand without coating is 15.2 mm, [6] measured by slide gauge, [7] (Hutchinson & Diederichs 1996).

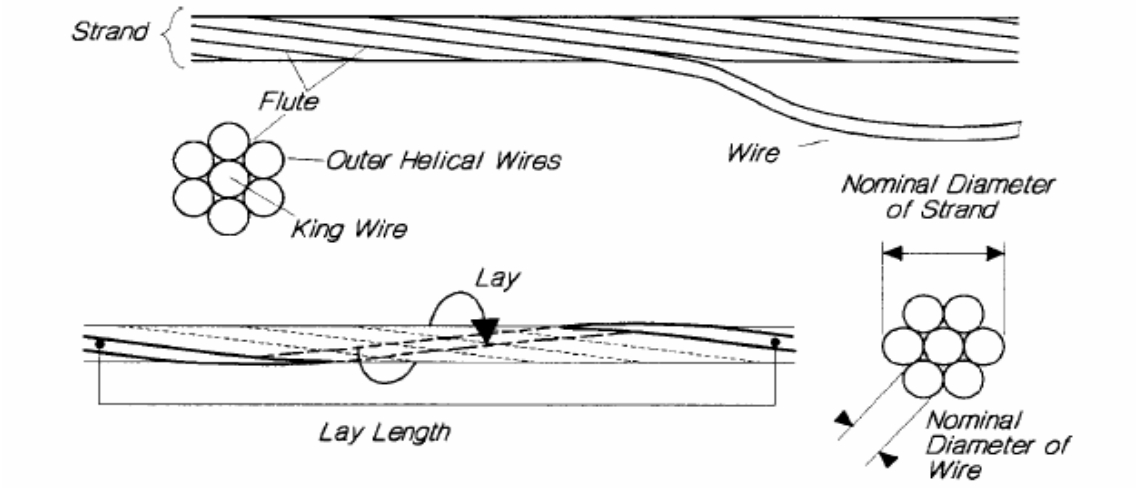

Figure 5. Standard steel strand (Hutchinson & Diederichs 1996).

The bulbed strand was worthy of interest because of its greater stiffness compared to the plain steel strand. The bulbed strand is formed by clamping a section of plain strand between two hydraulic grips and crimping the intervening section to create a deformed bulb (Figure 6). The geometry of the bulbed strand is thought to be more resistant to corrosion than the geometry of the plain strand. The king wire of the strand is placed on

the ring with the other wires in the bulbs so water cannot flow as easily along the king wire as it can along the plain steel strand. In the tests described in this report, the bulbed strand was not corrosion-protected. However, the bulbed strand can also be galvanized or have an epoxy coating. The bulbed strand to be tested had two bulbs per meter.

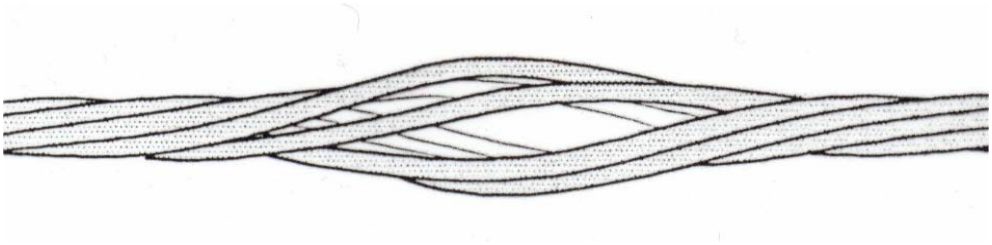

Figure 6. Bulbed strand (after Hutchinson & Diederichs 1996).

Figure 7. Test bolt types. From left: Rebar (with hot-dip galvanizing in the figure), bulbed strand, standard steel strand, hot-dip galvanized steel strand and epoxy-coated steel strand (Satola & Hakala 2001b).

3.3 Grouting

3.3.1 Grouting and installation of the test bolts

Empty steel pipes were put in a cradle where they lay in an inclined position. The steel pipes were washed to remove all oil from the internal surfaces of the pipes before

grouting. The lower end of the steel pipe system was plugged so that the grout could not drain out of the pipes during grouting. The upper end of the pipe systems was left open for a grout hose.

The grout was mixed in a cement mixer for 20 min before grouting. Test bolts were grouted using a 0.40 water-cement ratio grout with normal cement without any additives or aggregates (Table 2). The grout hose was placed inside the steel pipes from the upper end of the pipe system, and then the pipes were filled with the grout as the hose was retracted from the bottom to the upper end of the pipes.

After filling the pipes, the test bolt was manually inserted into them. A section of 0.3 - 0.5 m of the tests bolt was left out at both ends of the pipes so that the displacement transducers in double pipe tests might be connected. In the lower end of the steel pipe, this was possible without drainage problems because of the special plug system designed for that purpose. Bolt was not centralized inside the pipes.

The grouted test bolts were stored under stable conditions with a relative humidity of 98% and a temperature of 12°C for at least 30 days in the Research Tunnel of the Laboratory of Rock Engineering before testing.

Table 2. The properties of cement CEM II A 42.5 (Finnsementti 2001).

Blaine (m^2/kg)	**Blend components (%)**	**Setting time (20 °C) (min)**	**Strength, 2 days (MPa)**	**Strength, 28 days (MPa)**
380 ± 40	6 – 20	120 – 240	≥ 10	42.5 – 62.5

3.3.2 Quality control of the grout

Grout samples were taken from some of the batches during the grouting according to the SFS 5283 and SFS 5341 standards for uniaxial compressive tests and water-cement grout tests. The samples were taken from the mouth of the grout hose by filling the plastic cylinder with the grout. The cylinders were stored under the same conditions as the test bolts and were tested after 28 days.

The aim of the uniaxial compressive tests was to determine the compressive strength, Young's modulus and Poisson's ratio from the samples taken from the grout. The specimens were prepared according to the SFS 5441 standard and tested according to the suggested methods of International Society for Rock Mechanics (ISRM 1981) by the MTS 815 testing system at the Helsinki University of Technology. The compressive stress rate was 0.6 ± 0.4 MPa/s according to the SFS 4474 standard.

Young's modulus and Poisson's ratio were calculated between stress levels of 0% and 50% of the ultimate strength (compressive strength). The density of the samples was determined according to the SFS 5442 standard by measuring the dimensions and the weight of the samples. The mean value of the compressive strength was 55 MPa, the mean value of Young's modulus 15.6 GPa and the mean of Poisson's ratio 0.20. The results of the uniaxial compressive tests showed that the grouting mix had succeeded well.

The water-cement ratio of the grout was tested by taking samples of the fresh grout during grouting to ensure the correct water-cement ratio. Testing was performed using the procedure described in Satola & Hakala (2001a) and Hutchinson & Diederichs (1996). The grout samples were taken and the water-cement ratio was determined from every batch of the grout. Results showed that the water-cement ratio of the grout was very close to the desired value of 0.4 in every case.

3.4 Test sample preparation

Double pipe axial tests of the test bolts were conducted by grouting the test bolts inside steel pipes. The first test bolt samples with an embedment length of 2000 mm had a gap of 20 mm between the grout columns (between the steel pipes) for visual observation (Figure 8). However, this was considered useless and the rest of the test bolt samples in further tests had no gap between the steel pipes. In the tests with long embedment length, the length of the steel pipes was 2000 mm (Section 3.7). The thickness of the pipe wall was 9 mm (Table 3). The inside diameter of the steel pipe was 45 mm, which is very close to the common borehole diameter in Finnish and in Norwegian tunneling practice as well (Stjern 1995). A groove was turned in a lathe at one end of each steel pipe for the connection of the specially designed wedge system.

In the tests with short embedment length, the length of steel pipes was 1000 mm (Section 3.8). To ensure the exact length for the test sections, the rest of the test bolt outside the desired embedment length was debonded by plastic tubing.

In the tests with unequal embedment length, test samples consisted of two different lengths of steel pipes: 2000 mm and 500 mm (Section 3.9). In half of the samples, plates were attached to the test bolts. Square plates and nuts were used with the rebars and they were tightened manually to sit firm on the shorter embedment length end (steel pipe with a length of 500 mm). Typical barrel and wedge anchors with two component wedges were used with the steel strands and the galvanized steel strands. The barrel and wedge anchors were tightened manually instead of tensioning with the installation jack.

Table 3. The properties of the steel pipes used as host material (Satola & Hakala 2001a).

	Outside diameter (mm)	**Inside diameter (mm)**	**Thickness of the wall (mm)**	**Yield Limit (N/mm^2)**	**Breaking strength (N/mm^2)**	**Radial stiffness (MPa/mm)**
Steel pipe	63	45	9	470	620	2726

The radial stiffness (K_r) of the steel pipes (Table 3) was calculated from the thick-wall cylinder theory according to the equation:

$$K_r = \frac{2E}{(1+\nu)}\left\{\frac{d_o^{\,2} - d_i^{\,2}}{d_i\left[(1-2\nu)d_i^{\,2} + d_o^{\,2}\right]}\right\}, \tag{8}$$

where E is Young's modulus, ν is Poisson's ratio for the pipe material (E = 196 MPa and ν = 0.3 for steel), and d_i and d_o are the inside and outside diameters of the pipe, respectively (Hyett et al. 1992b).

Steel strand will tend to rotate in pull tests unless rotation is prevented. To prevent the rotation of the steel pipes relative to each other, two round rods were welded on each of the steel pipes (Figure 8). The welded round rods allow the steel pipes to move axially

to each other but not rotationally. The effect of the friction between round rods on the results was considered insignificant.

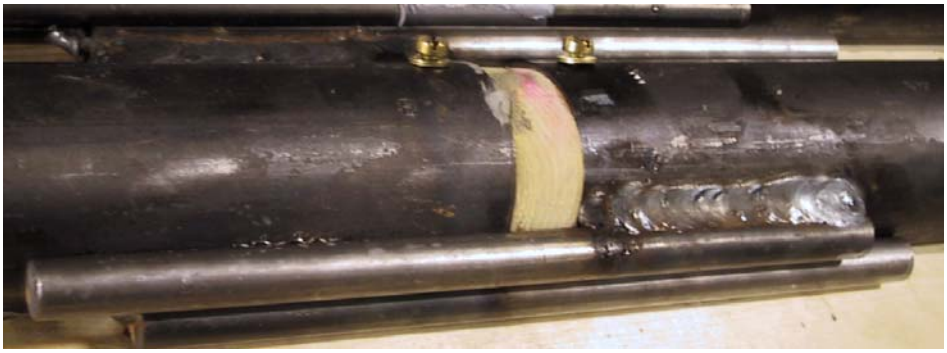

Figure 8. Welded round rods preventing the rotation of the pipes during pull-out tests (Satola & Hakala 2001a).

It was suspected that the bond between the smooth inside surface of the steel pipe and the grout was not strong enough to transfer the load from the steel pipe to the grout and then further to the test bolt. There was a concern that the steel pipe would slip away from the grout column resulting in unsuccessful test behavior. To prevent the grout column from slipping, a ring was welded to the inside surface of each steel pipe to create a ridge at the same end of the pipe where the round rods were welded (Figure 9).

Figure 9.The split test pipe and the grout column after the test. Welded ring inside surface of the pipe (30 mm from the end of the pipe in the figure).

3.5 Test procedure

The steel pipes with the grouted test bolt inside were put through from one end of the RHS -test frame, through the hydraulic jack and placed into the double pipe test machine. The wedges were placed into the grooves made for them at the outer end of both steel pipes to connect the steel pipes to the double pipe test machine. Then, the slack was taken up so that the wedges sat firmly in the grooves.

After placing the test sample in the correct position in the double pipe test machine, the displacement transducers were put in their places and all the values were set to zero. The test began, and increasing the pressure from the hydraulic pump, the load steadily rose at a rate of 10 kN/min. The test bolt was loaded until the failure of the test bolt occurred or the stroke was completed.

The pressure transducer measured the pressure applied to the hydraulic jack from the hydraulic pump. The computer, via the Spider amplifier system with a sampling interval of 0.5 s, recorded all the information data from the pressure transducer and displacement transducers. The load was calculated from the pressure values and working areas of the hydraulic jack.

3.6 Analyses of the test data

The test sample preparation and the pull tests were time consuming and expensive. Within the resources and time available, the number of identical tests had to be limited to a maximum of three samples for each test series. The pull-test procedure and the data obtained were first analyzed by observing the performance of the test bolt as it was tested and identifying and recording inconsistencies. If the tests were successful, the data were analyzed by evaluating the following parameters:

$\mathbf{F_{(bond)}}$: Pull-out load when the first bond failure is detected along the full embedment length on one of the embedment sections. The test bolt starts to slip, relative to the grout column along its full length. The value is identified by the change in the shape of the load-time curve (Figure 10).

$F_{(2nd\ bond)}$: Pull-out load which occurs in the other embedment section after the first bond failure has already occurred (Figure 10).

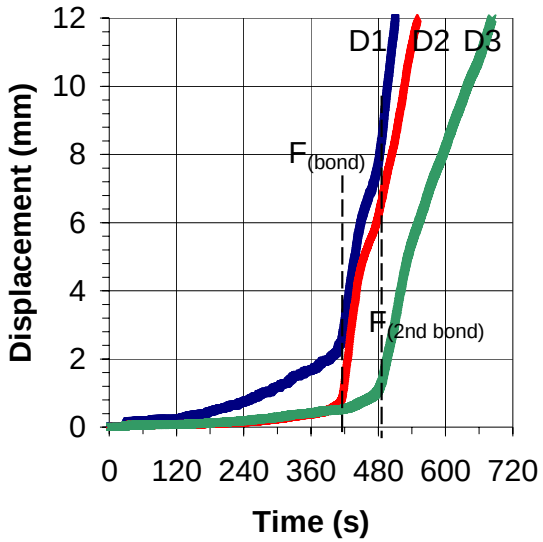

Figure 10. Evaluation of the bond strength.

$D_{(204\ kN)}$: Because of the structure of the steel strand, the yield load cannot be uniquely determined. Instead of the yield load, the 0.2 limit defined in the Finnish standard (SFS 3173) is used as a reference value. According to the strength qualification for strand for prestressed structures, the 0.2 limit ($R_{p\ 0.2}$) is 1470 N/mm^2, corresponding to a load of 204 kN (SFS 1265) (Figure 11).

$F_{(10\ mm)}$: Pull-out load at the displacement (D1) of 10 mm (Figure 11).

$F_{(max)}$: The maximum pull-out load during the test (Figure 11).

$F_{(break)}$: Pull-out load when the bolt failure occurs (Figure 11).

UBS: Ultimate bond strength is calculated using the true contact area of the test bolt and the maximum pull-out load during the test ($F_{(max)}$) (Stillborg 1984). Defined as N/mm^2.

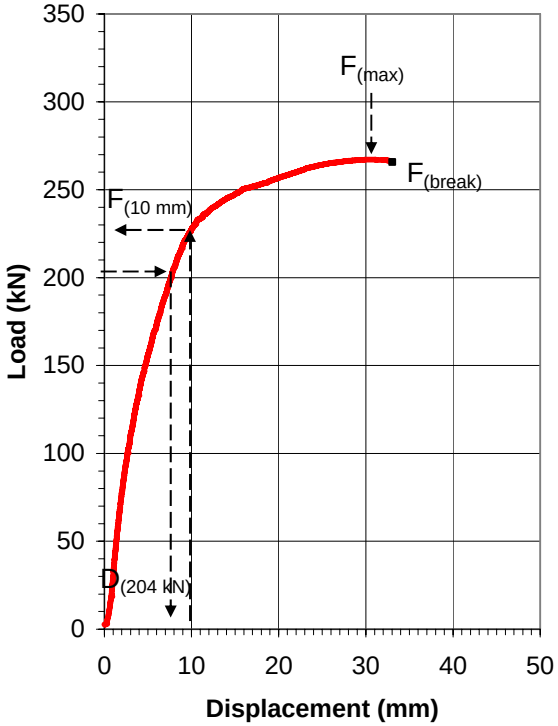

Figure 11. Evaluation of the parameters. Displacement is the value measured between steel pipes (D1).

The circumference of the strand was calculated by the equation:

$$C_S = N \times 3.14 \times D\left[\left(\frac{\sin\left(\frac{360}{2N}\right)}{\sin\left(\frac{360}{2N}\right)+1}\right)\right]\left(0.5+\frac{1}{N}\right), \quad (9)$$

where C_S is the circumference of the strand, N is the number of outer wires of the strand and D is the diameter of the strand (Goris 1991a, Stheeman 1982). The contact area of the steel strand was then calculated by multiplying the circumference by the length of embedded strand in the test pipe.

If serious disturbances occur during the test or if the test failed, the test result was rejected. All the rejected tests are reported in the test results section. All load-displacement curves for each test period were averaged using an Excel macro, so that the load-displacement trends could be evaluated.

3.7 Long embedment length

3.7.1 Aim of the tests

The aim of the pull tests with long embedment lengths was to induce the failure of each test bolt and, thus, obtain the total load-axial behavior of the test bolts from the load of 0 kN up to the breakage load.

3.7.2 Test bolt types

Five different bolt types were tested with an embedment length of 2000 mm: galvanized rebar, standard steel strand, hot-dip galvanized steel strand, epoxy-coated steel strand, and bulbed strand (Table 4).

Table 4. The number of tests of bolts with an embedment length of 2000 mm.

Bolt type	**Diameter (mm)**	**Number of tests**
Galvanized rebar	25	3
Steel strand	15.2	3
Galvanized steel strand	15.7[(5)]	5
Epoxy-coated steel strand	16.8[(5)]	5
Bulbed strand	15.2 / 28.0	4 *

* One of the tests was rejected, see section 3.7.3. [(5)] The diameter of the steel strand without coating is 15.2 mm.

3.7.3 Results

The behavior of different test bolts is illustrated in the load-displacement diagram where the curve of the average value of each test bolt type is presented in (Figure 12). The full test data of each test are presented in the appendices (Appendix A and C). All the test bolts broke off in the double pipe tests as expected. The averaged reference values taken from test data are presented in (Table 5).

Table 5. The averaged test results of the pull-out tests with an embedment length of 2000 mm. Abbreviations are explained in Section 3.6.

Bolt type	**$F_{(bond)}$ (kN)**	**$F_{(2nd\ bond)}$ (kN)**	**$D_{(204\ kN)}$ (mm)**	**$F_{(10mm)}$ (kN)**	**$F_{(max)}$ (kN)**	**$F_{(break)}$ (kN)**	**UBS (N/mm^2)**
Epoxy-coated strand	227.5	260.9	9.5	208.8	281.6	277.6	2.0
Galvanized strand	[a]	[a]	8.3	221.4	268.4	267.1	[b]
Steel strand	109.3	124.2	28.1	131.9	267.5	267.3	2.1
Bulbed strand	[a]	[a]	5.3	261.8	281.8	280.4	[b]
Galvanized rebar	[a]	[a]	1.4	309.0	334.4	286.4	[b]

[a] bond failure didn't occur, [b] UBS was not defined

One of the tests of galvanized rebar with an embedment length of 2000 mm failed because of problems with measuring and recording the data during the test. The test was rejected.

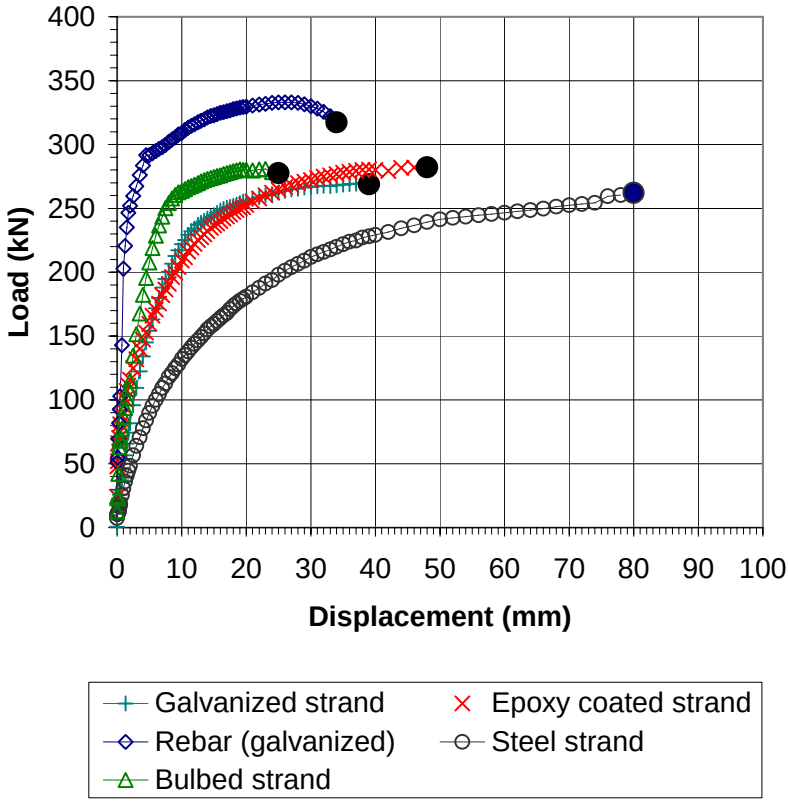

Figure 12. Axial double pipe test results. The average load-displacement curves of each test bolt type with an embedment length of 2000 mm. Displacement is the value measured between steel pipes (D1). Symbol ● denotes that test bolt ruptured (after Satola & Aromaa 2004).

3.7.4 Discussion

There was only a small difference in breaking loads between each test strand type. The breaking load of the test bolts obviously corresponded to the breaking strength of the bolt material, being a slightly higher, whereas the shapes of the curves and the displacement at the failure point were more interesting to analyze. When comparing the displacement at failure, there was a distinct difference between standard steel strand and the other strands. Corrosion protection treatment on the surface of the test strand improved the bond strength between the test strand and the grout because of an increase in roughness of the surface and bond area, resulting in a higher axial stiffness of the grouted steel strand.

The displacement at the proportional yield limit (204 kN) for epoxy-coated steel strand was only 34% of the value of the steel strand. The corresponding value was 30% for the galvanized steel strand, 19% for the bulbed strand and only 4% for the rebar (Table 6).

Table 6. Comparison of $D_{(204\ kN)}$ between different bolt types. Embedment length of 2000 mm.

Bolt type	**$D_{(204\ kN)}$ (mm)**	**F_i / F_{ref}**
Epoxy-coated steel strand (F_i)	9.5	0.34
Galvanized steel strand (F_i)	8.3	0.30
Steel strand (F_{ref})	28.1	1
Bulbed strand (F_i)	5.3	0.19
Rebar (F_i)	1.4	0.04

The bond failure occurred in both embedment sections for the plain strand at the quite low loads. The first bond failure value was 108% higher for the epoxy-coated steel strand (228 kN) than that of the plain steel strand (109 kN). The result was about the same for the second bond failure. Despite the high flexibility of the steel strand, the test bolt finally broke off instead of just slipping out of the grout column.

The bulbed strand had a high degree of stiffness mostly because of the bulbs that functioned as anchors. Galvanized steel strands and epoxy-coated steel strands behaved in a very similar way in the tests. This was clearly seen from the shapes of the curves of the epoxy-coated steel strands and the galvanized steel strands. The displacement at failure was clearly shorter for corrosion-protected steel strands than normal steel strand. The epoxy-coated steel strand and the galvanized steel strand behaved almost equally in the double pipe tests, despite the fact that the corrosion protection materials were so different.

In the tests with an embedment length of 2000 mm, the section of ungrouted test bolt between the steel pipes (20 mm) is free to stretch according to the material properties of the test bolt, and might result in higher displacement values in D1 than in the case, when there is no gap between the steel pipes, especially with the steel strands. However, the effect of the gap on test results was considered insignificant.

The steel pipe and grout around the test bolt were split after the double pipe tests. The compactness as well as the fractures in the grout and in the corrosion protection material on the bolt caused by loading, were all inspected visually. No significant air holes were found in the grout and the compactness of the grout was found to be good.

The bulbs of the bulbed strand were examined carefully after splitting. The visual examination showed that the bulbs were filled with the grout and no holes in the grout were found inside the bulbs (Figure 13). This indicates that the bulbs can be completely filled with the grout when inserting the bulbed strand into the borehole after grouting. This is an important observation for mechanized cable bolting, in particular.

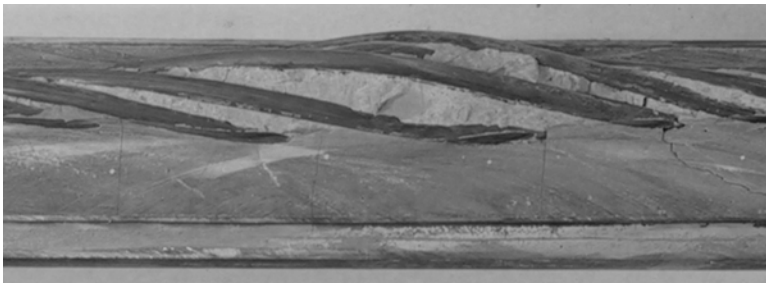

Figure 13. The split test pipe and grout column of the bulbed strand test sample (Satola & Hakala 2001a).

The bulbed strand had a high degree of stiffness because of its modified geometry. The bulbs were filled with the grout and they worked as anchors increasing the bond strength.

The end of the curve corresponding to the failure of the rebar test bolt was cut in the interpolated averaged load-displacement curve in (Figure 12). The values presented in the Table 5 are taken from the original test data and the real break load is presented there.

3.8 Short embedment lengths

3.8.1 Aim of the tests

The aim of the tests was to determine the effect of shorter embedment lengths on axial load-displacement behavior of each test bolt type and to estimate the average load transfer and critical embedment length if possible.

3.8.2 Test bolt types

Five different bolt types were tested: rebar, standard steel strand, hot-dip galvanized steel strand, epoxy-coated steel strand, and bulbed strand (Table 7.).

Table 7. The number of tests of bolts with different embedment lengths.

Bolt type	**Diameter**	**Embedment length (E.L.)**			
	(mm)	**250 mm**	**500 mm**	**750 mm**	**1000 mm**
Rebar	25	3	3	3	3
Steel strand	15.2	0	0	0	3
Galvanized steel strand	15.7	3	2 *	2 *	2 *
Epoxy-coated steel strand	16.8	3	2 *	3	3
Bulbed strand	15.2 / 28.0	3	0	3	3

* One of the tests was rejected, see Section 3.8.3

3.8.3 Test results

The behavior of different test bolts is illustrated in the load-displacement diagrams where the average curves of each test bolt type are presented (Figures 14-17). The full test data of each test are presented in the Appendix A and C. The averaged reference values taken from test data are presented in (Table 8, Table 9, Table 10 and Table 11).

With an embedment length of 1000 mm, all the test bolts broke off in the double pipe tests except steel strands and one test of the galvanized steel strand (Figure 14). The averaged breaking load of the galvanized steel strand presented in Table 8 is higher than the maximum load, because the break load value is from one test and the maximum load is the averaged value from two tests.

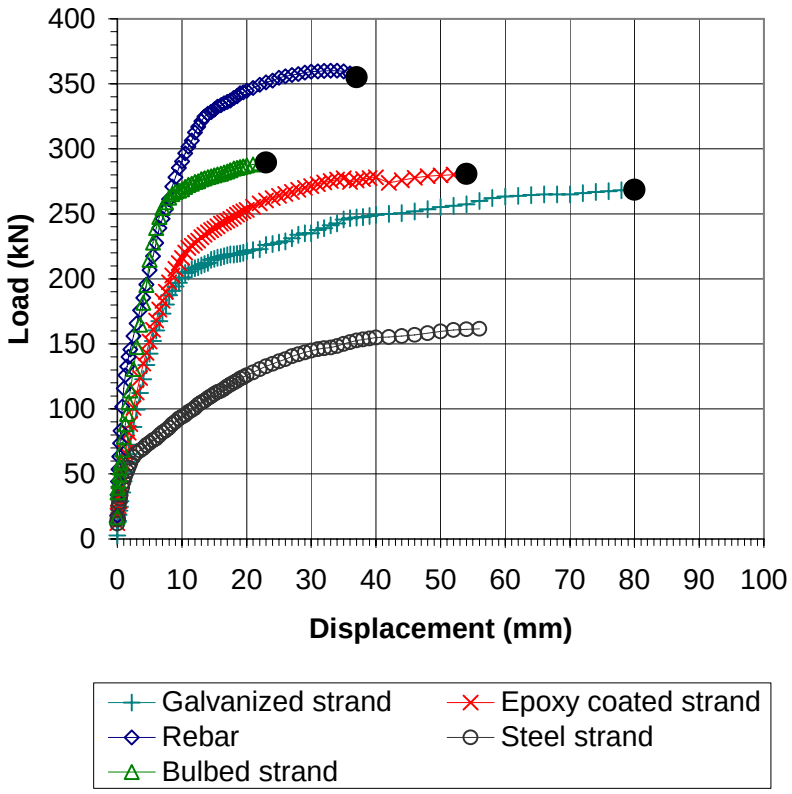

Figure 14. Axial double pipe test results. The average load-displacement curves of each test bolt type with an embedment length of 1000 mm. Symbol ● denotes that test bolt ruptured (after Satola & Aromaa 2004).

One test of the galvanized steel strand with an embedment length of 1000 mm was rejected because of exceptionally low load values. Low load values were considered to be caused by air holes detected in the split grout column.

Table 8. The averaged test results of the pull-out test with an embedment length of 1000 mm. Abbreviations are explained in Section 3.6.

Bolt type	**$F_{(bond)}$ (kN)**	**$F_{(2nd\ bond)}$ (kN)**	**$D_{(204\ kN)}$ (mm)**	**$F_{(10mm)}$ (kN)**	**$F_{(max)}$ (kN)**	**$F_{(break)}$ (kN)**	**UBS (N/mm^2)**
Epoxy-coated strand	247.4	268.6	6.9	239.7	284.7	284.1	4.0
Galvanized strand	203.4	234.1	12.6	201.0	269.5 [g]	270.9 [h]	4.1
Steel strand	64.4	71.4	[d]	87.5	172.1	[c]	2.7
Bulbed strand	[a]	[a]	4.7	269.0	288.1	286.3	[b]
Rebar	[a]	[a]	5.3	290.5	361.4	317.9	[b]

[a] bond failure didn't occur, [b] UBS was not defined, [c] bolt failure didn't occur, [d] a force of 204 kN was not reached in the tests, [g] two tests, [h] only one test, because in one of the tests slippage occurred instead of failure

With an embedment length of 750 mm, only galvanized steel strand and epoxy-coated steel strand were tested. None of the test bolts broke off. The end section from 62 mm to 80 mm of the averaged curve of galvanized steel strand was cut in the interpolated averaged load-displacement curve in Figure 15. The values presented in the Table 9 are taken from the original test data and the real maximum load is presented there. It has to been pointed out that in one test of two of the galvanized steel strand the bond failure occurred at exceptionally low load value. The both original curves are presented in Appendix A.

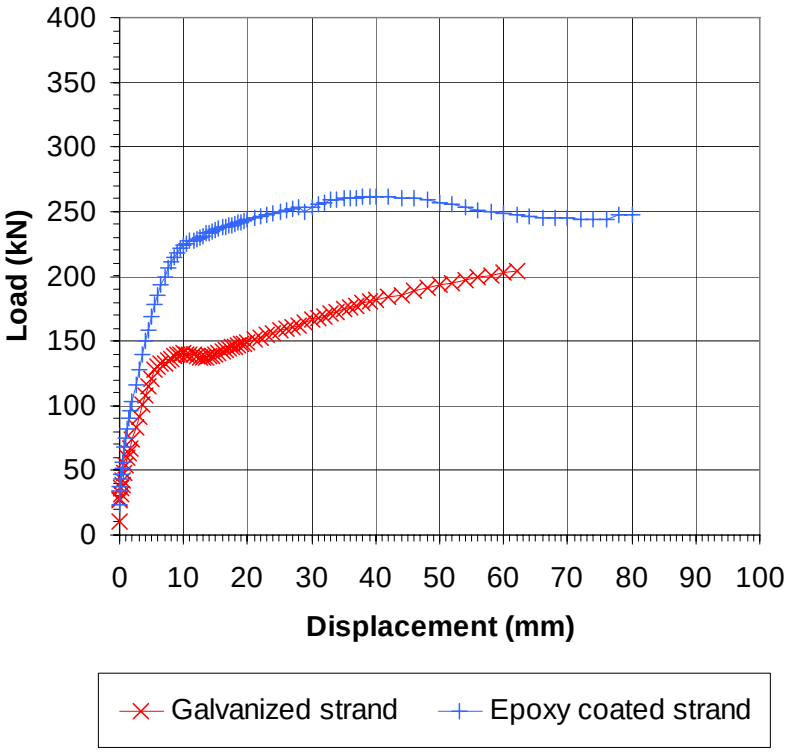

Figure 15. Axial double pipe test results. The average load-displacement curves of two test bolt type with an embedment length of 750 mm (Satola & Aromaa 2004).

Table 9. The averaged test results of pull-out test with embedment length of 750 mm. Abbreviations are explained in Section 3.6.

Bolt type	**$F_{(bond)}$ (kN)**	**$F_{(2nd\ bond)}$ (kN)**	**$D_{(204\ kN)}$ (mm)**	**$F_{(10mm)}$ (kN)**	**$F_{(max)}$ (kN)**	**$F_{(break)}$ (kN)**	**UBS (N/mm^2)**
Epoxy-coated strand	227.0	235.7	7.3	223.2	261.9	[c]	5.0
Galvanized strand	132.9 [i]	153.5 [i]	57.7	140.3	220.0	[c]	4.5
Steel strand	[e]						
Bulbed strand	[e]						
Rebar	[e]						

[c] bolt failure didn't occur, [e] the bolt types were not tested with this embedment length, [i] in one test exceptionally low load values

With an embedment length of 500 mm, the rebar broke off in one single test, whereas in two identical tests, slippage occurred without bolt failure. All bulbed strands broke off. One test of the galvanized steel strand with an embedment length of 500 mm failed because of problems with recording the test data during the test. One test of the epoxy-

coated steel strand with an embedment length of 500 mm was rejected because of exceptionally low load values. The test samples were not split after tests and thus it is impossible to say what the reason for the low load values was.

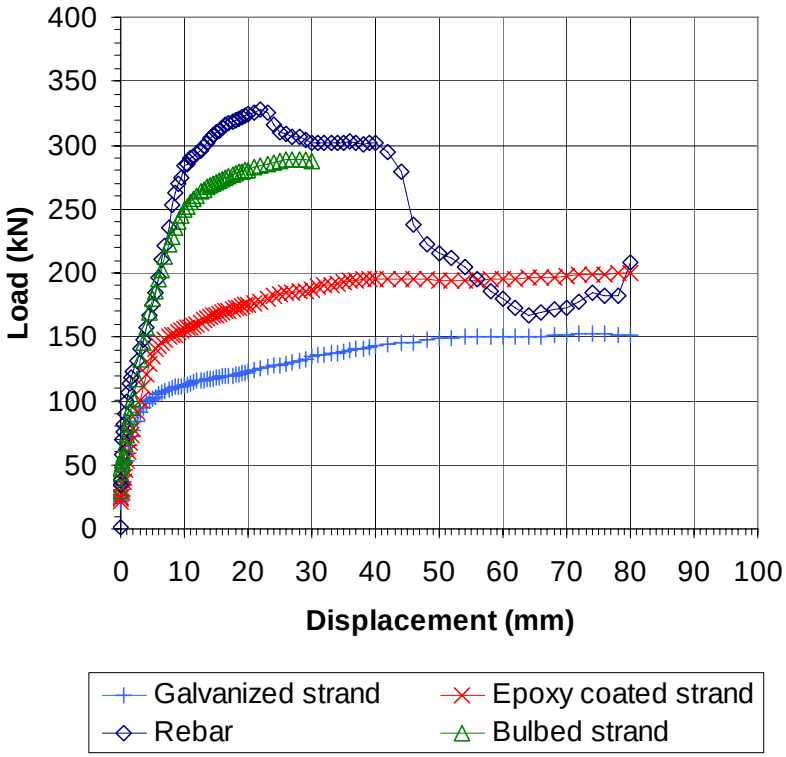

Figure 16. Axial double pipe test results. The average load-displacement curves of each test bolt type with an embedment length of 500 mm (Satola & Aromaa 2004).

Table 10. The averaged test results of pull-out test with an embedment length of 500 mm. Abbreviations are explained in Section 3.6.

Bolt type	**$F_{(bond)}$ (kN)**	**$F_{(2nd\ bond)}$ (kN)**	**$D_{(204\ kN)}$ (mm)**	**$F_{(10mm)}$ (kN)**	**$F_{(max)}$ (kN)**	**$F_{(break)}$ (kN)**	**UBS (N/mm^2)**
Epoxy-coated strand	146.6	178.5	25.7 [g]	156.2	201.2	[c]	5.7
Galvanized strand	104.2	113.8	[d]	112.3	160.7	[c]	4.9
Steel strand	[e]						
Bulbed strand	[a]	[a]	6.5	249.0	289.2	286.5	[b]
Rebar	319.0	[a]	6.9	282.1	334.0	311 [h]	8.5

[a] bond failure didn't occur, [b] UBS was not defined, [c] bolt failure didn't occur, [d] a force of 204 kN was not reached in the tests, [e] the bolt types were not tested with this embedment length, [g] force of 204 kN was not reached in one of the test, [h] in two out of three tests, slippage occurred instead of the failure

With an embedment length of 250 mm, none of the test bolts broke off (Figure 17). The averaged results are presented in Table 11.

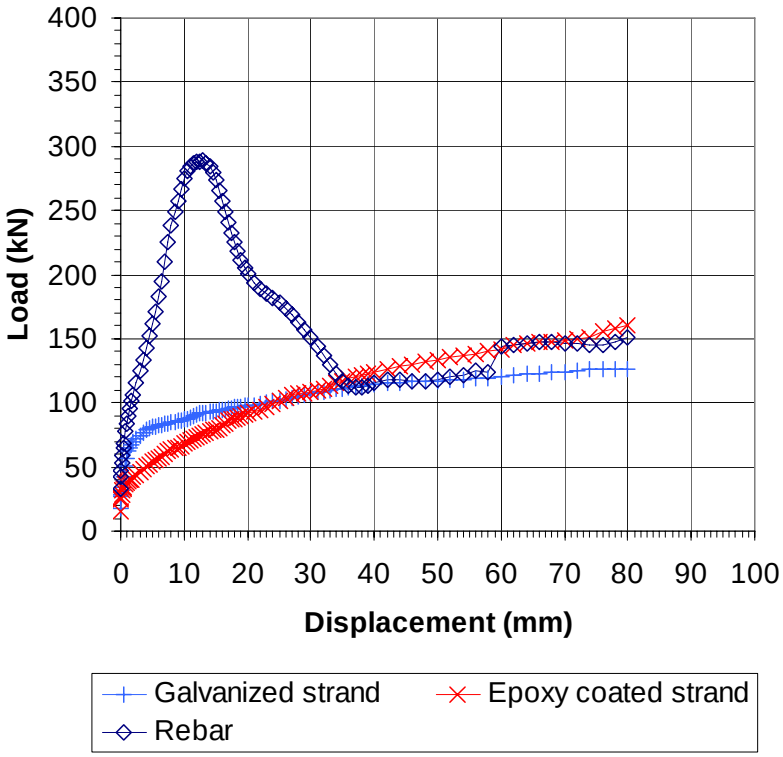

Figure 17. Axial double pipe test results. The average load-displacement curves of each test bolt type with an embedment length of 250 mm (Satola & Aromaa 2004).

Table 11. The averaged test results of pull-out test with an embedment length of 250 mm. Abbreviations are explained in Section 3.6.

Bolt type	**$F_{(bond)}$ (kN)**	**$F_{(2nd\ bond)}$ (kN)**	**$D_{(204\ kN)}$ (mm)**	**$F_{(10mm)}$ (kN)**	**$F_{(max)}$ (kN)**	**$F_{(break)}$ (kN)**	**UBS (N/mm^2)**
Epoxy-coated strand	35.3	51.6	[d]	68.4	159.5	[c]	9.1
Galvanized strand	73.8	84.0	[d]	86.9	131.4	[c]	8.0
Steel strand	[e]						
Bulbed strand	[e]						
Rebar	290.7	[a]	6.9	275.3	291.2	[c]	14.8

[a] bond failure didn't occur, [c] bolt failure didn't occur, [d] a force of 204 kN was not reached in the test, [e] the bolt types were not tested with this embedment length

3.8.4 Discussion

The corrosion protection treatment on the surface of the test strand increased the friction between the strand and the grout and thus improved the bond strength and the stiffness of the grouted strand meaning shorter displacements for given loads. This was clearly seen from the shapes of the curves of the epoxy-coated steel strands and the galvanized steel strands with every tested embedment length: 1000 mm, 750 mm, 500 mm and 250 mm (Figures 14-17)

Embedment length of 1000 mm

The axial load-displacement behavior of the rebar, bulbed strand and epoxy-coated steel strand was very close to the behavior they displayed in the tests with an embedment length of 2000 mm, whereas the behavior of the galvanized steel strand and steel strand was more flexible than that of the tests with an embedment length of 2000 mm.

Epoxy–coated steel strand had higher load values at bond failure, maximum load and break load than galvanized steel strand. The load at the first bond failure for the epoxy-coated steel strand was 22% higher than that of the galvanized steel strand. Higher load values are probably due to the grit surface of the epoxy, which generates more friction to resist pull-out.

The maximum load value for the epoxy-coated steel strand was slightly higher than that of the galvanized steel strand. The corresponding values for steel strand were distinctly lower. Bond failure took place in both embedment sections for the standards steel strand at the quite low loads. The first bond failure value was only 26% of that of epoxy-coated steel strand and 32% of that of the galvanized steel strand (Table 8). The surface of the steel strand is smooth generating very low friction between the surface of the grout and the steel. As presented earlier in this thesis, the untwisting mechanism of the steel strand plays a very important role in bond strength and thus the friction at the interface of the grout and steel is more dominant than the mechanical interlocking and dilation, especially in the tests with short embedment lengths.

The displacement at the proportional yield limit ($D_{(204\ kN)}$) for epoxy-coated steel strand was only 55% of the value of the galvanized steel strand. The corresponding percentage

was 37% for the bulbed strand and 42% for the rebar (Table 12). Bulbed strand had a lower displacement value than rebar, which was surprising. In tests of steel strand, a load of 204 kN was not reached because of the slippage of the strand at a lower load. The maximum load was 189 kN at a displacement of 58 mm.

Table 12. Comparison of $D_{(204\ kN)}$ values between different bolt types. Embedment length of 1000 mm.

Bolt type	**$D_{(204\ kN)}$ (mm)**	**F_i / F_{ref}**
Epoxy-coated steel strand	6.9	0.55
Galvanized steel strand (F_{ref})	12.6	1
Steel strand	[d]	-
Bulbed strand	4.7	0.37
Rebar	5.3	0.42

[d] a force of 204 kN was not reached in the test

The bulbed strand had a high degree of stiffness mostly because of the bulbs that functioned as anchors. The axial behavior and the maximum load value and breaking value were very close to the values obtained from the tests with an embedment length of 2000 mm. It is natural that the pull-out resistance of the bulbed strand is based on the anchoring mechanism produced by the bulbs and the effect of the embedment length is minor compared to the anchoring mechanism.

Embedment length of 750 mm.

In one test of the galvanized steel strand the bond failure occurred at exceptionally low load value, and thus the averaged load values presented in Table 9 and in Figure 15 are lower than they should be.

Embedment length of 500 mm

The axial load-displacement behavior of the bulbed strand with an embedment length of 500 mm was very close to its behavior with an embedment length of 1000 mm. The values were just slightly lower. The axial stiffness and the reference force values were highest for the bulbed strand compared to the other strands.

Epoxy-coated steel strand had a higher degree of stiffness than galvanized steel strand. For the galvanized steel strand, the load at bond failure was 71%, maximum load 80% and UBS 86% of those of epoxy-coated steel strand. The 0.2 limit value (204 kN) was not reached in the galvanized steel strand tests.

Embedment length of 250 mm

Epoxy-coated steel strand started to slip relative to the grout column earlier than galvanized steel strand. The bond failure value of the epoxy-coated steel strand was 48% of the value of the galvanized steel strand. However the maximum load was higher for the epoxy-coated steel strand than for the galvanized steel strand. The maximum load value of the latter was 82% of the former. The 0.2 limit value of 204 kN was not reached in the test for either of the test bolt types. No explanation for the difference between the behavior of galvanized steel strand and epoxy-coated steel strand could be given.

Rebar had still very high values. The value at the bond failure was at the same level as the yielding load of rebar and about 8.2 times higher than that of the epoxy-coated steel strand and about four times higher than that of the galvanized steel strand.

3.9 Bolts with plates and unequal embedment lengths

3.9.1 Aim of the tests

The aim of the test was to determine the effect of plates and barrels/wedges on the axial behavior of test bolts. One of the goals was also to determine the effect of unequal embedment lengths on the axial behavior of test bolts. The idea behind the unequal embedment lengths (2000 mm/500 mm) was that the shorter embedment section (E.L. = 500 mm) represents a rock block falling and pulling away from a bolt, while the longer embedment section (E.L. = 2000 mm) represents the anchor section.

3.9.2 Test bolt types

The following test bolt types were tested: galvanized rebar, steel strand and galvanized steel strand (Table 13).

Table 13. The number of double pipe axial tests with unequal embedment lengths (2000 mm/500 mm). Test bolts were tested both with and without plates.

Bolt type	**Diameter**		
	(mm)	**Plates**	**No plates**
Galvanized rebar	25	2	2
Steel strand	15.2	2	2
Galvanized steel strand	15.7	2	2

3.9.3 Test results

Test results of rebars showed that the full capacity of the rebars was obtained even without plates (Figure 18) (Table 14). In one test without plates, the rebar slippage instead of failure occurred indicating that the critical embedment length was about 500 mm.

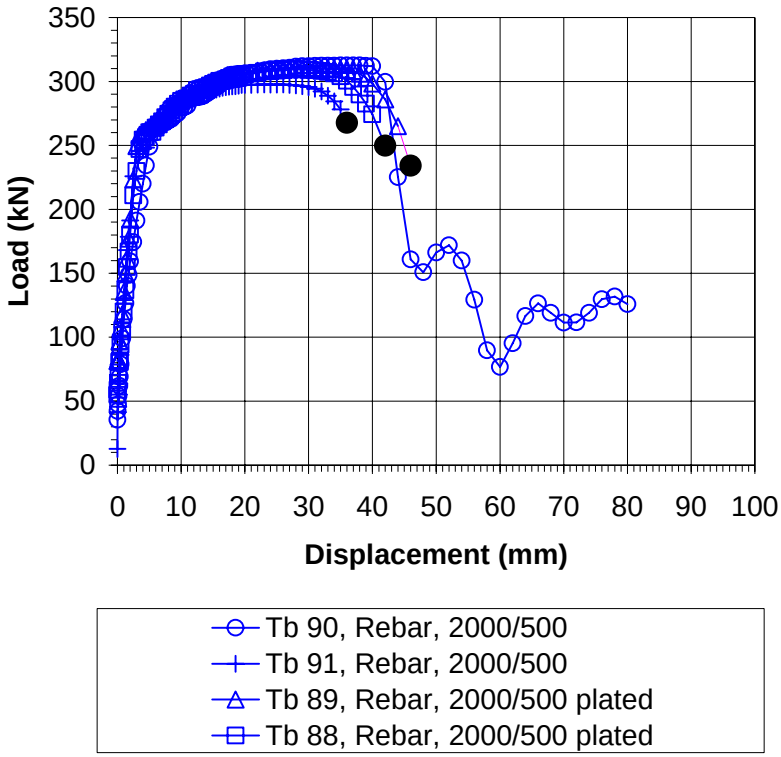

Figure 18. Axial double pipe test results of galvanized rebars of unequal embedment lengths (2000 mm/500 mm) and plates. Symbol ● denotes that test bolt ruptured.

Table 14. The averaged test results of pull-out test with embedment length of 2000 mm/500 mm. Abbreviations are explained in Section 3.6.

Bolt type	**$F_{(bond)}$ (kN)**	**$F_{(2nd\ bond)}$ (kN)**	**$D_{(204\ kN)}$ (mm)**	**$F_{(10mm)}$ (kN)**	**$F_{(max)}$ (kN)**	**$F_{(break)}$ (kN)**	**UBS (N/mm^2)**
Galvanized strand	51.5	[a]	[d]	41.9	82.3	[c]	2.5
Galvanized strand (plated)	47.5	137.0	68.2	74.2	254.8	294.8	7.8
Steel strand	34.0	[a]	[d]	48.0	95.1	[c]	2.9
Steel strand (plated)	37.6	138.1	32.0	78.6	263.0	246.8	8.0
Galvanized rebar	312.0	[a]	2.8	279.7	305.2	247.3	9.3
Galvanized rebar (plated)	[a]	[a]	2.4	285.7	310.3	230.9	[b]

[a] bond failure didn't occur, [b] UBS was not defined, [c] bolt failure didn't occur, [d] a force of 204 kN was not reached in the test

Test results of steel strand showed a significant difference in the axial behavior between plated and unplated tests (Figure 19). In both plated tests, the test bolt broke off.

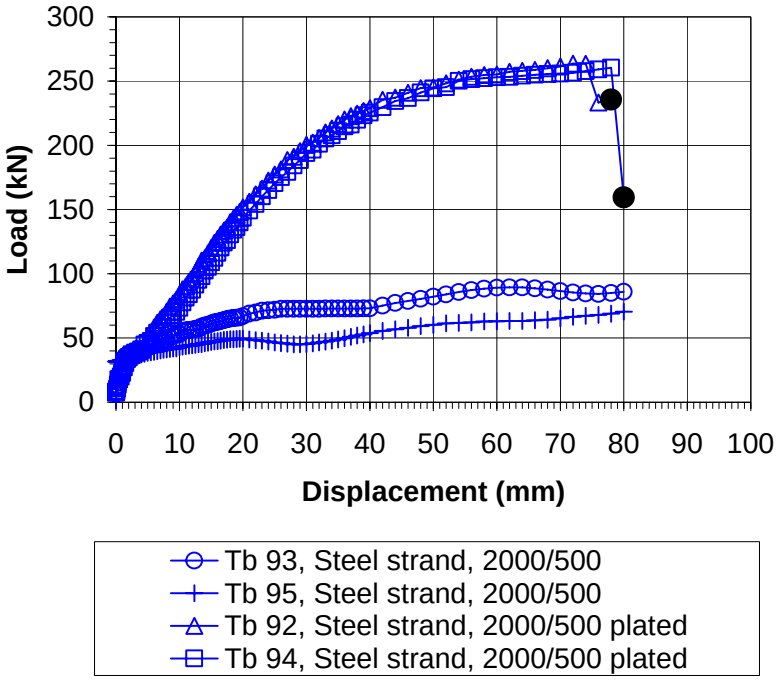

Figure 19. Axial double pipe test results of steel strands of unequal embedment lengths (2000 mm/500 mm) and plates. Symbol ● denotes that test bolt ruptured.

Test results of galvanized steel strand showed a difference in axial behavior between plated and unplated tests (Figure 20). One of the plated galvanized steel strands broke off (no. 86) and another test was stopped at the load of about 214 kN (no. 87) because of the problems with the connection of the displacement transducer.

Because the barrel and wedge anchors were not tensioned with the installation jack, the displacement values in (Figure 19) and (Figure 20) also include the displacement caused by taking up the slack between the barrel, wedges and plates.

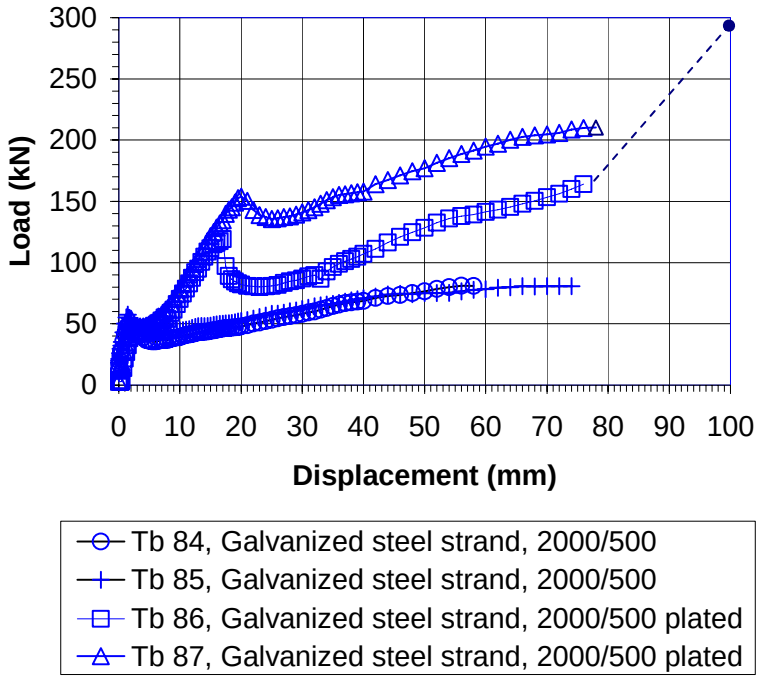

Figure 20. Axial double pipe test results of galvanized steel strands of unequal embedment lengths (2000 mm/500 mm) and plates. Recording the test data at the end of the test no. 86 failed because of problems with displacement transducers (spotted line). Symbol ● denotes that test bolt ruptured.

3.9.4 Discussion

When comparing the results of galvanized steel strands with embedment lengths of 2000 mm/500 mm, some very interesting observations can be made (Figure 21). The stiffness of the grouted galvanized steel strand with an embedment length of 2000 mm/500 mm is significantly lower than at an embedment length of 500 mm/500 mm. This behavior can be explained by the untwisting mechanism of the

strand. The torque absorbed in the strand during the test can not be released at the end of longer embedment (2000 mm) which in turn causes untwisting to occur earlier along the shorter embedment section (500 mm) and the strand slips at a lower load.

Another interesting observation is the behavior of plated galvanized steel strand (2000 mm/500 mm) compared to that of galvanized steel strand with an embedment length of 2000 mm/2000 mm (unplated). The plated galvanized strand showed a slippage at a load of 150 kN at the end of the embedment section of 2000 mm. The explanation is related to the untwisting mechanism in this case also.

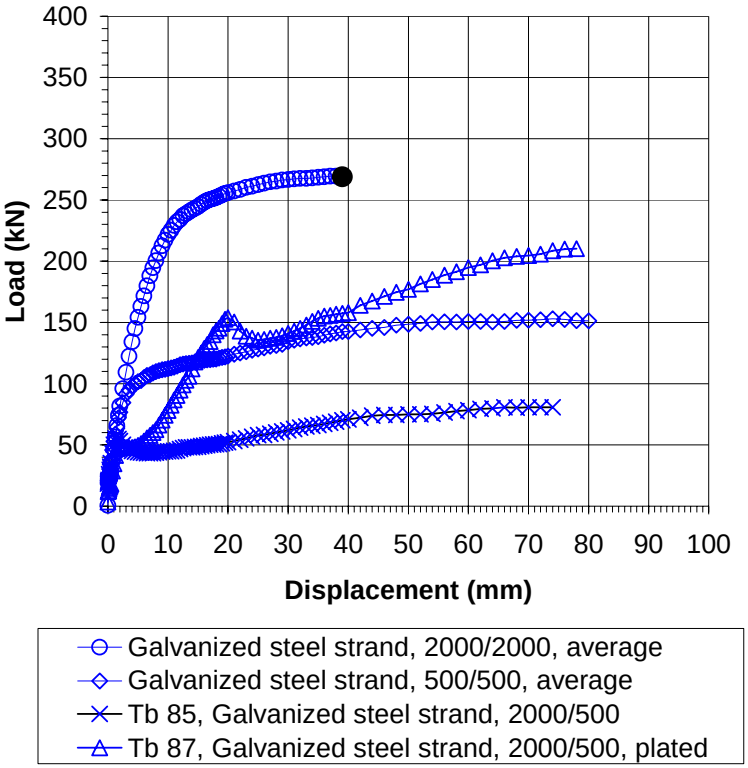

Figure 21. The difference in the axial behavior of galvanized steel strand with different embedment length variations and plated strands. Symbol ● denotes that test bolt ruptured.

The behavior of plated galvanized steel strand can be divided into the following stages (Figure 22):

Stage 0 - 1 (0 - 57 kN): The strand starts to lengthen in the section between two embedment sections. The bond between the grout and the strand starts to break off and the strand starts to debond itself from the joint opening point and debonding proceeds to both embedment sections. Finally, the strand has debonded itself from the grout at the full length of the shorter embedment section (on the both embedment section).

Stage 1 - 2 (57 - 48 kN): The torsional energy absorbed by the strand causes the strand to untwist and slip rapidly until the wedges inside the barrel are start to tighten against the strand and the barrel.

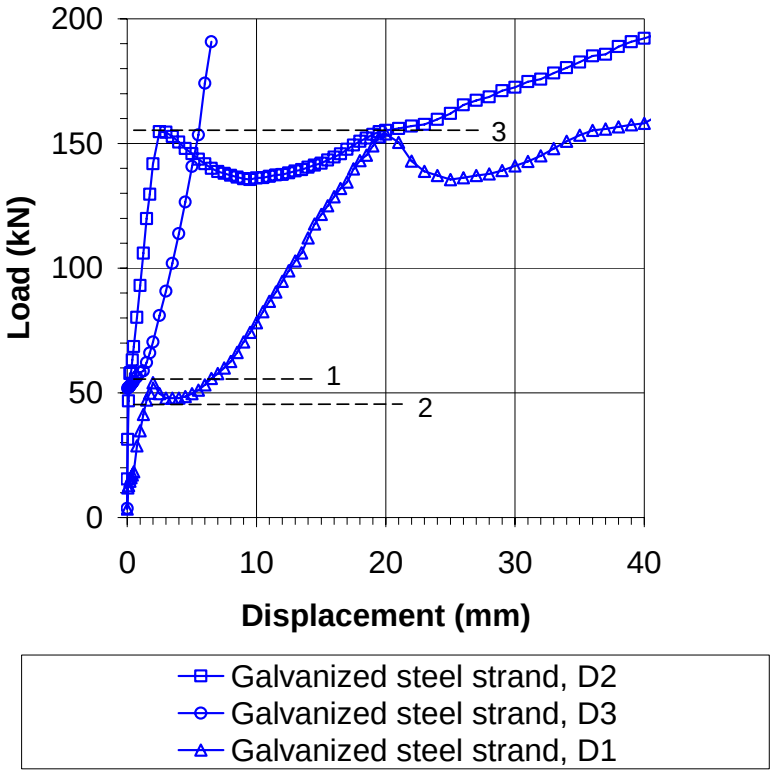

Figure 22. Example of different stages of axial behavior of galvanized steel strand with unequal embedment lengths (2000 mm/500 mm, plated). Test bolt no. 87.

Stage 2 - 3 (48 - 156 kN): The slack is taken up between the barrel/wedges and between the barrel/wedges and the end of the steel pipe. Rotation is prevented on the shorter embedment section because the slack has been taken off and the barrel/wedge and the plate prevent the rotation. The grout compresses. The strand continues to debond itself

from the grout in the longer embedment section and the decoupling front (bond failure front) propagates further along the grout column.

Stage 3 - (156 kN -): The decoupling front has propagated along the whole length of the embedment and bond failure occurs along the full length of the embedment. The end of the strand (pull-in end) moves into the grout column as the strand moves along the grout column for its full length.

When comparing the test results of the strands to that of the rebars, it has to be noted that the barrel and wedge anchors were not tensioned with the installation jack and thus the displacement values of the strands also contain the displacement caused by taking up the slack between the barrel, wedges and plates.

In a normal situation in cable bolting reinforcement, the barrel and wedge anchors are usually attached to the cable bolt after the bolt is tensioned at the pre-load of 50 kN. This load is enough to take up the slack of the surface fixtures of the cable bolt. Tensioning certainly has an influence also on the bond between the grout and bolt near the loading point. It is very likely that the load of 50 kN pointed towards the end of the strand, deteriorates the bond at section of dozens of centimeters from the loading point. How this affects the axial behavior of the strands should be determined. However, this was not the topic of this research.

3.10 Ungrouted steel strand

One single test was performed on the ungrouted steel strand to ascertain, how it behaves in the double pipe test (Figure 23). The test length of the steel strand was 4020 mm.

The strand was connected to the test frame with a plate and barrel and wedge anchors at both ends of the strand. In the beginning of the test, the slack was taken up from the barrel and wedge anchors (from 0 mm to 18 mm). At a load of approximately 240 kN, failure of the first wire(s) occurred. The failure of the next strand occurred at a load of 220 kN. It has to be pointed out that in the pull tests, when failure or sudden slippage occurs, the load is dropped to the lower level and then it starts to increase again.

In the real situation the load is constant and corresponds to the weight of the block or rock mass falling, leading to the breakage of all the wires at the same time (or within a very short time anyway).

The load corresponding to the theoretical 0.2 limit (204 kN) was reached after a displacement of about 55 mm.

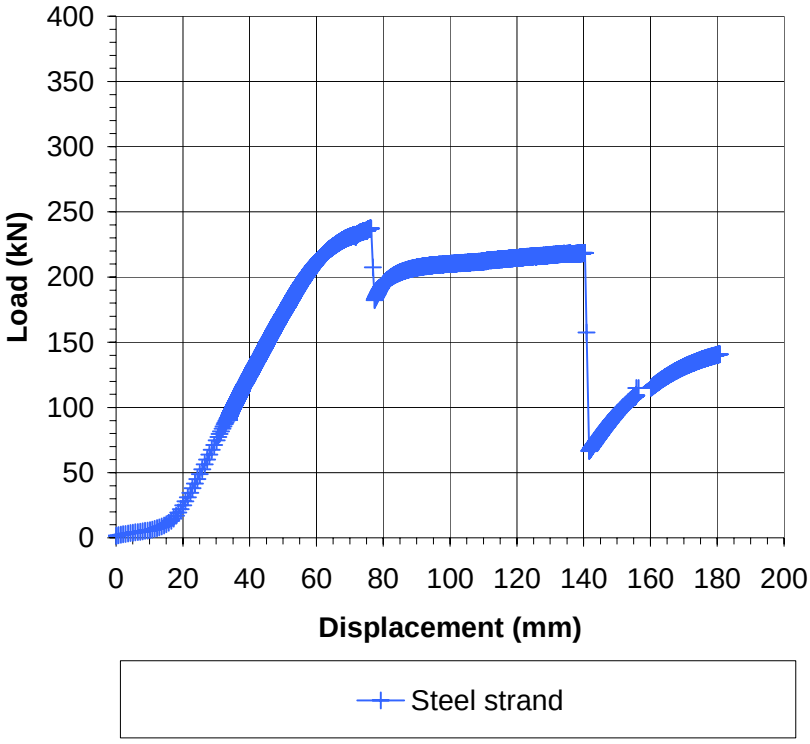

Figure 23. Load-displacement behavior of ungrouted steel strand with a test length of 4020 mm. The test was performed by a double pipe test machine.

3.11 Effect of debonding material on bond strength (Licentiate thesis)

3.11.1 General

This part of the research was done in a project on the development of a mechanized cable bolting system during 1996 - 1999 and is reported by the author in his licentiate thesis (Satola 1999a) and in a refereed conference paper (Satola 1999b). The aim of the licentiate thesis was to find the main factors and mechanisms affecting the behavior of the cable bolt reinforcement. Determining, whether those factors could be changed to

achieve a more flexible cable bolt in order to increase the cable bolt's displacement capacity was also important. This kind of solution, "a yielding cable bolt", would be a very applicable reinforcement structure in rock masses with large deformations. The main limitation of the study was to develop a solution suitable for mechanized cable bolting using standardized seven-wire steel strand being at the same time safe, technically practicable and economically viable.

3.11.2 Aim of the tests

The aim of the pull-out test was to determine the axial load-displacement behavior of debonded steel strands during loading. The idea of these tests was to test the applicability of a yielding cable bolt achieved by debonding by a very simple test procedure using steel pipes. Also, the aim was to determine the applicability of three different materials as debonding materials for steel strands.

3.11.3 Test sample preparation

The test bolt type was a steel strand described in Section 3.2. Three different materials were tested on the surfaces of the steel strands: paraffin, lubricating oil and silicone spray. Each material was tested on the surface of the three steel strands. Three reference steel strands were tested without any surface treatment (Table 15).

Table 15. The number of test samples with different debonding materials in unconstrained pull-out tests (Satola 1999a,b).

Bolt type	Diameter (mm)	Debonding material	Embedment length (mm)	Number
Steel strand	15.2	Paraffin	1000	3
Steel strand	15.2	Silicone spray	1000	3
Steel strand	15.2	Lubricating oil	1000	3
Steel strand	15.2	-	1000	3

The steel strands were placed in a horizontal position and the debonding treatment was performed on that part of the steel strand to be grouted inside the steel pipe. Lubricating

oil was spread on the surface of the strand in a thin layer with a paintbrush. The silicone spray was sprayed on from a distance of about 200 mm. The paraffin was first melted and then spread with a paintbrush. The paraffin cooled very fast and set solidly on the surface of the steel strand.

3.11.4 Grouting and installation of the test steel strands

Cement CEM II A 42.5 was used as the grouting material and the water-cement ratio was about 0.4. The portion of cement was weighed with scales and then mixed with a measured amount of water in a large tub. The water-cement mixture was mixed manually with an electric drill and beater in a tub. No additives or aggregates were used.

The test steel strands were grouted into the steel pipes. The inside diameter of the steel pipe was 44 mm and the length was 1000 mm. The thickness of the wall of the steel pipe was 2.3 mm. One end of the steel pipe was closed and sealed with a welded steel plate. The steel pipes were filled with the grout poured from a can into the steel pipes. Steel pipes were filled with the grout in several steps. The grout was compacted with a tamping bar between every step. Steel strands were inserted manually into the steel pipes. The grouted test steel strands were stored in a vertical position under constant conditions with a relative humidity of 98% and a temperature of +11ºC at the research tunnel of the Laboratory of Rock Engineering before testing.

3.11.5 Pull-out tests

Pull-out tests were performed in the research tunnel of Sandvik Tamrock Ltd. in Tampere in September 1997. The pull-out test equipment consisted of a hydraulic jack with an electric pump and measuring instruments. The measuring instruments consisted of a measuring program, a data logging modulus, two pressure transmitters and a telltale to measure the displacement of the steel strand. The hydraulic jack with the electric pump was capable of applying a maximum load of 300 kN. The stroke of the hydraulic jack was about 300 mm. The load was calculated from the pressures and working areas of each side of the hydraulic jack. The pressures were measured by two pressure transmitters. Pressures were calibrated by using computational values. The telltale was connected to the data logging modulus through a message converter. The telltale was

calibrated by using measuring tape. The measuring range was selected between 0 and 100 mm to reach an adequate resolution.

3.11.6 Test procedure

The steel strand was put through the hydraulic jack. A steel plate was then placed between the end of the steel pipe and the hydraulic jack. The steel strand was connected to the hydraulic jack by another plate, a barrel and wedges. The plate was tightened against the hydraulic jack by the barrel and wedge anchor. A small load was applied to the strand so that the plates, barrel and wedge anchor and hydraulic jack would sit firmly on each other and the direction of the pull was axial to the strand.

The telltale was connected to the hydraulic jack by the steel band and the line of the telltale was tied to the holder, which was connected to the free end of the steel strand. After taking up the slack in the equipment, the telltale was tied to the holder. The rate of the load 10 kN/min was in the line with the suggested methods of the ISRM (1981). The load from the electric pump was steadily increased until the bolt moved/stretched the amount of the stroke or failure occurred. The pressure and displacement readings were taken at increments of 0.5 s and they were recorded automatically by the computer. After each pull-out test the line of the telltale was released and the strand was cut off in order to remove the strand from the hydraulic jack.

3.11.7 Test results

The averaged axial behavior of the test steel strands during pull-out testing is illustrated in the load –displacement diagram (Figure 24). Because of the calibration of the telltale it was possible to record the displacements of the first 100 mm. However, all the steel strands were pulled out the full amount of the stroke of the hydraulic jack (300 mm). All the test steel strands slipped out of the pipes instead of breaking. In every pull-out test the steel strands came out by untwisting.

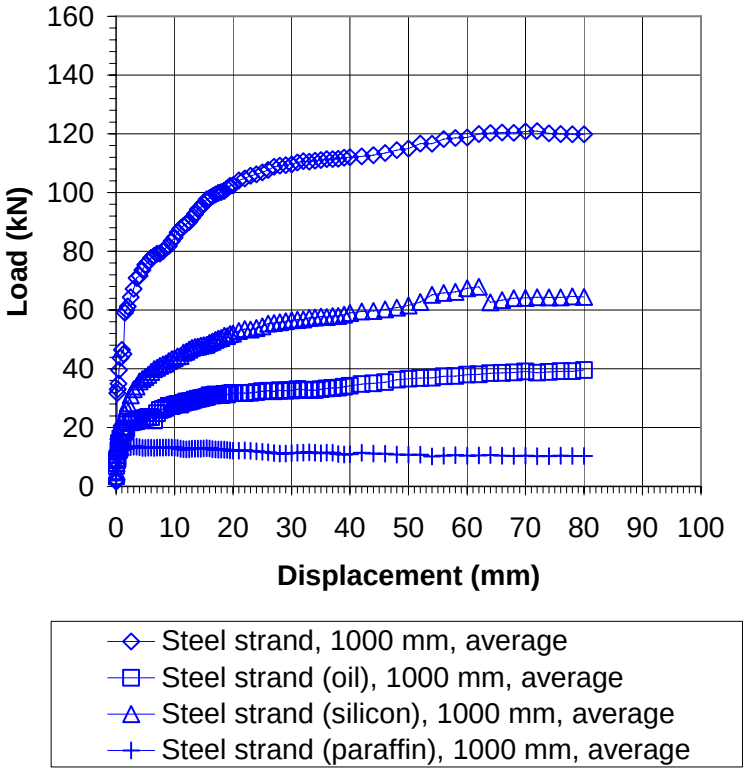

Figure 24. The averaged test results of steel strands with different debonding materials (after Satola 1999a,b).

3.11.8 Discussion

Reference wire strands came out of the steel pipes with quite low pull-out loads rather than a break in the wire strands. This was mainly because of the rotation of the wire strand during pull-out and the low radial stiffness of the steel pipes. Pull-out tests, where rotation is allowed, give lower pull-out resistances than tests where rotation is prevented (Hutchinson & Diederichs, 1996). The radial stiffness of the steel pipe affects the embedment length where the full cable capacity (240 kN) is attained (Hyett et al. 1992b). The lower the radial stiffness, the longer the embedment length required. In the reported pull-out tests, the thickness of the wall of the steel pipes was only 2.3 mm and thus the radial stiffness of the steel pipe was quite low.

The thickness of the layer of the debonding materials applied to the surface of the steel strand varied with each debonding material. Lubricating oil and paraffin were spread onto the surface of a steel strand by paintbrush. Thus, it was difficult to get those materials to spread uniformly. The thickness of the layers had a clear effect on the pull-

out loads. Increasing the thickness of the layer decreases the pull-out resistance. Silicon was easier to spread uniformly on the surface of the steel strand, because it was sprayed on. The thickness of the layer was also less and thus the pull-out resistance was higher than that of the steel strands debonded by the other debonding materials.

There was a clear difference between the mean values of maximum pull-out loads of debonded steel strands and reference steel strands (not debonded) (Table 16). The mean value of the pull-out loads of the steel strands debonded by paraffin was only 11% of that of the reference steel strands. The steel strands debonded by silicon spray had the highest pull-out loads of the debonded steel strand. The mean value of the pull-out loads of those steel strands was about 58% of the reference steel strands. The corresponding value was 34% for the steel strands debonded by lubricating oil. It should be pointed out that the mean values were calculated from three values and are thus only averages.

Table 16. The number of test samples with different debonding material in unconstrained pull-out tests (Satola 1999b).

Bolt type	**Diameter (mm)**	**Debonding material**	**F_{max} (kN)**	**F_i / F_{ref}**
Steel strand	15.2	No debonding	122 (F_{ref})	1
Steel strand	15.2	Silicone spray	71 (F_i)	0.58
Steel strand	15.2	Lubricating oil	42 (F_i)	0.34
Steel strand	15.2	Paraffin	14 (F_i)	0.11

3.12 Interpretation of the test results

To check the load values and calibrate the double pipe test system, the hydraulic jack was connected in the MTS 815 testing system and the calibration test was performed. The load values measured by the MTS 815 testing system were compared to those measured by the double pipe test system. The load measured by the MTS 815 testing system was 6% higher than that of the double pipe test at a load of 50 kN. When the load was increased from 50 kN to 400 kN the corresponding value decreased from 6% to 1% (Appendix B).

The artificial improvement of the bond strength by the welded ring inside the steel pipe cannot simulate the real bond between the grout and the surface of the borehole. However, the mechanisms affecting on the surface between the test bolt and the grout column were virtually the same.

The displacement (D1), the total opening between the pipes, has been defined as total displacement, although it is the sum of the elongation of the embedded test bolt, the elongation of the ungrouted section of test bolt between two pipes, the elongation of the pipe and grout column, and any initial movement in the testing apparatus when loading began.

It should be pointed out that the laboratory axial tests are mainly intended for a comparison of different variables between test bolts. The results are relative and comparison can be made only with the results obtained from tests performed in a similar way. None of the laboratory tests can simulate the real situation of a rock reinforcement element loaded in a rock mass. However, in double pipe axial tests the response of the reinforcing element at the interface between the two halves of the test specimen most closely represents the performance of a similar reinforcing element crossing a dilating discontinuity.

A minimum of five tests are usually required in rock bolt testing according to the ISRM Suggested Methods for Rock Bolt Testing (ISRM 1981). However in the tests described in this thesis, a very limited number of identical tests were performed because of the limited resources of and schedule available. Normally the number of identical tests was at least three, but in some tests only two successful identical tests were performed.

4 FINAL DISCUSSION

4.1 Effect of corrosion protection

The corrosion protection treatment on the surface of the test strand increased the friction at the interface between the strand and grout and improved the bond strength resulting in higher bond failure loads, maximum load and ultimate bond strength (Table 17). The bond failure loads ($F_{(bond)}$ and $F_{(2nd\ bond)}$) of the epoxy-coated steel strand with embedment length of 1000 mm were about 3.8 times that of the steel strand. The corresponding values of the galvanized steel strand were about 3.2 - 3.3 times that of the steel strand.

The maximum loads of the epoxy-coated steel strand and the galvanized steel strand were about 60% - 70% higher than that of the steel strand with an embedment length of 1000 mm and less than 10% higher with an embedment length of 2000 mm. $D_{(204\ kN)}$ of the epoxy-coated steel strand, with an embedment length of 2000 mm, was only 34% of that of the steel strand, whereas the $D_{(204\ kN)}$ of the galvanized steel strand was only 30% of that of the steel strand.

Table 17. The comparison between corrosion-protected steel strands and unprotected steel strand. Abbreviations are explained in the Section 3.6. V_i = values of the galvanized steel strand or epoxy-coated steel strand, V_{ref} = value of the steel strand.

Bolt type	**E.L. (mm)**	**$F_{(bond)}$ (V_i/V_{ref})**	**$F_{(2nd\ bond)}$ (V_i/V_{ref})**	**$D_{(204\ kN)}$ (V_i/V_{ref})**	**$F_{(max)}$ (V_i/V_{ref})**	**UBS (V_i/V_{ref})**
Epoxy-coated strand	1000	3.84	3.76	*	1.65	1.52
Epoxy-coated strand	2000	2.08	2.10	0.34	1.05	*
Galvanized strand	1000	3.16	3.28	*	1.57	1.52
Galvanized strand	2000	*	*	0.30	1.00	*

* could not be defined, see previous results

Epoxy-coated steel strand had higher load values at bond failure and maximum load than galvanized steel strand (Table 18). The $F_{(bond)}$ of the epoxy-coated steel strand was about 22% higher than that of the galvanized steel strand with an embedment length of

1000 mm. There was a distinct difference in $D_{(204\ kN)}$ values between the epoxy-coated and galvanized steel strands with an embedment length of the 1000 mm with that of the epoxy-coated steel strand being only 55% of that of the galvanized steel strand. With an embedment length of 2000 mm, epoxy-coated steel strand had, however, a higher (14%) $D_{(204\ kN)}$ value than galvanized steel strand.

Higher load values of the epoxy-coated steel strand with the embedment length of 1000 mm are probably because of the grit surface of the epoxy and larger contact area, which generates more friction and thus increased pull-out resistance. The effect of the grit and larger contact area decreased when the embedment length was increased. This can be seen from the results of the test strands with the embedment length of 2000 mm.

The maximum load value for the galvanized steel strand was slightly higher than that of the epoxy-coated steel strand.

Table 18. The comparison between epoxy-coated (E_i) and galvanized strand (G_i). Abbreviations are explained in Section 3.6.

Bolt type	**E.L. (mm)**	**$F_{(bond)}$ (E_i/G_i)**	**$F_{(2nd\ bond)}$ (E_i/G_i)**	**$D_{(204\ kN)}$ (E_i/G_i)**	**$F_{(max)}$ (E_i/G_i)**	**UBS (E_i/G_i)**
Relation	1000	1.22	1.15	0.55	1.06	0.98
	2000	*	*	1.14	1.05	*

* could not be defined, see previous results

4.2 Effect of the embedment length

Most of the axial pull tests were carried out in such a way that both embedment lengths were equally long in the same test. The results showed that the maximum load-carrying capacity of galvanized steel strand and epoxy-coated steel strand increased linearly as embedment length increased from 250 mm to 1000 mm (Figure 25). In the tests presented in this thesis, steel strand was tested with only two different embedment lengths (1000 mm and 2000 mm), and thus it is not reliable to present any thoughts about linearity as regards the behavior of steel strand. However, Goris (1990a) found a

linear behavior in his tests on steel strand for embedment lengths from 203 mm (8 inches) to 813 mm (32 inches).

The maximum loads of bulbed strands were about the same level at every embedment length tested. It is obvious that for the steel strands the maximum load increases when the embedment length increases, until the critical embedment length is reached (Figure 25).

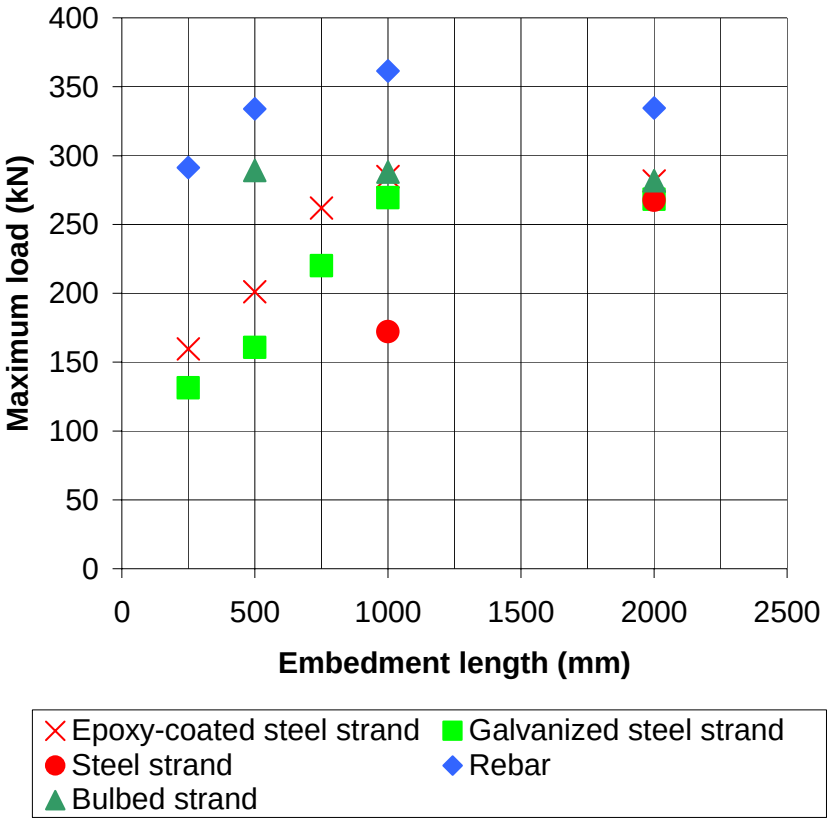

Figure 25. The averaged maximum load at the different embedment lengths.

The ultimate bond strength, i.e. the maximum load divided by the bond area, was calculated for every test bolt type with the embedment length tested in the cases when the bond failure was detected (Figure 26). Rebar and bulbed strand had the highest bond strength values with every embedment length tested.

The high pull-out resistance of the bulbed strands is based on the bulbs which work as anchors, and therefore the mechanisms affecting the pull-out resistance differs from that of other strands (Figure 7). The ultimate bond strength values for the bulbed strand were not defined because bond failures were not detected.

Epoxy-coated steel strand had higher UBS values than galvanized steel strand with every embedment length.

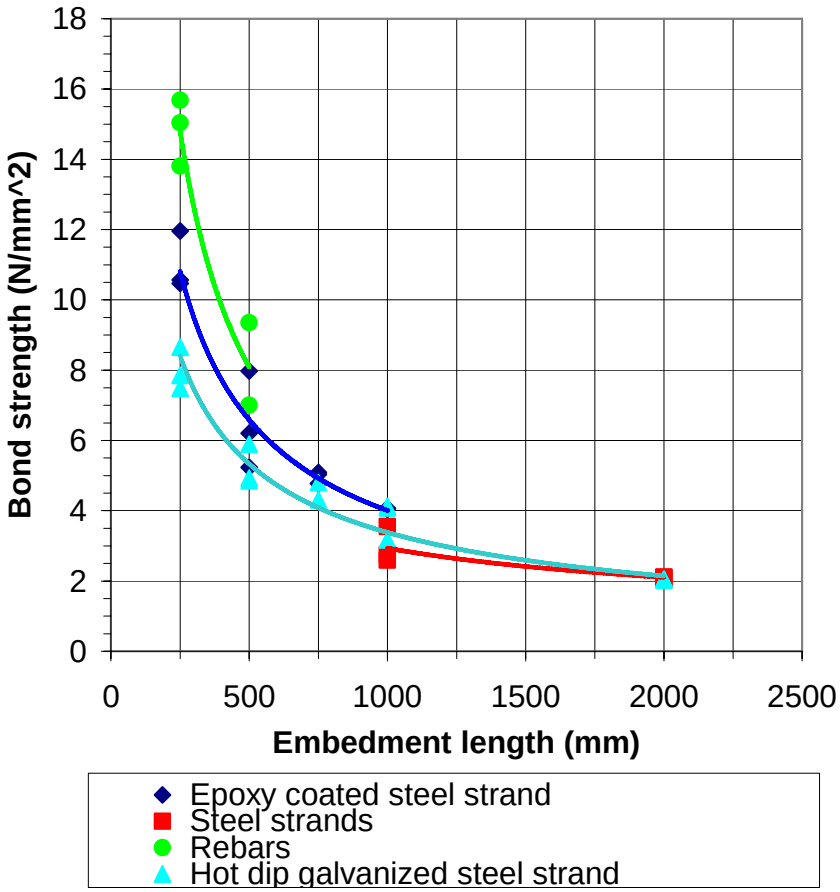

Figure 26. The ultimate bond strengths (UBS) of test bolt types with different embedment lengths. Bond strength is defined as the ultimate load divided by the bond area of the bolt.

Some of the axial pull tests were performed in such a way that that one of the embedment lengths was shorter (500 mm) and the other was longer (2000 mm) in the same test. The idea of this test system was to simulate a rock block falling from the roof

and pulling away from a support cable bolt. Also the effect of the plates on the axial behavior was tested.

It is obvious that the end of the test strand in the shorter embedment section (500 mm) offered the least resistance to pull-out and consequently pulled out of the grout as the load applied to the system was increased. The bond between the grout and strand was broken first at the junction of the steel pipes (joint opening point) and then propagated along the length of the steel strand in both 500-mm and 2000-mm embedment sections. When the bond along the entire length of the strand embedded in the 500-mm section was broken the grout began to slip along the surface of the strand. It is assumed that the bond was also broken along the 500 mm of the strand in the 2000-mm section.

Untwisting mechanism played a very important role in the tests and two very interesting observations were made. The stiffness of the grouted galvanized steel strand with the embedment lengths of 2000 mm and 500 mm (2000 mm/500 mm) was significantly lower than in the case of 500 mm and 500 mm (500 mm/500 mm). This behavior was explained by the untwisting mechanism of the strand. It is the author's opinion that the torque generated along the strand during the test cannot be released at the section of longer embedment (2000 mm), which in turn caused untwisting to occur earlier at the end of shorter embedment section (500 mm) and the strand slipped at a lower load.

Another interesting observation was the behavior of plated galvanized steel strand (2000 mm/500 mm) compared to that of galvanized steel strand with embedment lengths of 2000 mm and 2000 mm (unplated). Plated galvanized strand took a slippage at a load of 150 kN at the 2000-mm embedment end. This behavior is probably caused by the prevention of the rotation of the strand due to the plate.

4.3 Effect of the debonding material

The effect of the debonding material is based on the thickness of the debonding layer and the ability to decrease the friction between the strand and grout. The thickness of the layer plays a dominant role, because it smoothes the profile of the grout surrounding the debonding layer and thus the interlocking is decreased. The thickness of the layers

had a clear effect on the pull-out loads. The thicker the layer, the lower the pull-out resistance.

4.4 Effect of untwisting mechanism

As mentioned earlier in this thesis, the untwisting mechanism of the strand plays an even more important role in the axial behavior of plain strand than the other mechanisms: shear failure of the cement flutes and dilatational slip of the strand accommodated by radial splitting. This phenomenon was discussed earlier in the Section 2.4.

An untwisting mechanism was also detected in the axial pull tests presented in this thesis. The steel strand untwisted out of the grout column, instead of shearing the cement flutes or dilational slip during pull-out. Bond failure occurred by untwisting nearly the full length of the bond length and shearing of the grout flutes occurred only on the small section near the exit point of the strand.

The untwisting mechanism is very closely related to the torsional rigidity of the steel strand, the friction between the strand and grout, the strength of the grout and the stiffness of the host material (rock, steel pipe).

The effect of the untwisting mechanism has to be taken seriously in rock reinforcement design. The critical embedment length values of the plain strand presented in the literature are very often determined by single embedment length tests, where an untwisting mechanism is not presented because the torque is not generated in the strand. This leads to an unrealistic behavior of the steel strand under loading, and thus a longer critical embedment length than occurs in reality.

5 CONCLUSIONS

Due to the interest in the expanded use of cable bolting also in civil rock engineering, “Corrosion-protected cable bolts in long-term reinforcement” research projects were carried out in the Helsinki University of Technology in 1999 – 2003. The object of the projects was to study the applicability of corrosion-protected cable bolts in long-term reinforcement.

This thesis concentrated on one of the topics of the projects, related to the mechanical applicability of cable bolts in rock reinforcement for civil rock engineering and long-term reinforcement purposes. The scope of the thesis was to test and evaluate the axial load-displacement behavior of different types of steel strands applicable to rock reinforcement.

Of particular interest was to determine the effect of the corrosion protection (hot-dip galvanization and epoxy coating) on the axial load-displacement behavior of the steel strand.

A new modification for axial laboratory testing of rock reinforcement elements was designed and constructed for this research. The double pipe test apparatus enabled testing of different bolt types with embedment lengths from 250 mm up to 2000 mm with a loading capacity of 0 kN - 350 kN. The test apparatus worked as desired and was easy to operate.

A total of about 70 axial laboratory pull-out tests were performed, including different set-ups for the tests and different embedment lengths used. This was performed by conducting strictly controlled axial laboratory pull tests on full-scale standard steel strand, modified steel strand, galvanized steel strand and epoxy-coated steel strand, under axial loading. Rebars were tested as a reference given that they are the most commonly used bolt types in civil rock engineering in Finland.

An untwisting mechanism was detected in the axial pull tests. The results showed that untwisting mechanism dominates the axial behavior of the steel strands. This observation is in line with the results reported in the literature. The steel strand

untwisted out of the grout column, instead of shearing the cement flutes or dilatational slip of the strand during pull-out. Bond failure occurred by untwisting nearly along the full length of the bond length, and shearing of the grout flutes took place only on the small section near the exit point of the strand.

The main principle of axial behavior of the test bolt, despite the type of bolt, was the following: as the load was increased, the bond between the grout and strand was broken, first at the junction of the pipes and then propagating along the length of the bolt. If the load applied to the bolt is larger than the force resisting pull-out (i.e. bond strength), the bolt starts to slip out of the grout column. If the load applied to the bolt is less than the bond strength, the bond between the grout and the strand is broken to the definite point of embedment. In other words, if the embedment length is longer than the critical embedment length strand will break off. The length of the broken bond section (i.e. the point of embedment) is dependent on the factors affecting bond strength.

The bond failure loads ($F_{(bond)}$ and $F_{(2nd\ bond)}$) of the epoxy-coated steel strand and the galvanized steel strand with an embedment length of 1000 mm were significantly higher than that of the steel strand.

The maximum loads of the epoxy-coated steel strand and the galvanized steel strand were about 60% - 70% higher than that of the steel strand with an embedment length of 1000 mm. Displacement at a load of 204 kN ($D_{(204\ kN)}$) for the epoxy-coated steel strand and the galvanized steel strand was only about 30% - 34% of that of the steel strand with an embedment length of 2000 mm.

The results showed that the maximum load-carrying capacity of galvanized steel strand and epoxy-coated steel strand increased linearly as the embedment length increased from 250 mm to 1000 mm. The critical embedment length of those bolt types was between 750 and 1000 mm.

When making a comparison between the epoxy-coated steel strand and galvanized steel strand, the results showed that the epoxy-coated steel strand had higher load values at bond failures and maximum load than galvanized steel strand (Table 18). There was a distinct difference in $D_{(204\ kN)}$ values between the epoxy-coated and the galvanized steel

strand with an embedment length of 1000 mm such that the epoxy-coated steel strand were only 55% of those of the galvanized steel strand.

Rebar had the highest breaking load, the highest maximum load simultaneously allowing the shortest displacement values. Rebar was found to be the best bolt type tested for situation where minimum rock mass displacement is allowed. Bulbed strand acted most closely to the rebar. The load-displacement curves from 0 to 250 kN were similar between the rebar and the bulbed strand with an embedment length of 1000 mm and from 0 to 220 kN with an embedment length of 500 mm.

Tests with unequally long embedment lengths (2000 mm and 500 mm) were also carried out. It is obvious that, the end of the test strand in the shorter embedment section (500 mm) offered the least resistance to pull-out and, consequently, pulled out of the grout as the load applied to the system was increased. The bond between the grout and strand was broken first at the junction of the steel pipes (joint opening point) and was then propagated along the length of the steel strand in both 500-mm and 2000-mm embedment sections. When the bond along the entire length of the strand embedded in the 500-mm section was broken, the grout began to slip along the surface of the strand. Results showed that untwisting mechanism played a very important role also in the test with unequal embedment lengths.

To summarize the results, the corrosion protection on the surface of the steel strand significantly increased the bond strength and decreased the displacement in proportion to the loads and thus increased the stiffness of the grouted steel strand under axial loading.

The effect of the debonding material was found to be based both on the thickness of the debonding layer and the ability to decrease the friction between the strand and grout. The thickness of the layer plays a dominant role because it smoothes the profile of the grout surrounding the debonding layer, and thus decreases the interlocking between the grout and strand. Thickening the layer, decreases the pull-out resistance leading to lower pull-out loads.

6 RECOMMENDATIONS FOR FURTHER STUDIES

The test system designed for the purpose of this research was found to be very practical and successful. However, a test system, where test bolts are grouted inside rock or concrete blocks (Stillborg 1984), would simulate even more closely the real situation in rock mass, when it comes to the properties of the host material. The roughness of the borehole as well as the radial stiffness of the confining material should be closer to that of borehole in a rock mass. However, using rock or concrete blocks would require the determination of the stiffness of the confining material to ensure that the testing conditions are as identical as possible between different tests.

If possible more identical tests are recommended to ensure more reliable statistical analysis. The ISRM (1981) suggests that at least five identical tests should be performed. The author's opinion is that statistical analysis would require many more identical tests than the suggested five. However, the resources and the schedule available for research usually keep the amount of the tests to a minimum, and thus the ISRM recommendation seems very reasonable.

All necessary further research should be performed for approval of the use of cable bolts as a permanent reinforcement structure in rock construction in Finland. As needed, more corrosion tests on steel strands should be performed.

The flexibility of the fully grouted steel strand can be decreased by increasing the roughness of the surface of the strand or using modified cable bolts, such as bulbed strand. This kind of stiff axial behavior is usually desired in the civil rock engineering, where very limited displacement of the rock mass can be allowed on the surfaces of the rock construction and on structures on the earth. The opposite kind of behavior is often desired in reinforcing the stopes or drifts in underground mines, where rock bolts should withstand large rock mass deformation. Increasing the flexibility can be achieved by discharging the bond between the grout and the strand using debonding. The ideal rock bolt would be provided by a bolt that whose stiffness and corrosion protection can be adjusted as desired.

An applicable solution for a multipurpose rock bolt could be provided by the mechanized cable bolter which could spread debonding or corrosion protection material on the surface of the strand, as well as create a deformed bulb wherever desired by clamping and crimping a plain steel strand. The operator could increase and decrease the stiffness of the fully grouted cable bolts using debonded sections or bulbs where necessary, and add corrosion-resistant material to the surface of the bolt if necessary.

REFERENCES

Bawden, W. F., Hyett, A. J. & Lausch, P. 1992. An experimental procedure for the in situ testing of cable bolts. International Journal for Rock Mechanics and Mining Sciences & Geomechanics Abstracts. Vol 29, no. 5, p. 525–533.

Benmokrane, B. & Chekired, M. 1992**.** Instrumentation of injected rock anchors with vibrating wire strain gages. In: Kaiser, P. K. & McCreath, D. R. (eds.) Rock support in mining and underground construction. Proceedings of the international symposium on rock support. Sudbury, Ontario, Canada 16 – 19 June 1992. Rotterdam, Brookfield, A. A. Balkema. P. 327–333.

Benmokrane, B., Chennouf, A. & Ballivy, G. 1992. Study of bond strength behavior of steel cables and bars with different cement grouts. In: Kaiser, P. K. & McCreath, D. R. (eds.) Rock support in mining and underground construction. Proceedings of the international symposium on rock support. Sudbury, Ontario, Canada 16 – 19 June 1992. Rotterdam, Brookfield, A. A. Balkema. P. 293–301.

Finnsementti. 2001. Cement information brochures from the manufacturer. (In Finnish)

Fuller, P. & Cox, R. 1975. Mechanics of load transfer from steel tendons to cement based grouts. Proceedings of 5th Australasian conference on the mechanics of structures and materials. Melbourne, Australia. P. 189–203.

Goris, J. 1991. Laboratory evaluation of cable supports. CIM Bulletin. Vol. 84, no. 948, p. 44–50.

Goris, J. 1990a. Laboratory evaluation of cable bolt supports (in two parts). 1. Evaluation of supports using conventional cables. Report of investigations RI 9308, U.S. Department of the Interior, Bureau of Mines, Washington. 23 p.

Goris J. 1990b. Laboratory evaluation of cable bolt supports (in two parts). 2. Evaluation of supports using conventional cables with steel buttons, birdcage cables

and epoxy coated cables. Report of investigations RI 9342, U.S. Department of the Interior, Bureau of Mines, Washington. 14 p.

Hakala, M. Double pipe test system. FLAC 3.3 simulations. (unpubl.).

Hassani, F., Mitri, H., Khan, U. & Rajaie, H. 1992. Experimental and numerical studies of the cable bolt support systems. In: Kaiser, P. K. & McCreath, D. R. (eds.) Rock support in mining and underground construction. Proceedings of the international symposium on rock support. Sudbury, Ontario, Canada 16 – 19 June 1992. Rotterdam, Brookfield, A. A. Balkema. P. 411–417.

Hutchinson, D. & Diederichs, M. 1996. Cable bolting in underground mines. Richmond, Canada, BiTech Publisher Ltd. 406 p.

Hyett, A. J., Bawden, W. F., Hedrick, N. & Blackall, J. 1995a. A laboratory evaluation of the 25 mm Garford bulb anchor for cable bolt reinforcement. CIM Bulletin. Vol. 88, no. 992, p. 54–59.

Hyett, A., Bawden, W., MacSporran, G. & Moosavi, M. 1995b. A constitutive law for bond failure of fully-grouted cable bolts using a modified Hoek cell. International Journal for Rock Mechanics and Mining Sciences & Geomechanics Abstracts. Vol 32, no. 1, p. 11–36.

Hyett, A. J., Bawden & W. F., Coulson, A, L. 1992a. Physical and mechanical properties of normal Portland cement pertaining to fully grouted cable bolts. In: Kaiser, P. K. & McCreath, D. R. (eds.) Rock support in mining and underground construction. Proceedings of the international symposium on rock support. Sudbury, Ontario, Canada 16 – 19 June 1992. Rotterdam, Brookfield, A. A. Balkema. P. 341–349.

Hyett, A. J., Bawden, W. F. & Reichert, R. D. 1992b. The effect of rock mass confinement on the bond strength of fully grouted cable bolts. International Journal for Rock Mechanics and Mining Sciences & Geomechanics Abstracts. Vol 29, no. 5, p. 503–524.

ISRM. 1981. Rock characterization, testing and monitoring. In Brown, E. (ed.) ISRM Suggested methods. International Society for Rock Mechanics. Oxford, Pergamon Press. 211 p.

Ito, F., Nakahara, F., Kawano, R., Kang, S. & Obara, Y. 2001. Visualization of failure in a pull-out test of cable bolts using X-ray CT. Construction and building materials 15. Elsevier Science Ltd. P. 263–270.

Kaiser, P., Yazici, S. & Nosé, J. 1992. Effect of stress change on the bond strength of fully grouted cables. International Journal for Rock Mechanics and Mining Sciences & Geomechanics Abstracts. Vol 29, no. 3, p. 293–306.

Maloney, S., Fearon, R., Nosé, J. & Kaiser, P. 1992. Investigations into the effect of stress change on support capacity. In: Kaiser, P. K. & McCreath, D. R. (eds.) Rock support in mining and underground construction. Proceedings of the international symposium on rock support. Sudbury, Ontario, Canada 16 – 19 June 1992. Rotterdam, Brookfield, A. A. Balkema. P. 367–376.

Moosavi, M. 2002. A laboratory test program to investigate bond capacity of rock bolts under different boundary conditions. In: Hammah, R., Bawden, W., Curran, J. & Telesnicki, M. (eds.) Mining and tunneling innovation and opportunity. Proceedings of NARMS-TAC 2002. Toronto, Canada, 7 – 10 July 2002. Toronto, University of Toronto Press. P. 447–455.

Moosavi, M. 1997. Load distribution along fully grouted cable bolts based on constitutive models obtained from modified Hoek cells. Doctoral thesis. Queen's University, Kingston, Ontario, Canada. Doctoral thesis. 247 p.

Moosavi, M., Bawden, W. & Hyett, A. 1996. A comprehensive laboratory test program to study the behavior of modified geometry cable bolt support. In: Nelson & Laubach, (eds.) Rock Mechanics: Models and measurements challenges from industry. Rotterdam, A. A. Balkema. P. 209–216.

Satola, I. & Aromaa, J. 2004. The corrosion of rock bolts and cable bolts. In Villaescusa, E. & Potvin, Y. (eds) Ground support in mining and underground construction. Proceedings of the fifth international symposium on ground support. Perth, Western Australia, 28–30 September 2004. Leiden, London, New York, Philadelphia, Singapore, A. A. Balkema. P. 521–528.

Satola, I. & Aromaa, J. 2003. The corrosion of the rock bolts and the effect of the corrosion protection on the axial behaviour of cable bolts. Proceedings of the 10th International congress on rock mechanics, 8 – 12 September, Sandton City, South Africa. Johannesburg, the South African Instute of Mining and Metallurgy. P. 1039–1042.

Satola I, & Hakala, M. 2001a. Corrosion-protected cable bolts in long-term reinforcement. Research Report, TKK-KAL-A-28. Espoo, Finland, Helsinki University of Technology. 42 p. ISBN 951-22-5444-1.

Satola, I & Hakala, M. 2001b. Corrosion-protected cable bolts in long-term reinforcement. In Särkkä, P. & Eloranta, P. (eds) Rock mechanics a challenge for society. Proceedings of EUROCK 2001 Symposium on Rock Mechanics. Espoo, Finland 3 – 7 June 2001. Lisse, Abingdon, Exton, Tokyo, A. A. Balkema. P. 377–382.

Satola, I. 2001. Testing of corrosion-protected cable bolts by double pipe axial tests. In Elsworth, D., Tinucci, J. & Heasley, K (eds) Rock Mechanics in the National Interest. Proceedings of DC Rocks 2001, 38th U.S. Symposium on Rock Mechanics. Washington D.C., USA 7 – 10.7.2001. Lisse, Abingdon, Exton (pa), Tokyo, A. A. Balkema Publishers. P. 1021–1027.

Satola, I. 1999a. Yielding cable bolt for mechanized cable bolting. Licentiate thesis. Espoo, Finland, Helsinki University of Technology. 73 p.

Satola, I. 1999b. Testing of the yielding cable bolt achieved by debonding. In: G. Vouille & P. Berest (eds) Proceedings of the 9th International congress on rock mechanics. Paris, France, 25 – 28 August 1999. Rotterdam, Brookfield, A. A. Balkema. P. 1467–1470.

SFS 1265. Strand for prestressed structures. Low relaxation. The Finnish Standards Association SFS. 6 p. (In Finnish)

SFS 3173. 1975. Tensile testing of metals. The Finnish Standards Association SFS. 12 p. (In Finnish)

SFS 4474. 1978. Concrete. Compressive strength. The Finnish Standards Association SFS. 4 p. (In Finnish)

SFS 5283. 1987. Fresh concrete. Sampling. The Finnish Standards Association SFS. 2 p. (In Finnish)

SFS 5341. 1988. Concrete. Test specimens. Making and curing. The Finnish Standards Association SFS. 2 p. (In Finnish)

SFS 5441. 1988. Concrete. Core of hardened concrete. Taking, curing and making. The Finnish Standards Association SFS. (In Finnish)

SFS 5442. 1988. Concrete. Density. The Finnish Standards Association SFS. 2 p. (In Finnish)

State Technical Research Centre. 2002. Research report, no. val24-023361, 13.02.2002. Espoo Finland. 1 p.

Stheeman W. H. 1982. A practical solution to cable bolting problems at the Tsumeb Mine. CIM Bulletin. Vol. 75, no. 838, p. 65–77.

Stillborg, B. 1990. Rockbolt and cable bolt tensile testing in a joint. Research report. Luleå, Sweden, Mining and geotechnical consultants, James Askew Associates. 19 p.

Stillborg, B. 1984. Experimental investigation of steel cables for rock reinforcement in hard rock. Doctoral thesis. Luleå University of Technology, Division of Rock Mechanics. Luleå, 1984. 127 p.

Stjern, G. 1995. Practical performance of rock bolts. Doctoral Thesis. Trondheim, Norway, The Norwegian Institute of Technology, Department of Geology and Mineral Resources Engineering. 170 p.

Villaescusa, E. & Wright, J. 1999. Reinforcement of underground excavations using CT Bolt. In: E. Villaescusa, C. Windsor & A. Thompson (eds) Rock support and reinforcement practice in mining. Proceedings of the international symposium on ground support. Kalgoorlie, Western Australia 15-17 March 1999. Rotterdam, Brookfield, A. A. Balkema. P. 109–115.

Villaescusa, E., Sandy, M. & Bywater, S. 1992. Ground support investigations and practices at Mount Isa. In: P. Kaiser & D. McCreath (eds) Rock support in mining and underground construction. Proceedings of the international symposium on rock support. Sudbury, Ontario, Canada 16-19 June 1992. Rotterdam, Brookfield, A. A. Balkema. P. 185–193.

Windsor, C. 2004. A review of long, high capacity reinforcing systems in rock engineering. In Villaescusa, E. & Potvin, Y. (eds) Ground support in mining and underground construction. Proceedings of the fifth international symposium on ground support. Perth, Western Australia 28 – 30 September 2004. Leiden, London, New York, Philadelphia, Singapore, A. A. Balkema. P. 17–41.

Windsor, R. 1992. Cable bolting for underground and surface excavations. In: Kaiser, P. K. & McCreath, D. R. (eds.) Rock support in mining and underground construction. Proceedings of the international symposium on rock support. Sudbury, Ontario, Canada 16-19 June 1992. Rotterdam, Brookfield, A. A. Balkema. P. 349–367.

Windsor, C. & Thompson, A. 1993. Rock reinforcement - technology, testing, design and evaluation. In: Hudson, J (ed.) Comprehensive rock engineering: Principles, practice & projects, Volume 4: Excavation, support and monitoring. Oxford, U.K., Pergamon Press. P. 451–484.

APPENDICES

Appendix A: Test results from double pipe axial tests. Load-displacement diagrams.

Appendix B: Calibration curve of the hydraulic jack.

Appendix C: Test results from double pipe axial tests. Time-displacement diagrams.

Appendix D: Double pipe test system. FLAC 3.3 simulations.

APPENDIX A

AXIAL DOUBLE PIPE TEST RESULTS

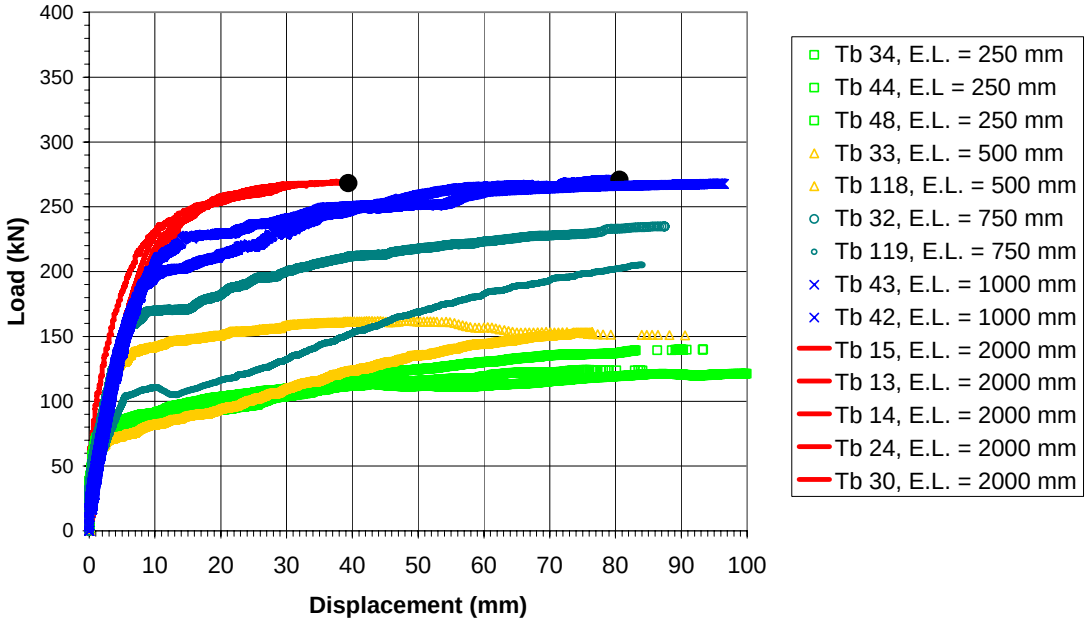

Figure A.1. The axial double pipe test results of hot-dip galvanized steel strand with embedment lengths of 250 mm, 500 mm, 750 mm, 1000 mm and 2000 mm. Symbol ● denotes that test bolt ruptured.

APPENDIX A

AXIAL DOUBLE PIPE TEST RESULTS

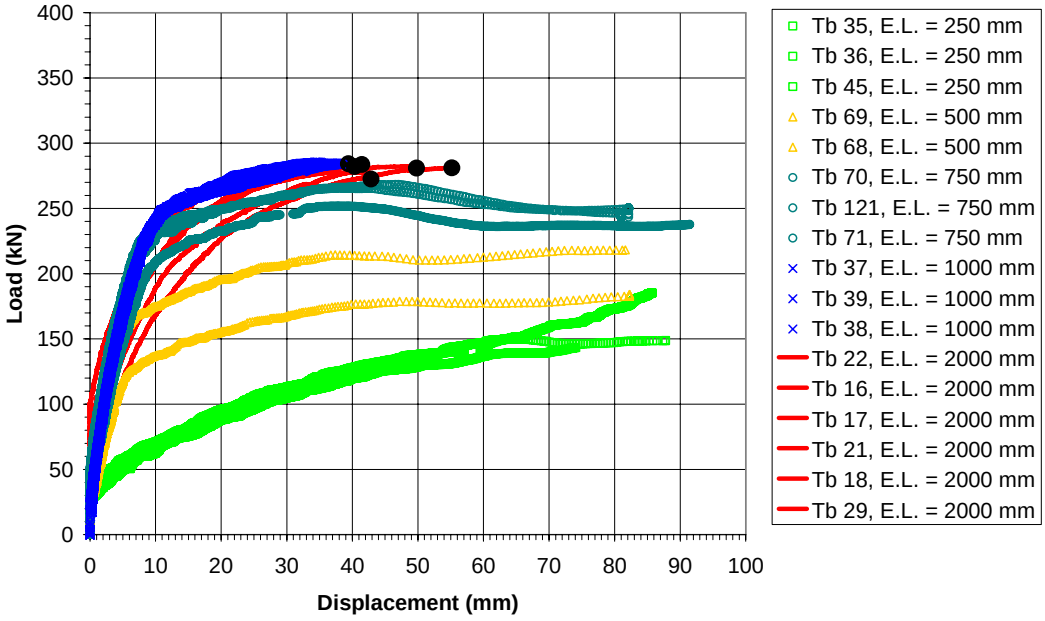

Figure A.2. The axial double pipe test results of epoxy-coated steel strand with embedment lengths of 250 mm, 500 mm, 750 mm, 1000 mm and 2000 mm. Symbol ● denotes that test bolt ruptured.

APPENDIX A

AXIAL DOUBLE PIPE TEST RESULTS

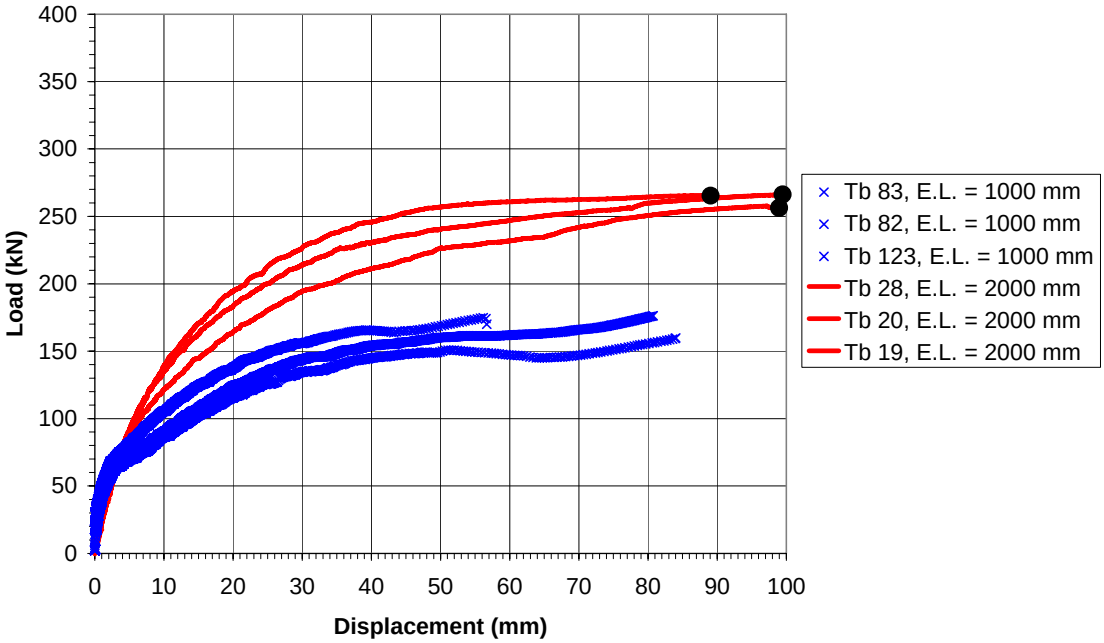

Figure A.3. The axial double pipe test results of steel strand with embedment lengths of 1000 mm and 2000 mm. Symbol ● denotes that test bolt ruptured.

APPENDIX A

AXIAL DOUBLE PIPE TEST RESULTS

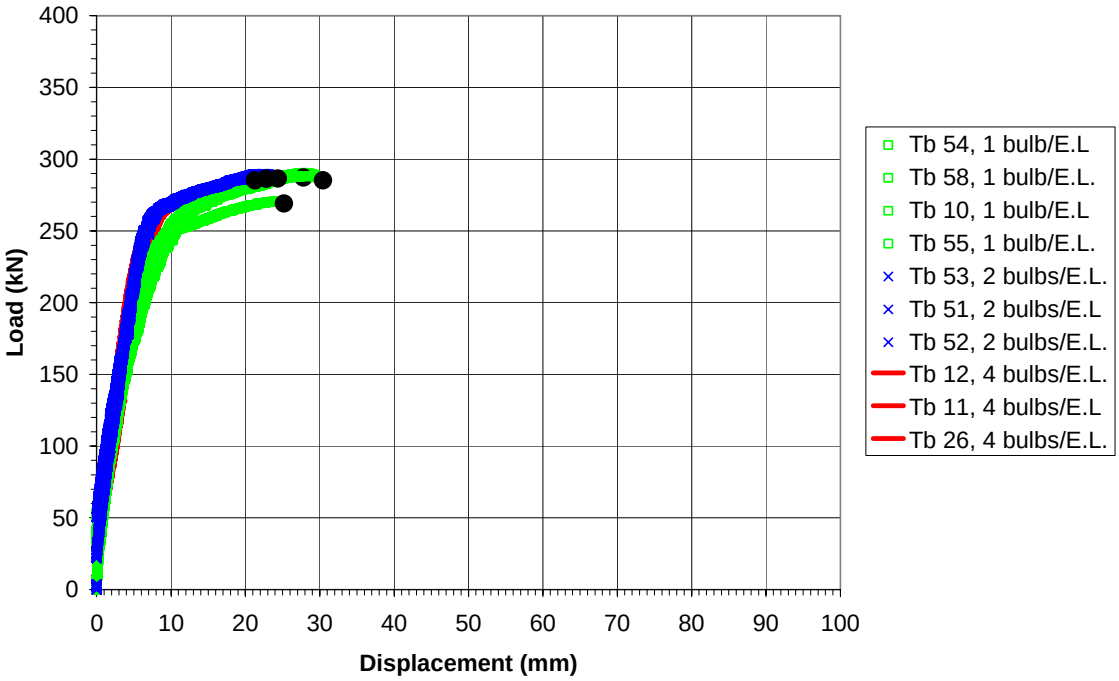

Figure A.4. The axial double pipe test results of bulbed strand with embedment lengths of 250 mm, 1000 mm and 2000 mm. Symbol ● denotes that test bolt ruptured. All the test bolts broke off.

APPENDIX A

AXIAL DOUBLE PIPE TEST RESULTS

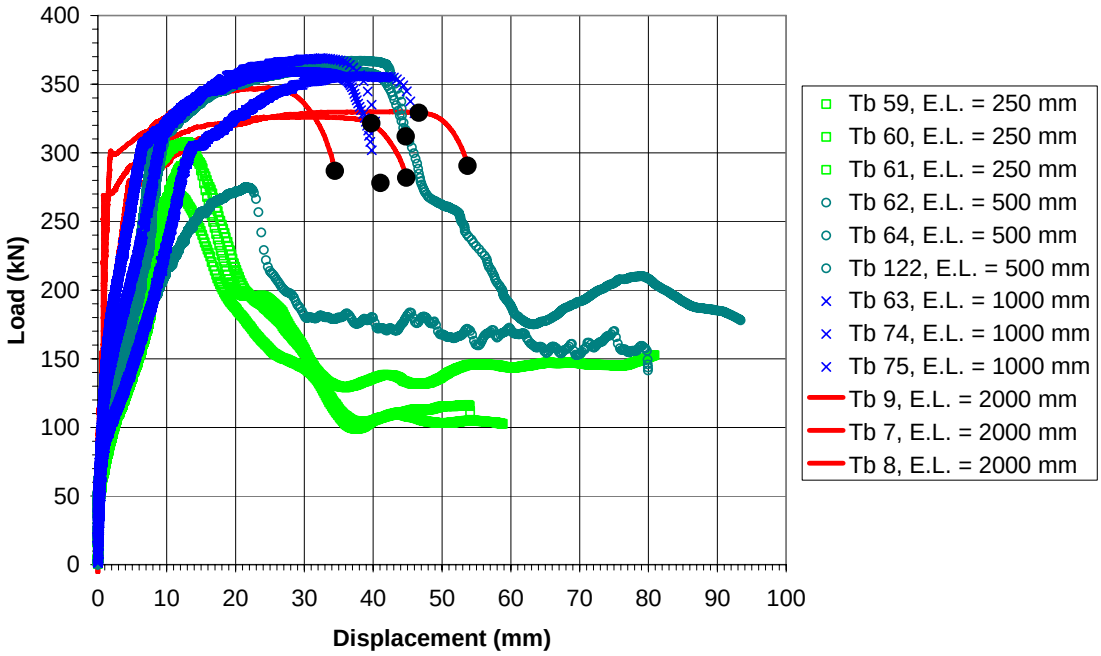

Figure A.5. The axial double pipe test results of rebar with embedment lengths of 250 mm, 500 mm and 1000 mm and galvanized rebar of 2000 mm. Symbol ● denotes that test bolt ruptured.

APPENDIX B

CALIBRATION OF THE HYDRAULIC JACK

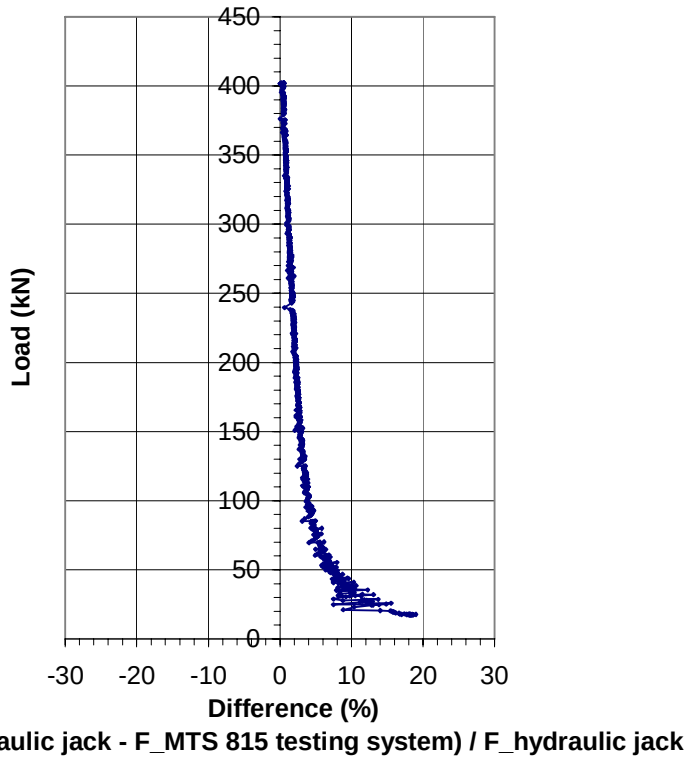

Figure B.1. *The calibration curve of the hydraulic jack (double pipe) by the MTS 815 testing system.*

APPENDIX C

AXIAL DOUBLE PIPE TEST RESULTS. TIME-DISPLACEMENT DIAGRAMS

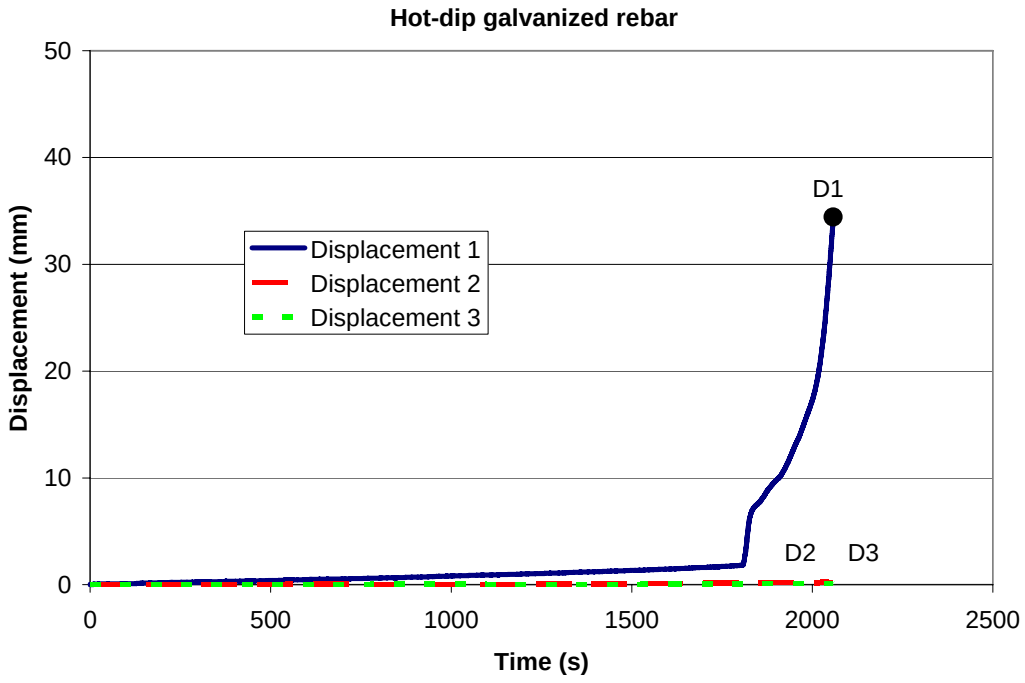

Figure C. 1. Time-displacement diagram of hot-dip galvanized rebar with embedment length of 2000 mm (test bolt no. 7). Symbol ● denotes that bolt ruptured.

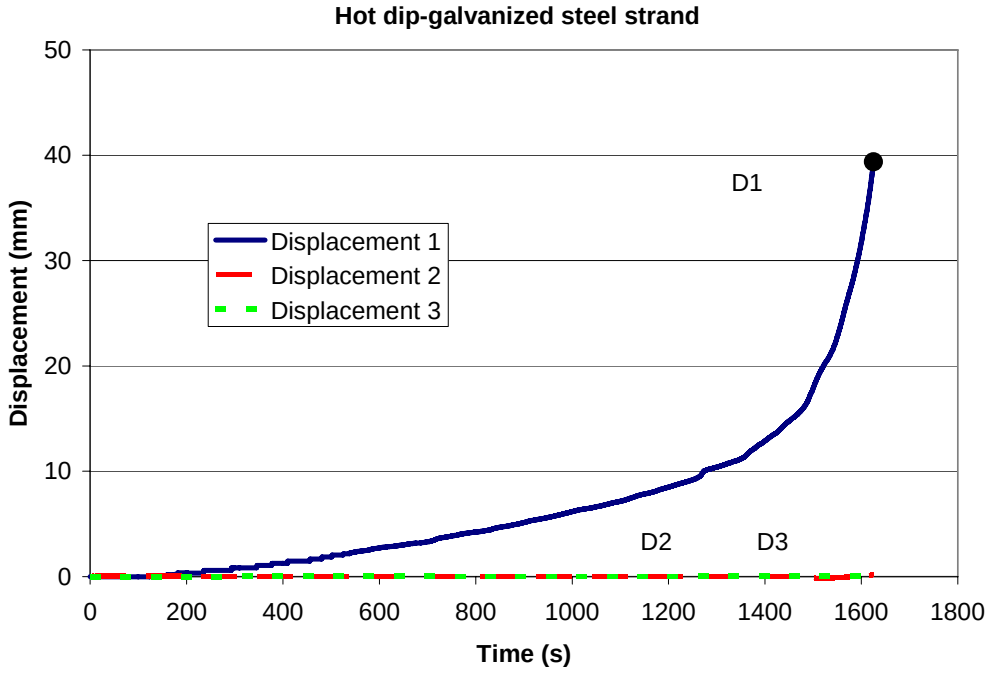

Figure C. 2. Time-displacement diagram of hot-dip galvanized steel strands with embedment length of 2000 mm (test bolt no. 24). Symbol ● denotes that bolt ruptured.

APPENDIX C

AXIAL DOUBLE PIPE TEST RESULTS. TIME-DISPLACEMENT DIAGRAMS

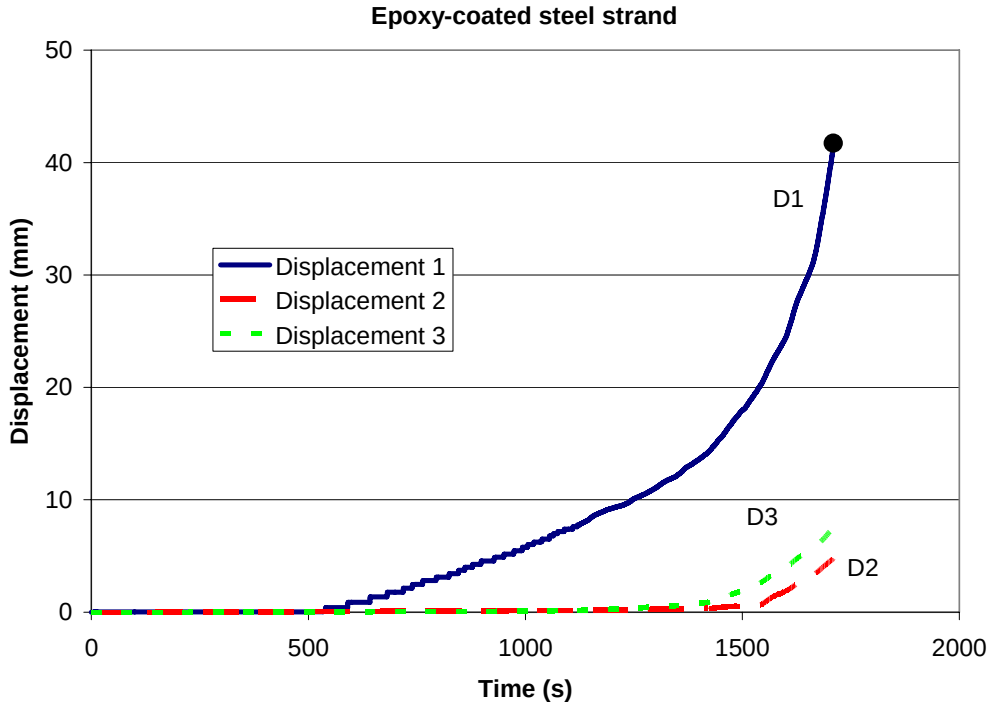

Figure C. 3. Time-displacement diagram of epoxy-coated steel strand with embedment length of 2000 mm (test bolt no. 22). Symbol ● denotes that bolt ruptured.

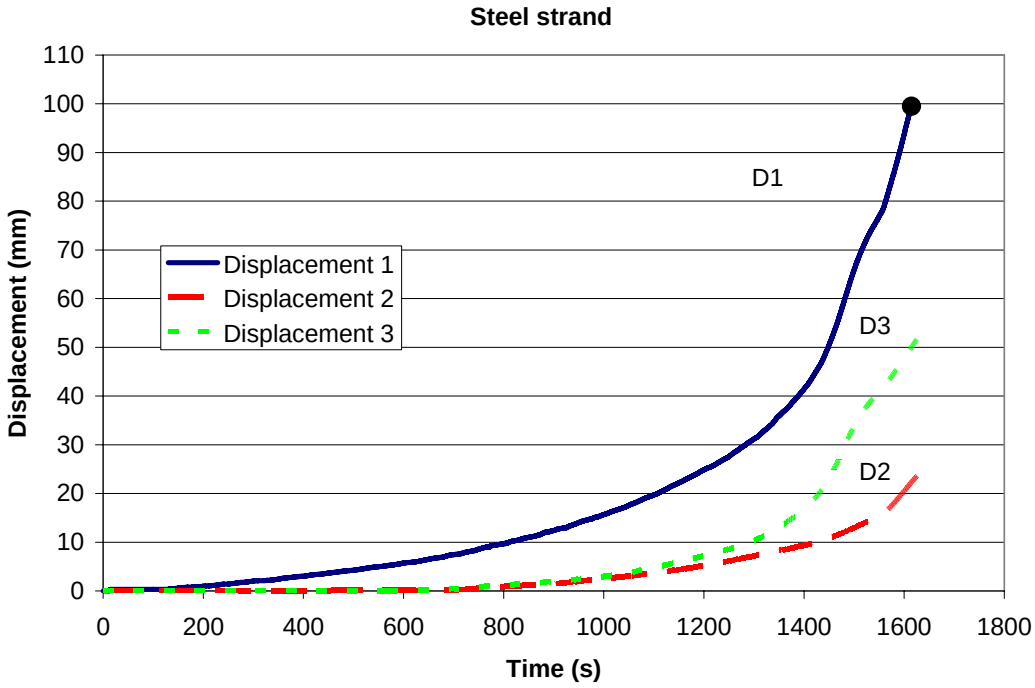

Figure C. 4. Time-displacement diagram of standard steel strand with embedment length of 2000 mm (test bolt no. 28). Symbol ● denotes that bolt ruptured.

APPENDIX C

AXIAL DOUBLE PIPE TEST RESULTS. TIME-DISPLACEMENT DIAGRAMS

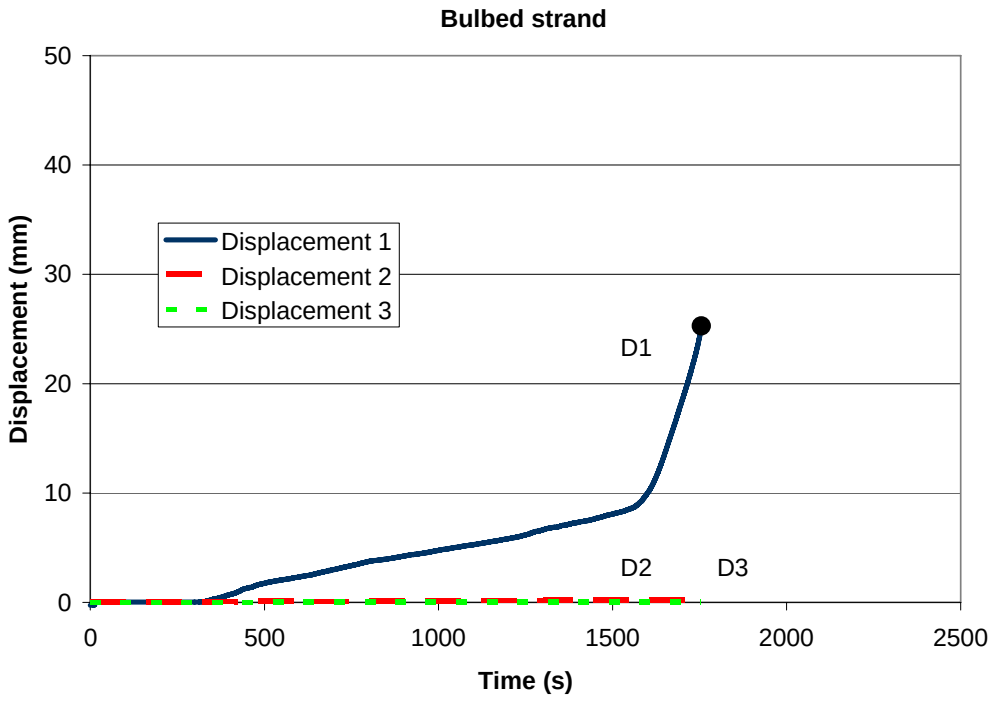

Figure C. 5. Time-displacement diagram of bulbed strand with embedment length of 2000 mm (test bolt no. 11). Symbol ● denotes that bolt ruptured.

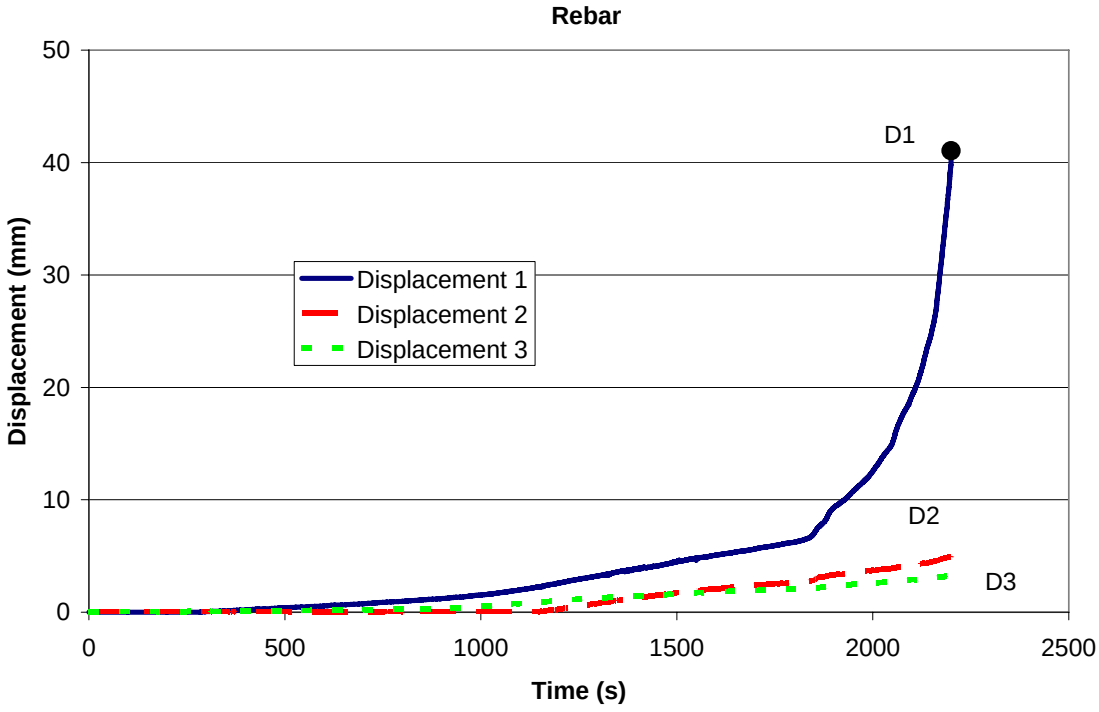

Figure C. 6. Time-displacement diagram of rebar with embedment length of 1000 mm (test bolt no. 63). Symbol ● denotes that bolt ruptured.

APPENDIX C

AXIAL DOUBLE PIPE TEST RESULTS. TIME-DISPLACEMENT DIAGRAMS

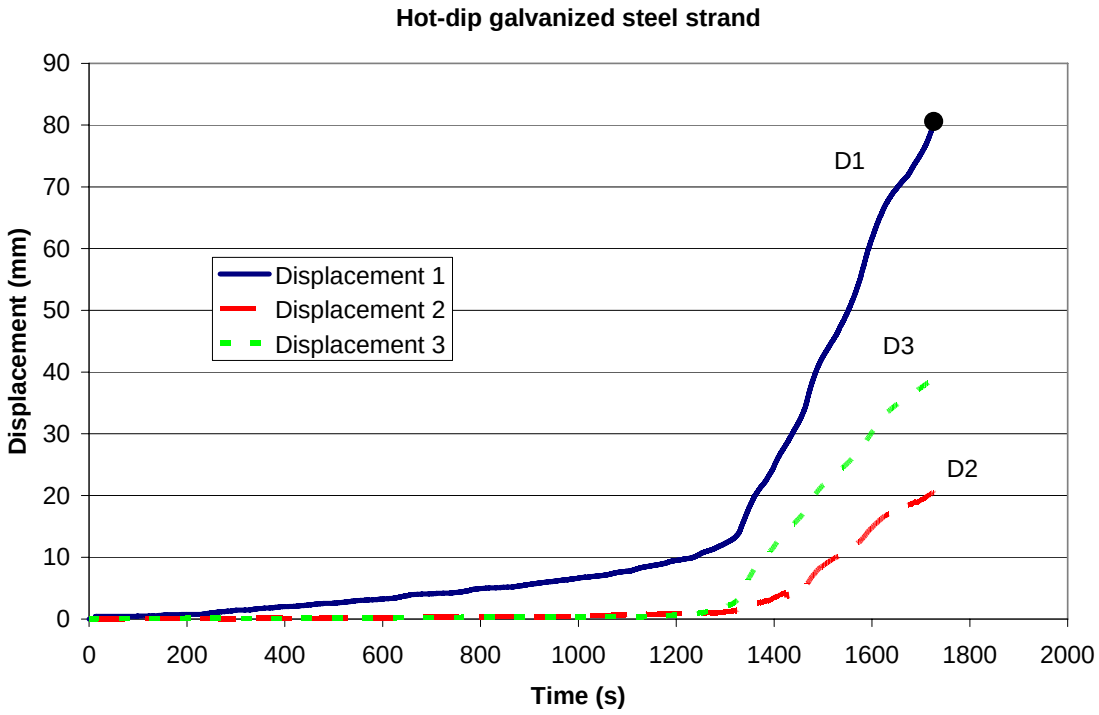

Figure C. 7. Time-displacement diagram of hot-dip galvanized steel strand with embedment length of 1000 mm (test bolt no. 43). Symbol ● denotes that bolt ruptured.

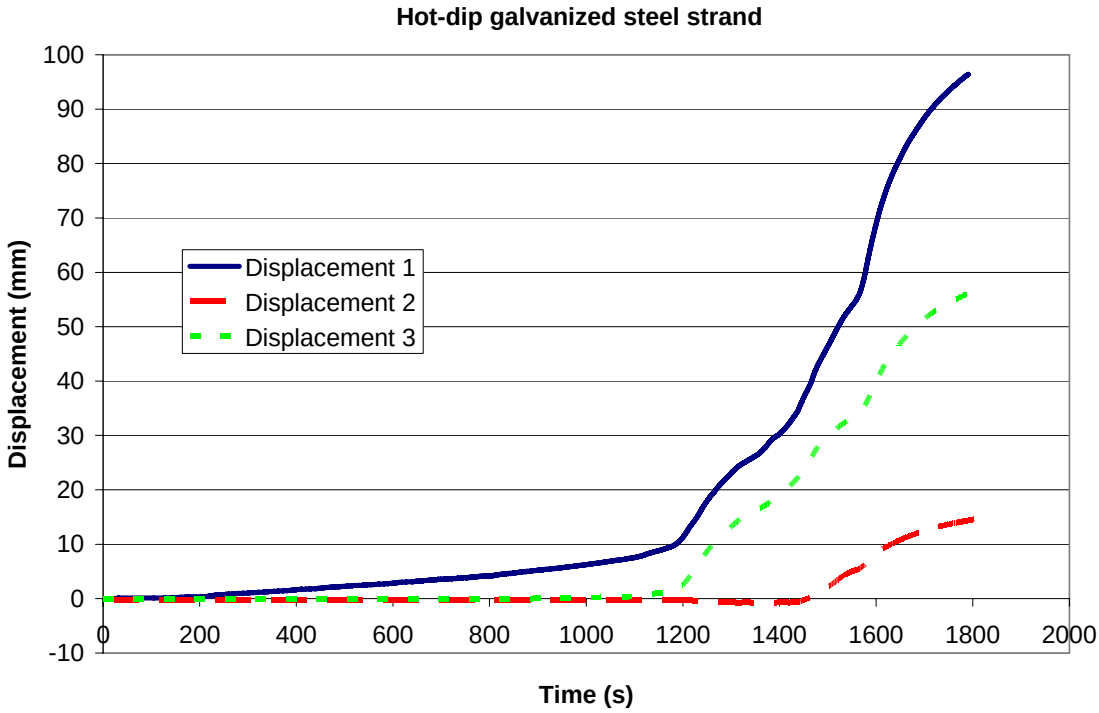

Figure C. 8. Time-displacement diagram of hot-dip galvanized steel strand with embedment length of 1000 mm (test bolt no. 42). Instead of rupture, test bolt slipped (see also Figure C.7).

APPENDIX C

AXIAL DOUBLE PIPE TEST RESULTS. TIME-DISPLACEMENT DIAGRAMS

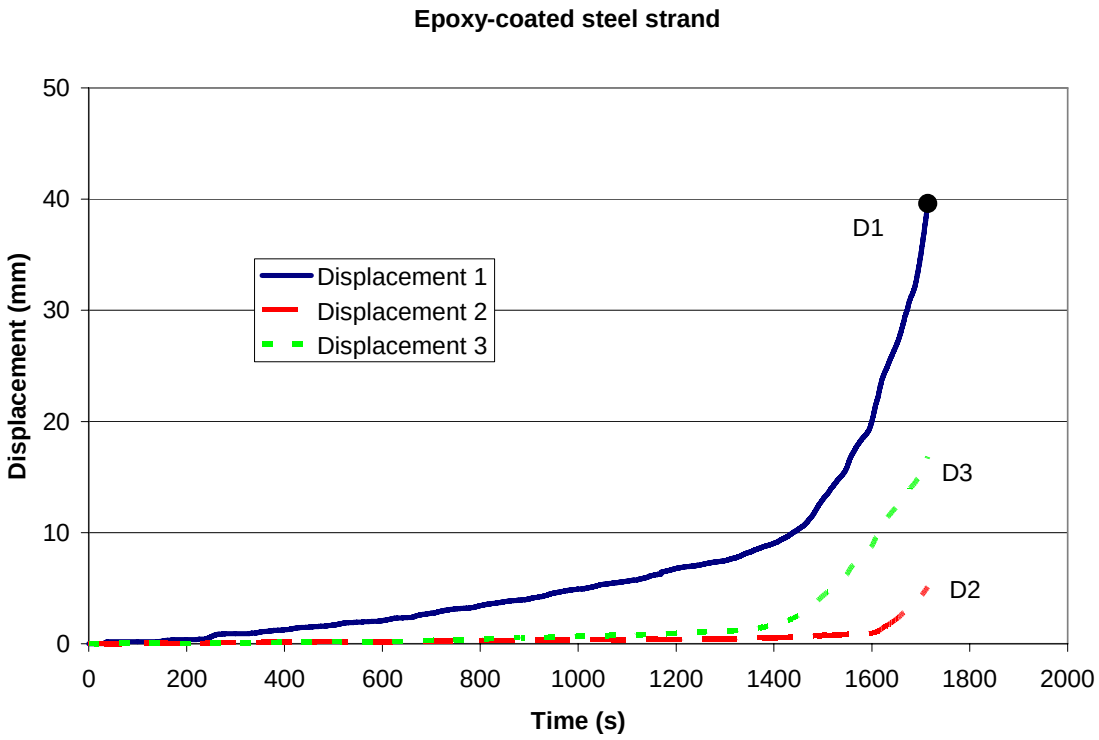

Figure C. 9. Time-displacement diagram of epoxy-coated steel strand with embedment length of 1000 mm (test bolt no. 38). Symbol ● denotes that bolt ruptured.

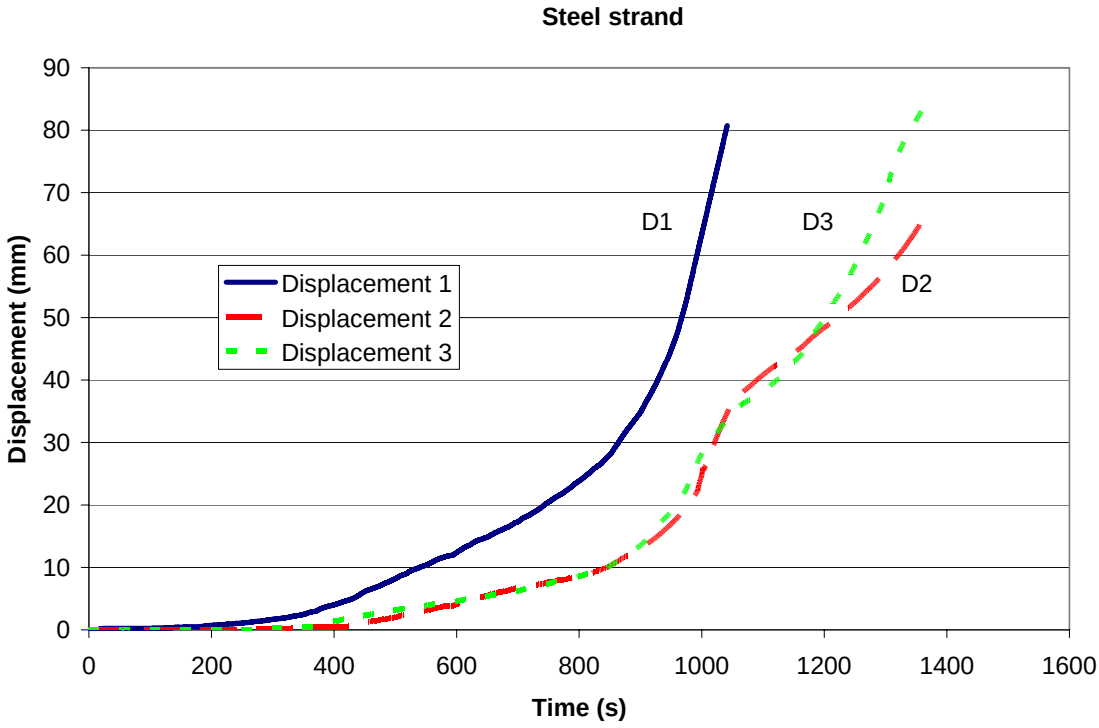

Figure C. 10. Time-displacement diagram of standard steel strand with embedment length of 1000 mm (test bolt no. 123).

APPENDIX C

AXIAL DOUBLE PIPE TEST RESULTS. TIME-DISPLACEMENT DIAGRAMS

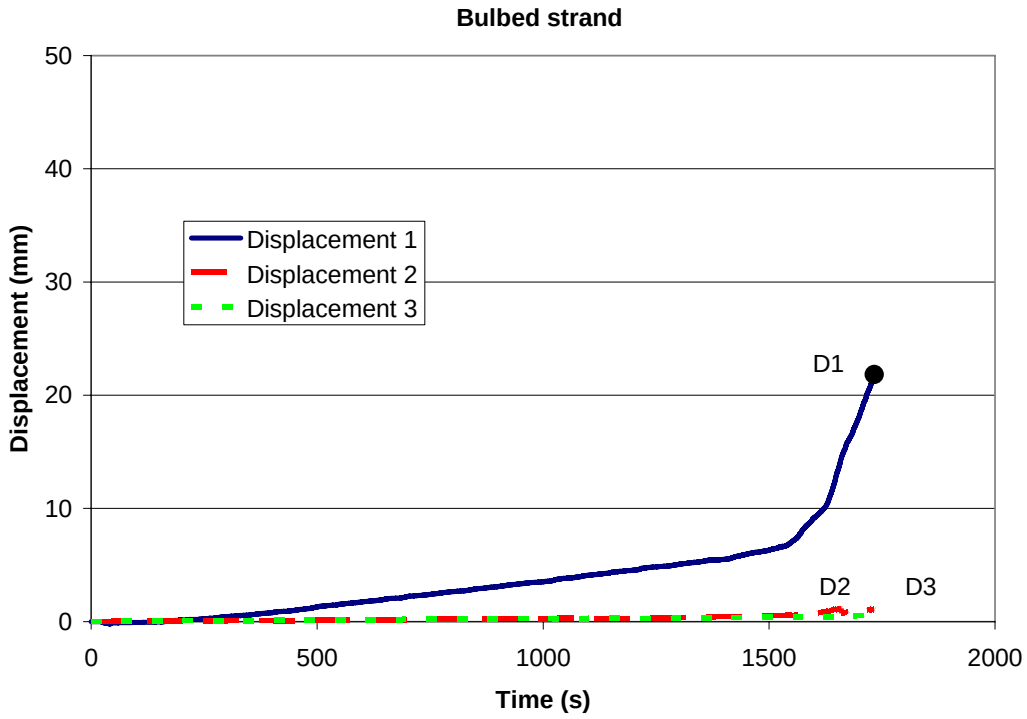

Figure C. 11. Time-displacement diagram of bulbed strand with embedment length of 1000 mm (test bolt no. 51). Symbol ● denotes that bolt ruptured.

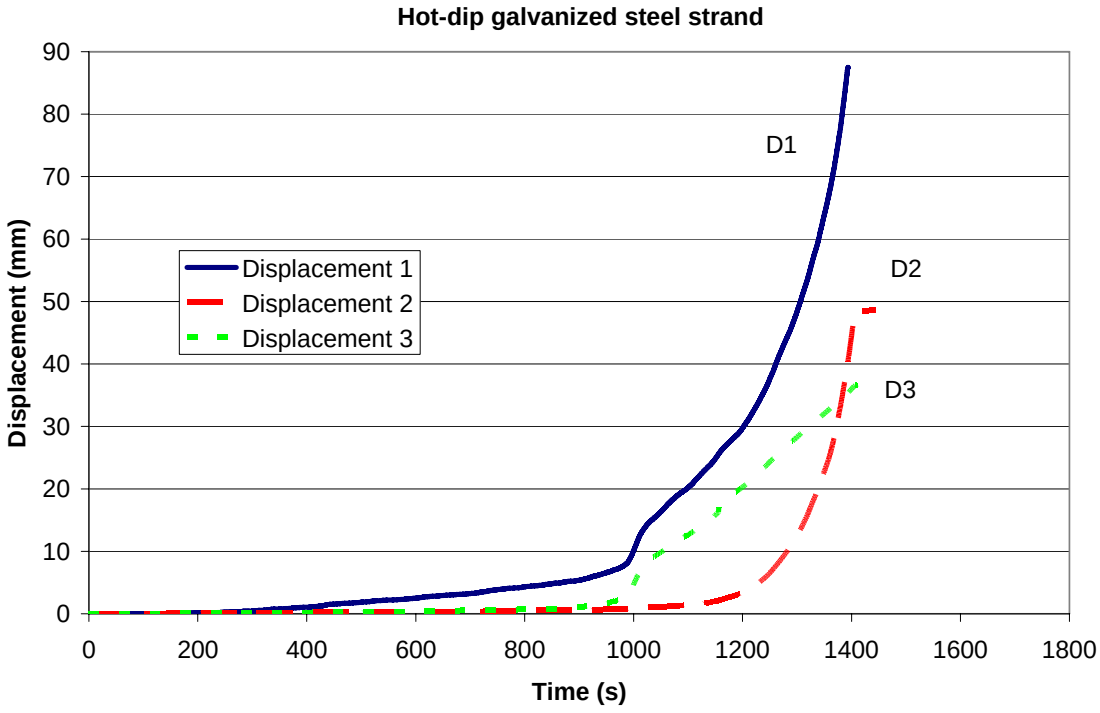

Figure C. 12. Time-displacement diagram of hot-dip galvanized steel strand with embedment length of 750 mm (test bolt no. 32).

APPENDIX C

AXIAL DOUBLE PIPE TEST RESULTS. TIME-DISPLACEMENT DIAGRAMS

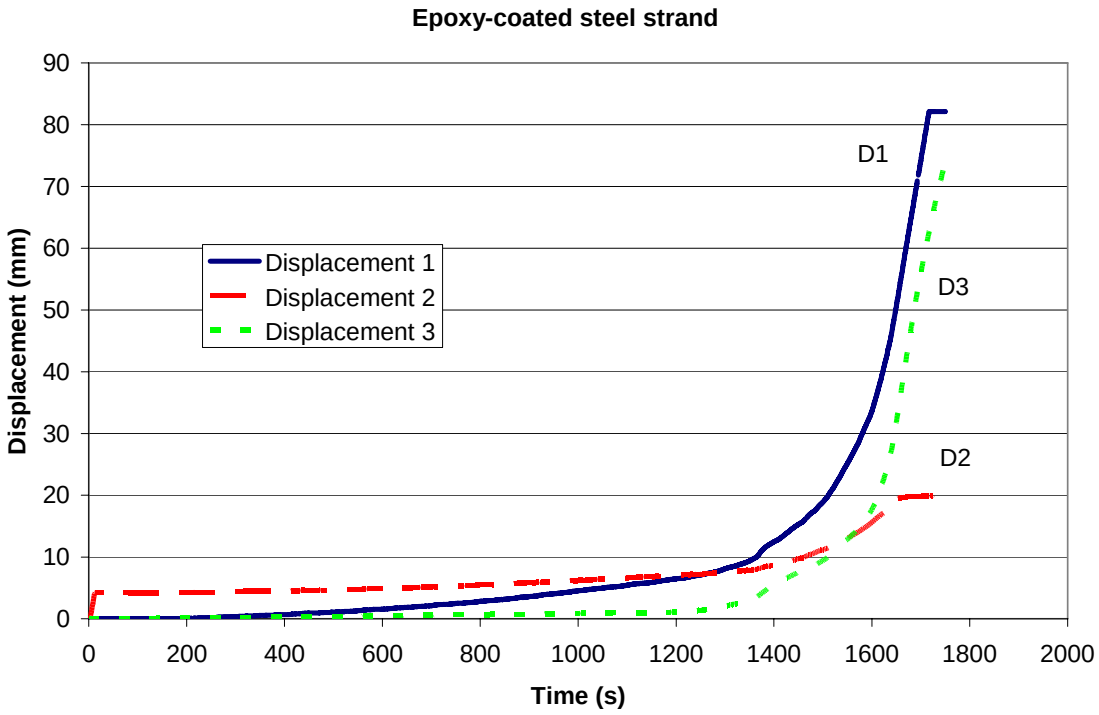

Figure C. 13. Time-displacement diagram of epoxy-coated steel strand with embedment length of 750 mm (test bolt no. 71).

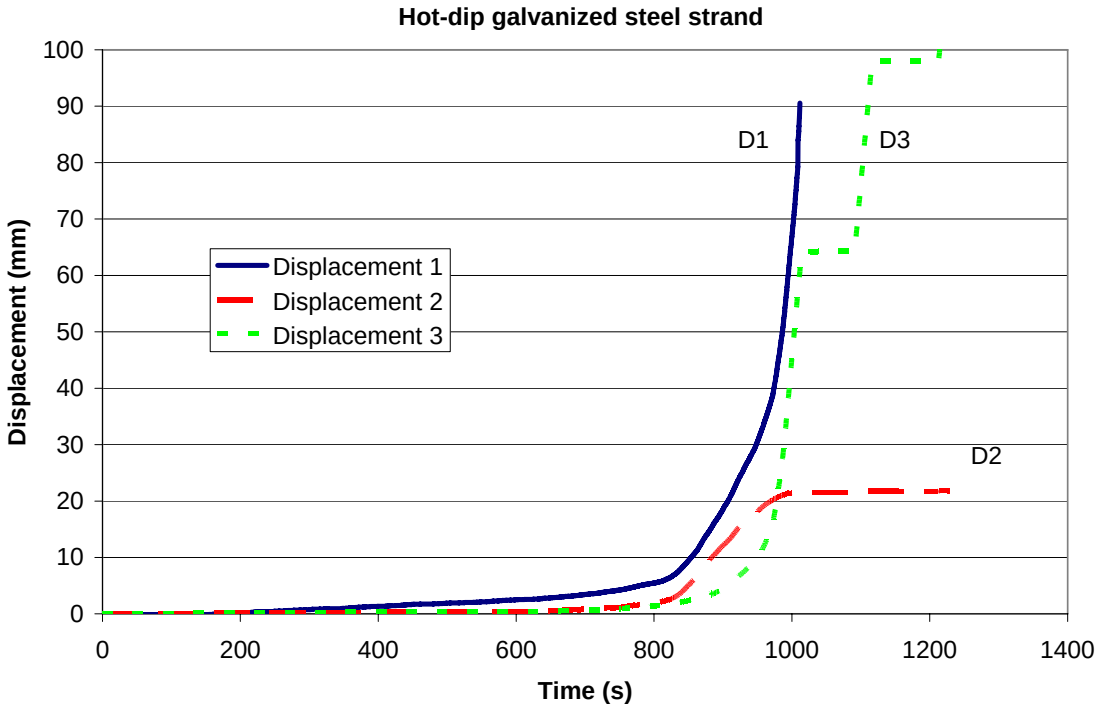

Figure C. 14. Time-displacement diagram hot-dip galvanized steel strand with embedment length of 500 mm (test bolt no. 33).

APPENDIX C

AXIAL DOUBLE PIPE TEST RESULTS. TIME-DISPLACEMENT DIAGRAMS

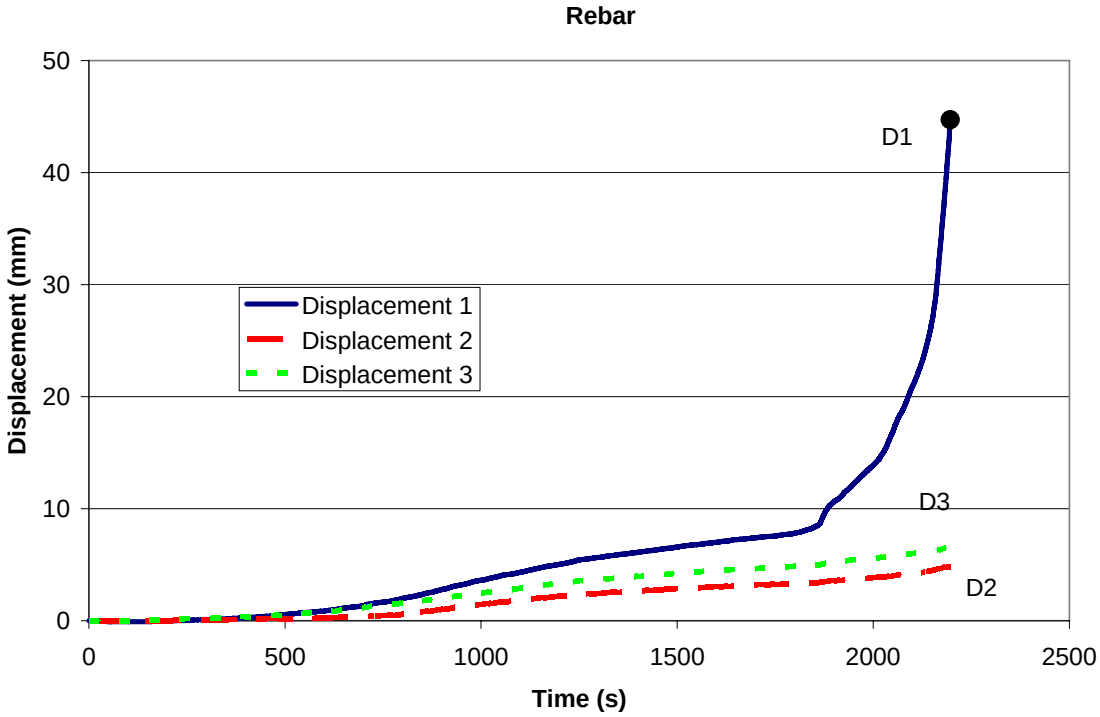

Figure C. 15. Time-displacement diagram of rebar with embedment length of 500 mm (test bolt no. 64). Symbol ● denotes that bolt ruptured.

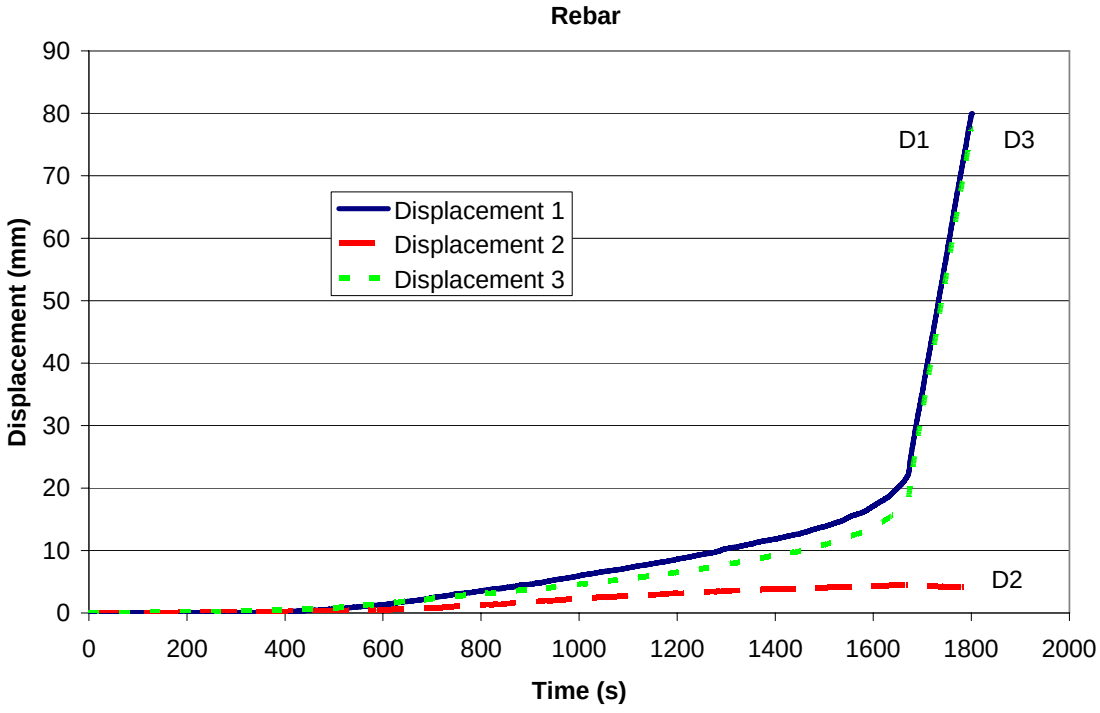

Figure C. 16. Time-displacement diagram of rebar with embedment length of 500 mm (test bolt no. 122). Instead of rupture test bolt slipped (see also Figure C.15).

APPENDIX C

AXIAL DOUBLE PIPE TEST RESULTS. TIME-DISPLACEMENT DIAGRAMS

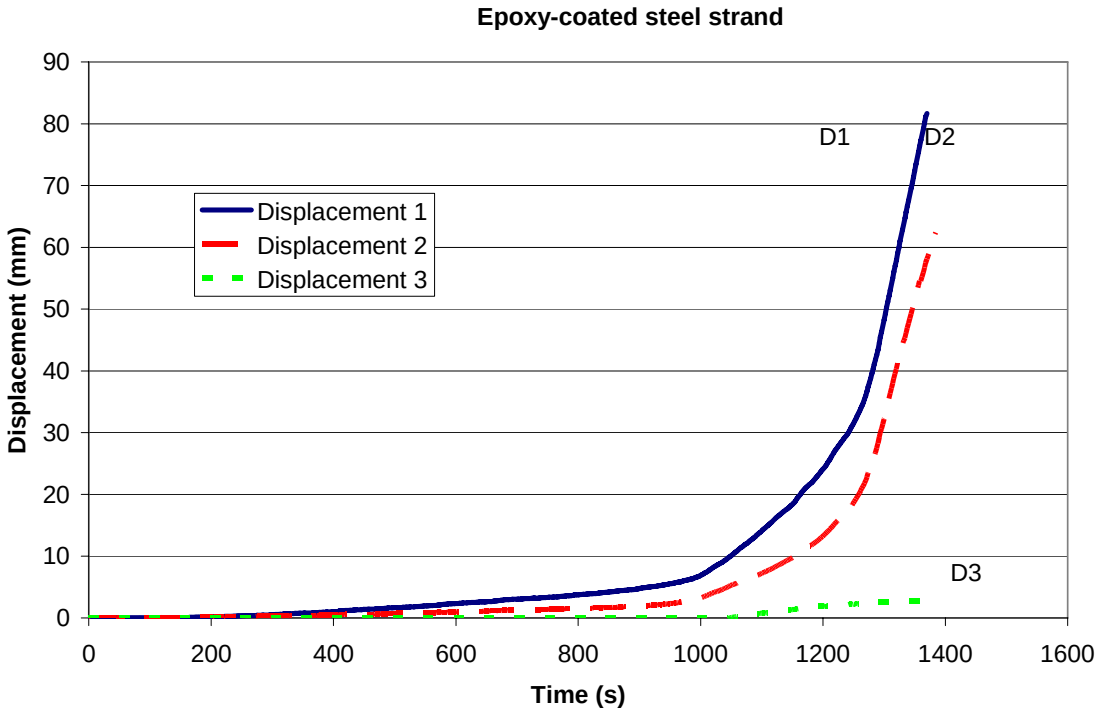

Figure C. 17. Time-displacement diagram of epoxy-coated steel strand with embedment length of 500 mm (test bolt no. 68).

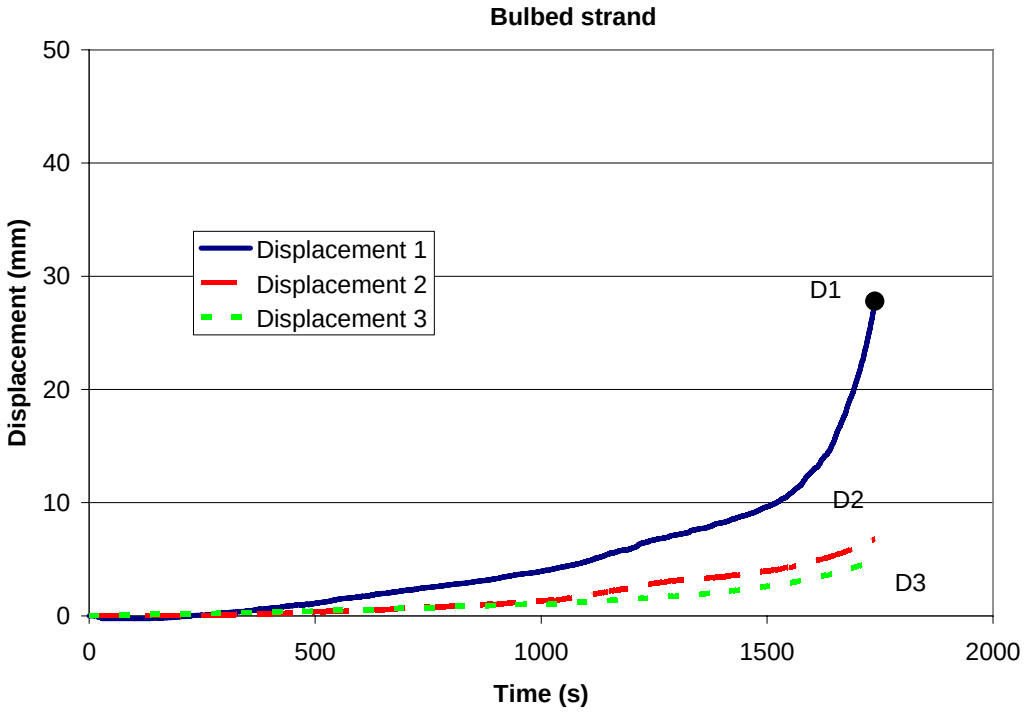

Figure C. 18. Time-displacement diagram of bulbed strand with embedment length of 500 mm (test bolt no. 58). Symbol ● denotes that bolt ruptured.

APPENDIX C

AXIAL DOUBLE PIPE TEST RESULTS. TIME-DISPLACEMENT DIAGRAMS

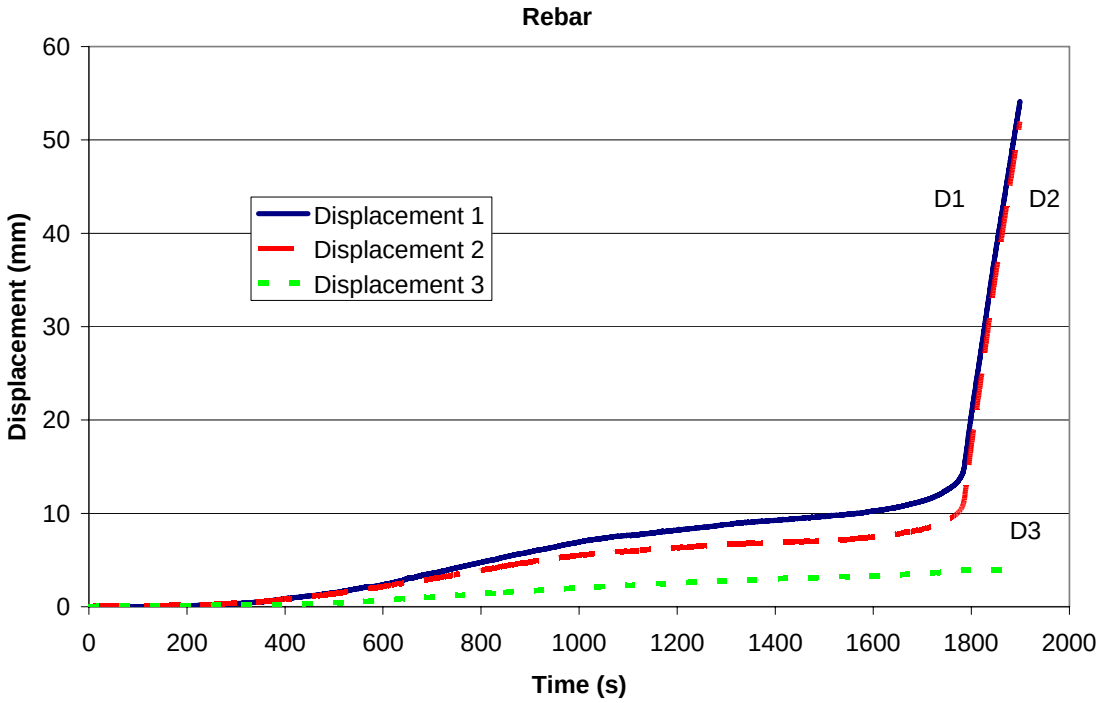

Figure C. 19. Time-displacement diagram of rebar with embedment length of 250 mm (test bolt no. 59).

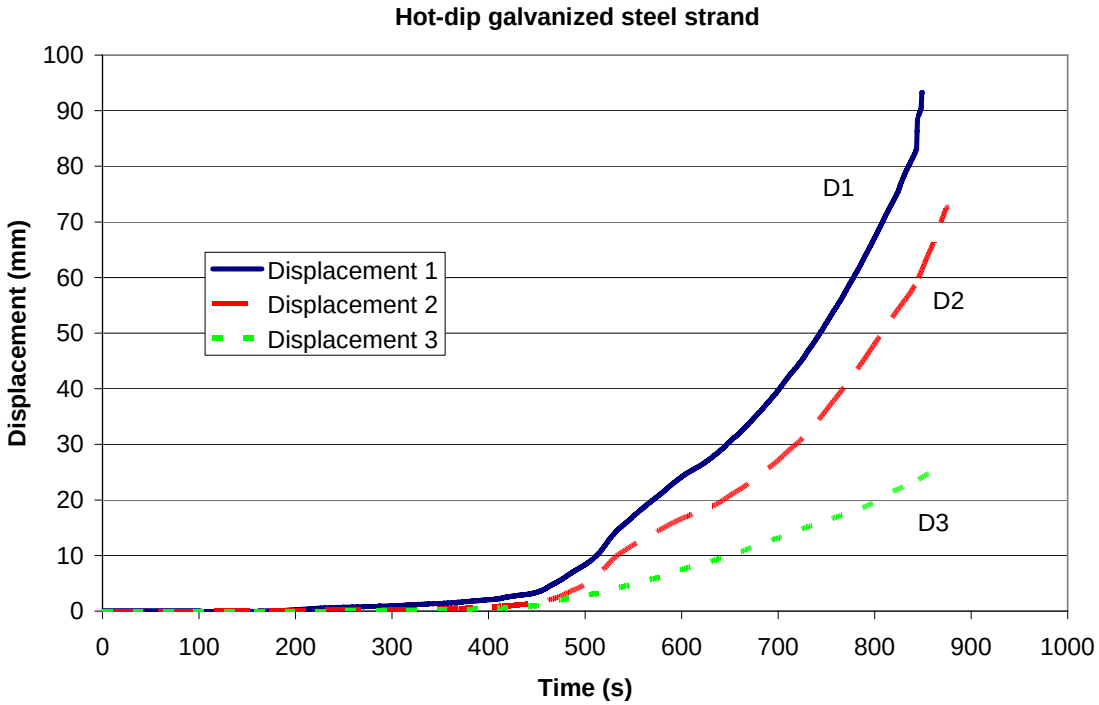

Figure C. 20. Time-displacement diagram of hot-dip galvanized steel strand with embedment length of 250 mm (test bolt no. 44).

APPENDIX C

AXIAL DOUBLE PIPE TEST RESULTS. TIME-DISPLACEMENT DIAGRAMS

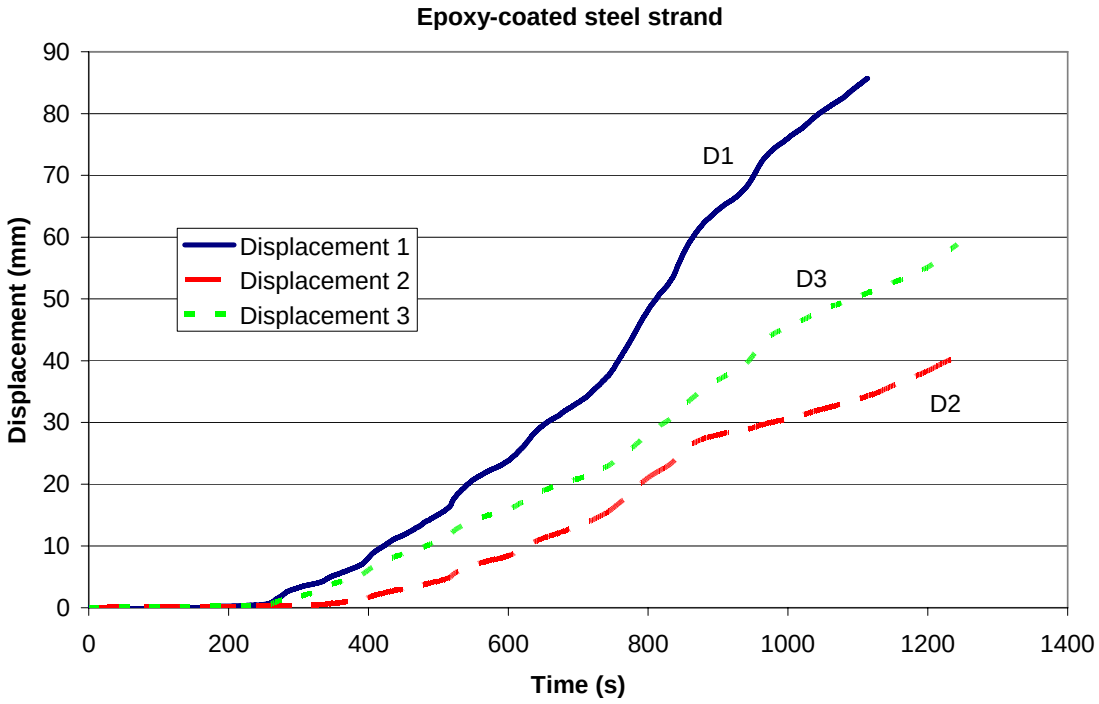

Figure C. 21. Time-displacement diagram of epoxy-coated steel strand with embedment length of 250 mm (test bolt no. 35).

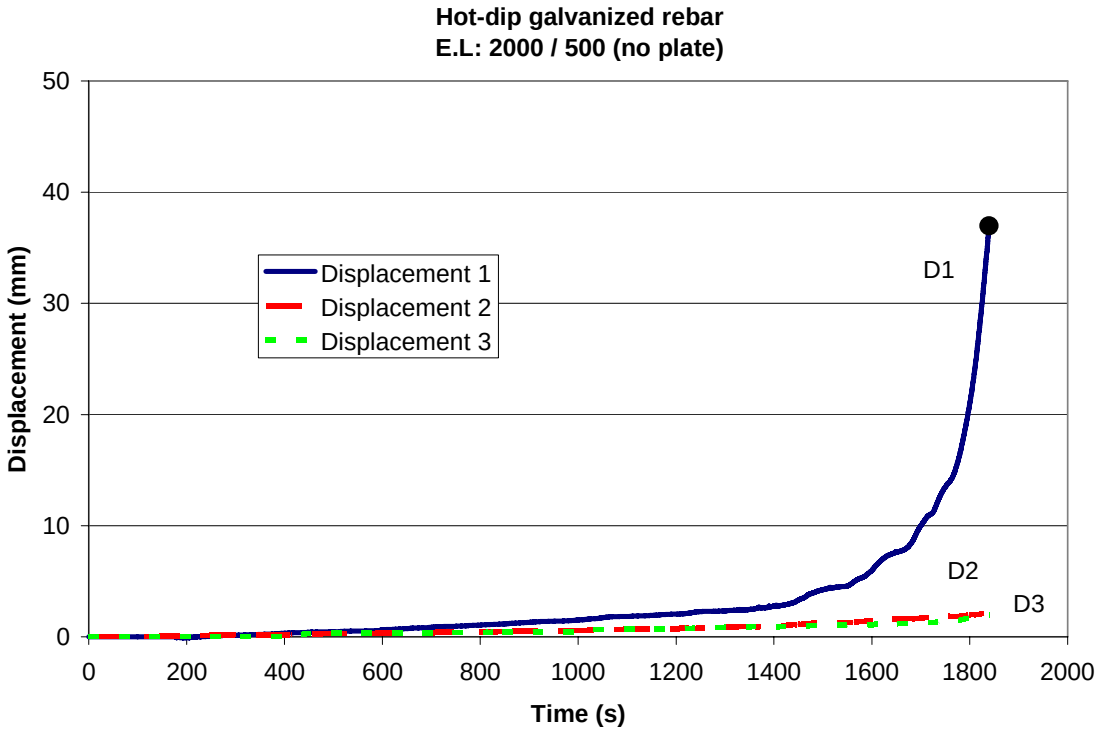

Figure C. 22. Time-displacement diagram of hot-dip galvanized rebar with embedment lengths of 2000 mm and 500 mm (test bolt no. 91). Symbol ● denotes that bolt ruptured.

APPENDIX C

AXIAL DOUBLE PIPE TEST RESULTS. TIME-DISPLACEMENT DIAGRAMS

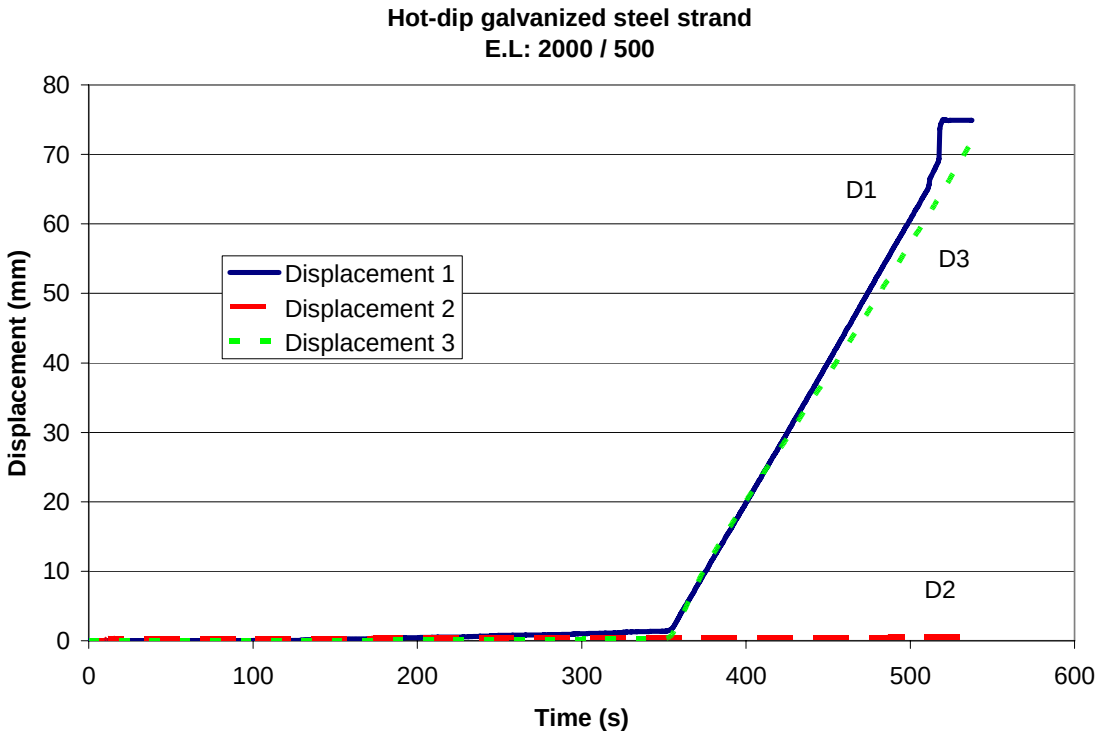

Figure C. 23. Time-displacement diagram of hot-dip galvanized steel strand with embedment lengths of 2000 mm and 500 mm (test bolt no. 85).

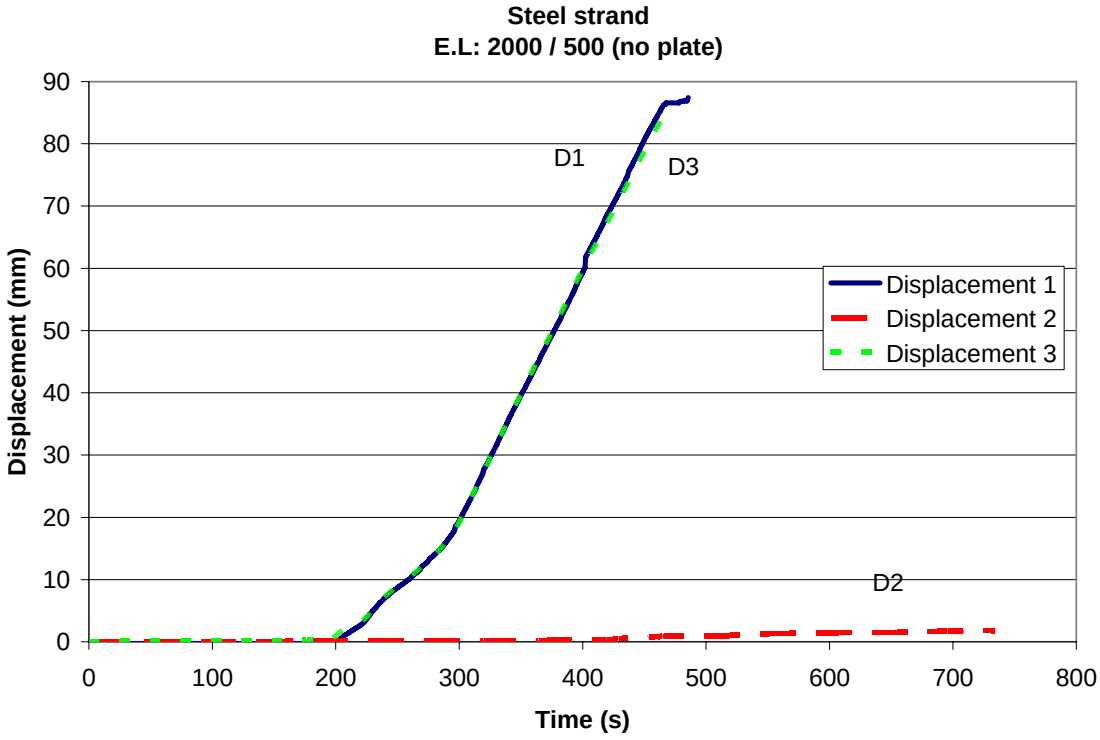

Figure C. 24. Time-displacement diagram of standard steel strand with embedment lengths of 2000 mm and 500 mm (test bolt no. 95).

APPENDIX C

AXIAL DOUBLE PIPE TEST RESULTS. TIME-DISPLACEMENT DIAGRAMS

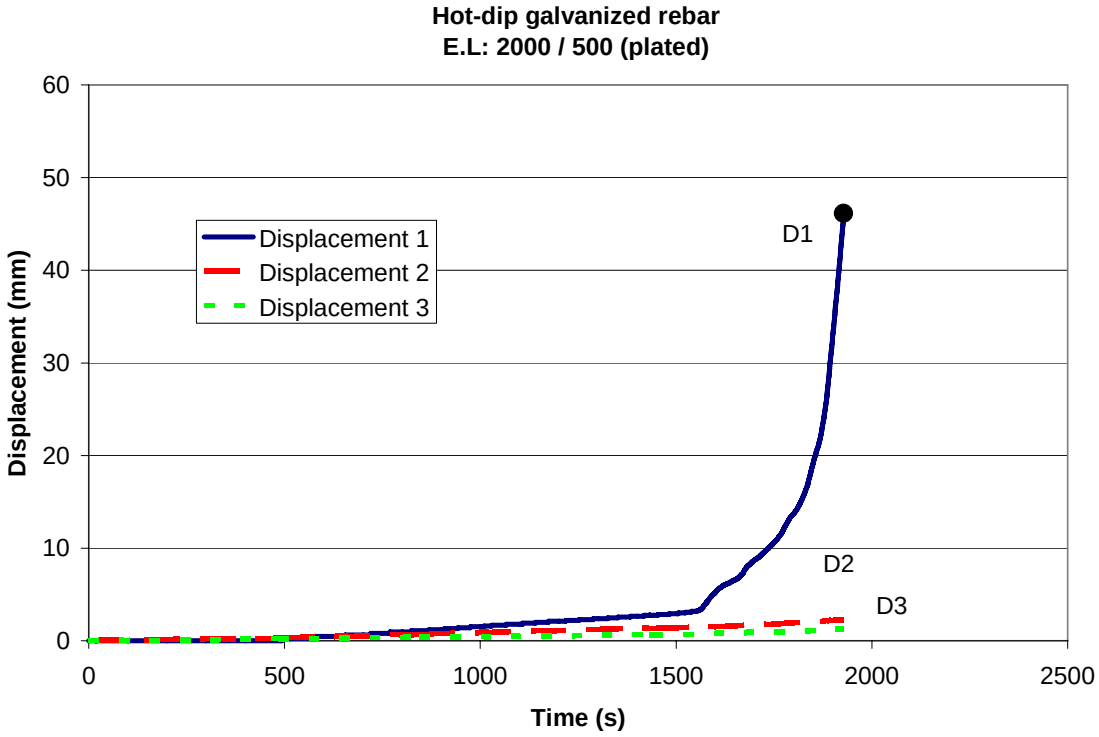

Figure C. 25. Time-displacement diagram of hot-dip galvanized rebar with embedment lengths of 2000 mm and 500 mm (plated) (test bolt no. 89). Symbol ● denotes that bolt ruptured.

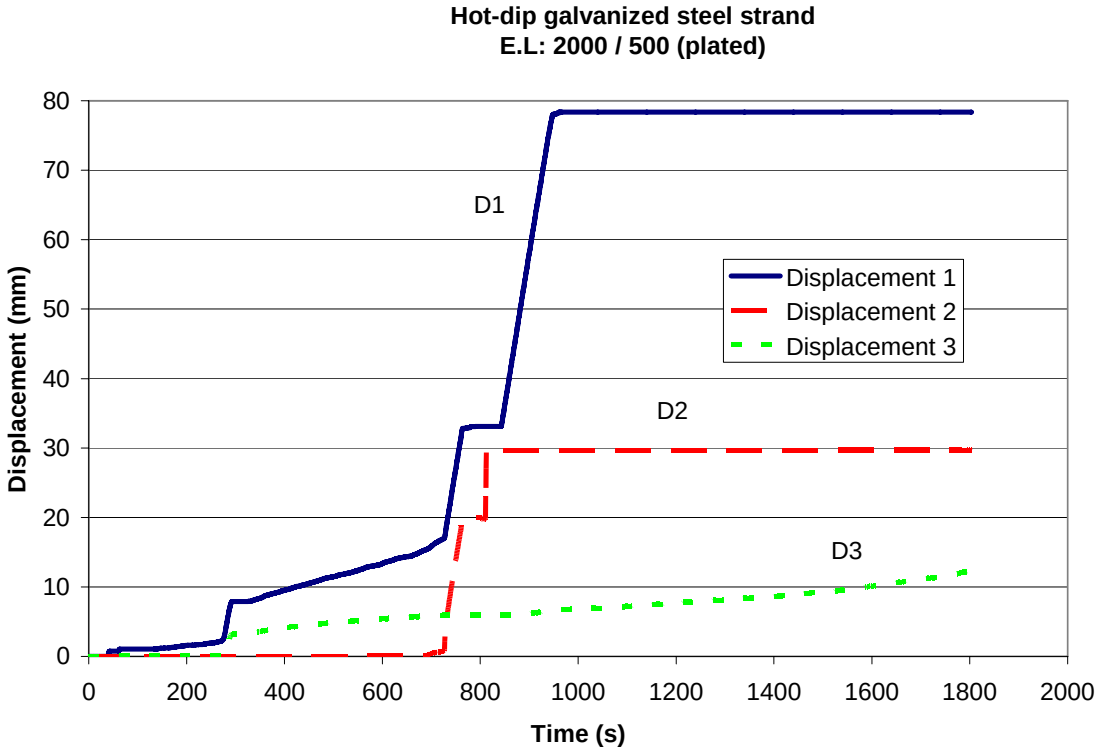

Figure C. 26. Time-displacement diagram of hot-dip galvanized steel strand with embedment lengths of 2000 mm and 500 mm (plated) (test bolt no. 86).

APPENDIX C

AXIAL DOUBLE PIPE TEST RESULTS. TIME-DISPLACEMENT DIAGRAMS

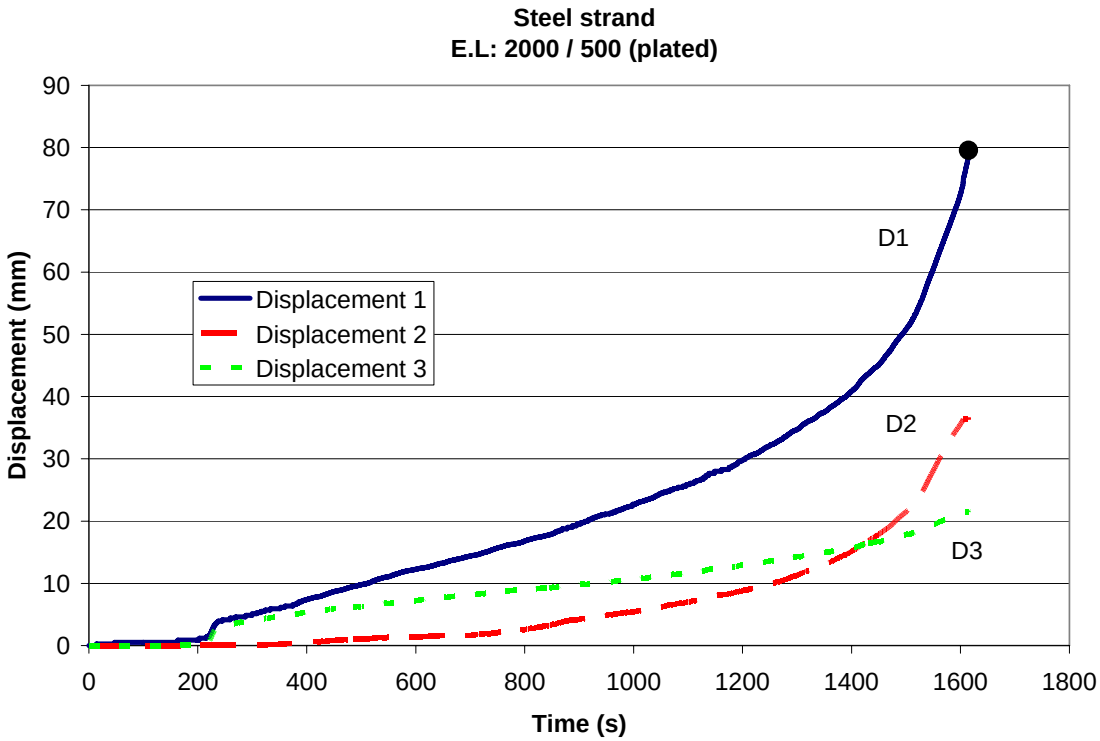

Figure C. 27. Time-displacement diagram of standard steel strand with embedment lengths of 2000 mm and 500 mm (plated) (test bolt no. 92). Symbol ● denotes that bolt ruptured.

APPENDIX D

DOUBLE PIPE TEST SYSTEM. FLAC 3.3 SIMULATIONS

FLAC 3.3 SIMULATIONS (Hakala, unpubl.)

1. Simulation

The effect of the connection points on the steel pipes in the test machine was studied in three different cases (Figure D.1):

1. The connection points of steel pipes to the RHS test frame were at the outer edges of the steel pipes. Pipes were separated from each others by pulling at the connection points (Case A)
2. One of the connection point was at the outer edge of the pipe and another connection point was at the inner edge of the other pipe (Case B)
3. One of the connection point was at the outer edge of the pipe and another connection point was in the middle of the other pipe (Case C)

The simulations were done with two dimensional finite difference code FLAC version 3.3. An axi-symmetric model was used to simulate the double pipe test (Figure D.2). The 3D-construct of steel strand was simulated with surface of repeatable slopes and anisotropic Young's modulus. In cable-grout and grout-steel pipe contacts interface elements capable to deform, slip and separate were used.

In simulation the pulling device itself was not modelled instead the displacement at pulling device contact was increased with a constant rate. The pull was stopped at the displacement step of 0.5 mm, 1.5 mm, 3.0 mm, 5.0 mm, 7.5 mm and 10 mm and the model was run to an equilibrium state. This was done to get comparable results without any ongoing dynamic effects.

2. Parameter values for simulation

Steel strand

- Young's modulus: E_axial = 196 GPa, E_radial = 2 GPa
- Poisson's ratio_axi/rad = 0.25
- Anisotropic, elastic material

Grout

- Young's modulus: E = 13.8 GPa
- Poisson's ratio = 0.25
- Cohesion = 16.5 MPa or 8 MPa
- Friction angle = 30º
- Tensile strength = 4 MPa or 2 MPa
- Dilatation = 10º

Steel pipes

- Young's modulus: E = 196 GPa
- Poisson's ratio = 0.3

Steel strand/grout contact and grout/steel pipe contact

- Normal stiffness = 1000 GPa/m

APPENDIX D

DOUBLE PIPE TEST SYSTEM. FLAC 3.3 SIMULATIONS

- Shear stiffness = 10 GPa
- Friction angle = 22º
- Cohesion = 2 MPa
- Tensile strength = 2 MPa

3. Conclusions

The simulation results shoved that in Case A the failure starts in the middle as a bond failure between cable and grout. With increasing load the failure proceeds as grout yielding. First the grout is cut in to 20 cm to 30 cm sections by tension (Figure D.4) and later the tensile failure propagates through the entire grouting. At highest loading bound failure in cable-grout contact is observed.

Case B connection type induces unwanted bond failure at grout-steel pipe contact (Figure D.3). In case C the grouting outside the RHS-pipe is subjected to less tension in the beginning of loading and therefore the grouting inside the RHS-pipe fails and major strains are taking place in that section. Case C is not recommended because of the length of efficiently working grouting is hard to predict and the overall mechanical behaviour is two-parted (Figure D.4).

APPENDIX D

DOUBLE PIPE TEST SYSTEM. FLAC 3.3 SIMULATIONS

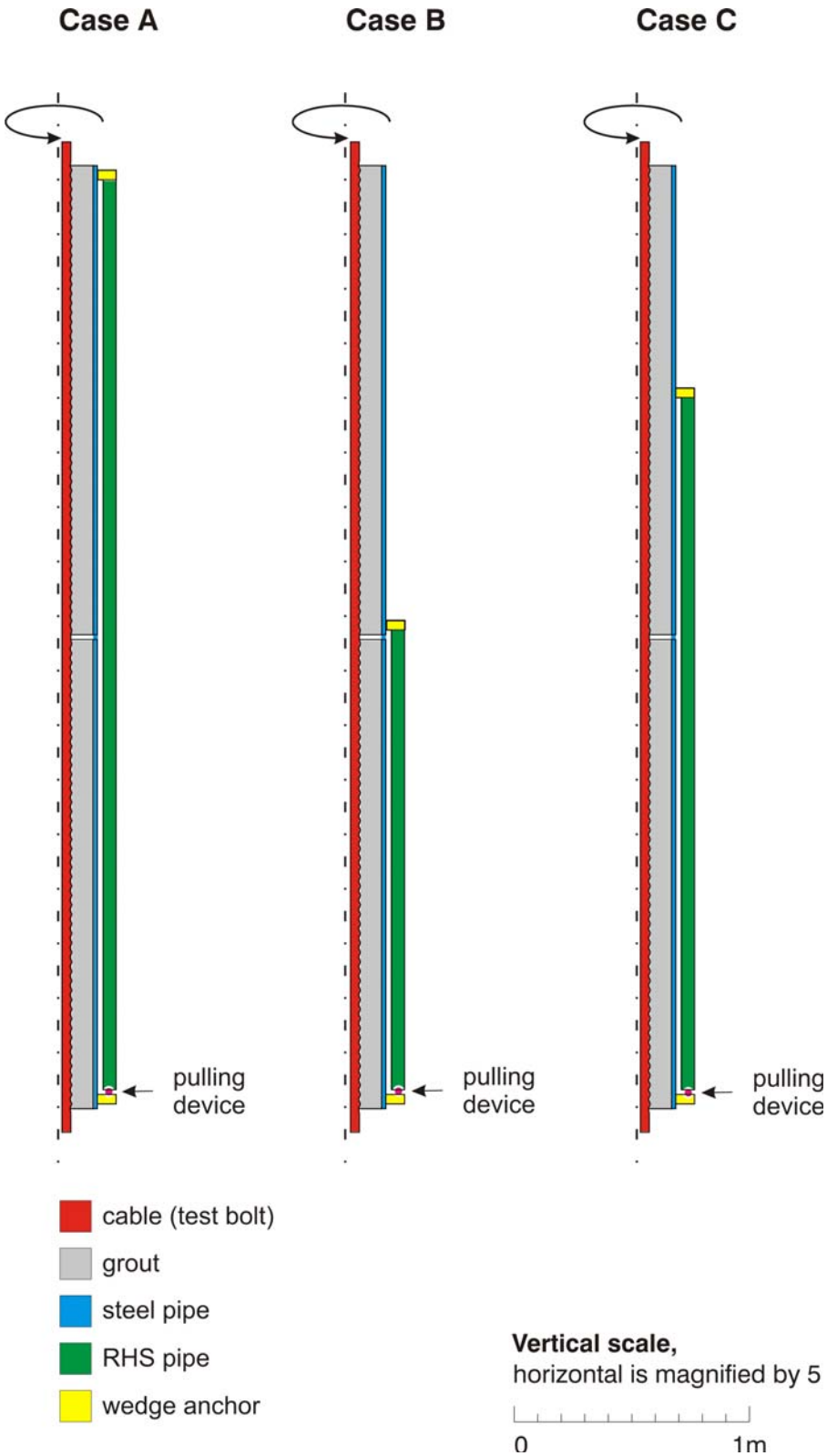

Figure D.1. Simulated cases, anchoring point of RHS-pipe varies, pulling device is simulated with constant velocity boundary condition (Hakala, unpubl.).

APPENDIX D

DOUBLE PIPE TEST SYSTEM. FLAC 3.3 SIMULATIONS

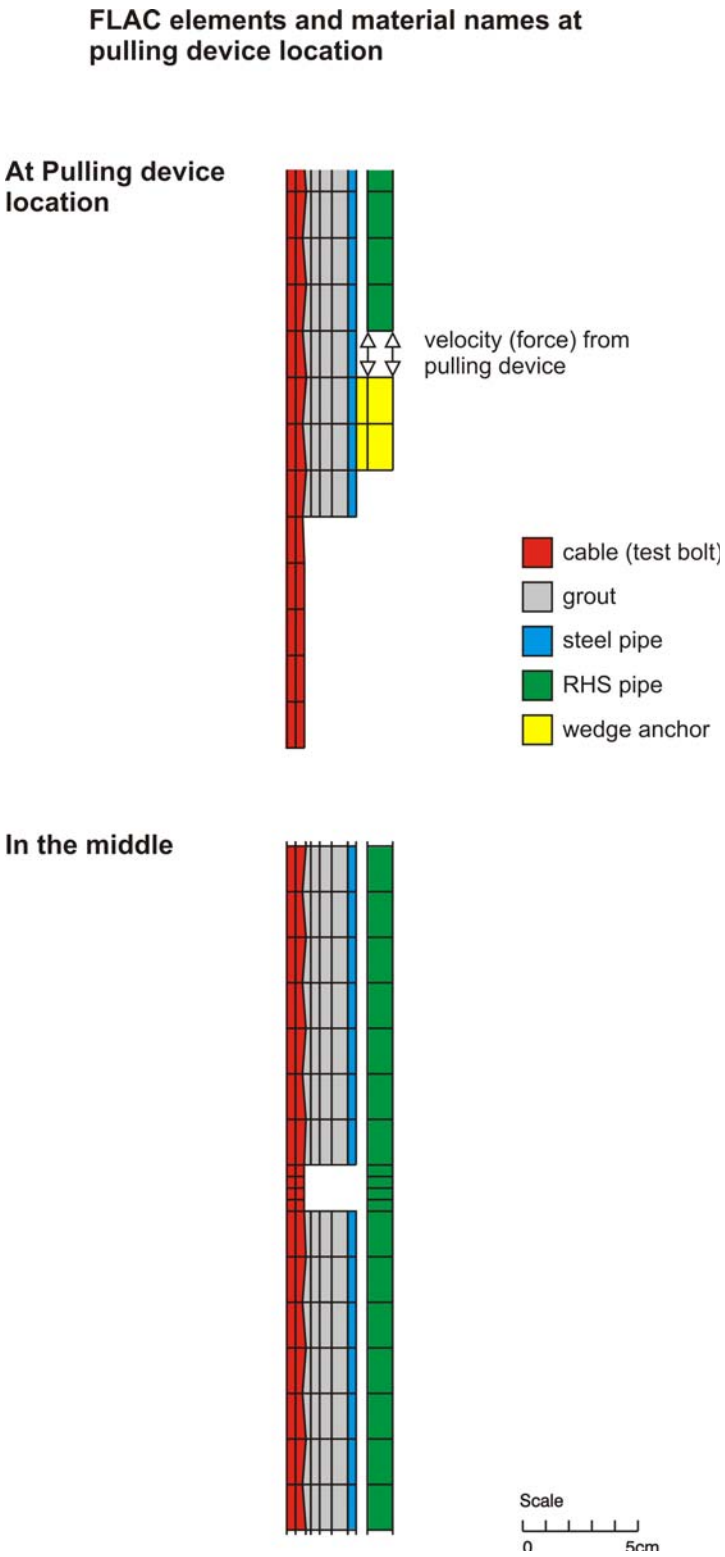

Figure D.2. FLAC elements and materials (Hakala, unpubl.).

APPENDIX D

DOUBLE PIPE TEST SYSTEM. FLAC 3.3 SIMULATIONS

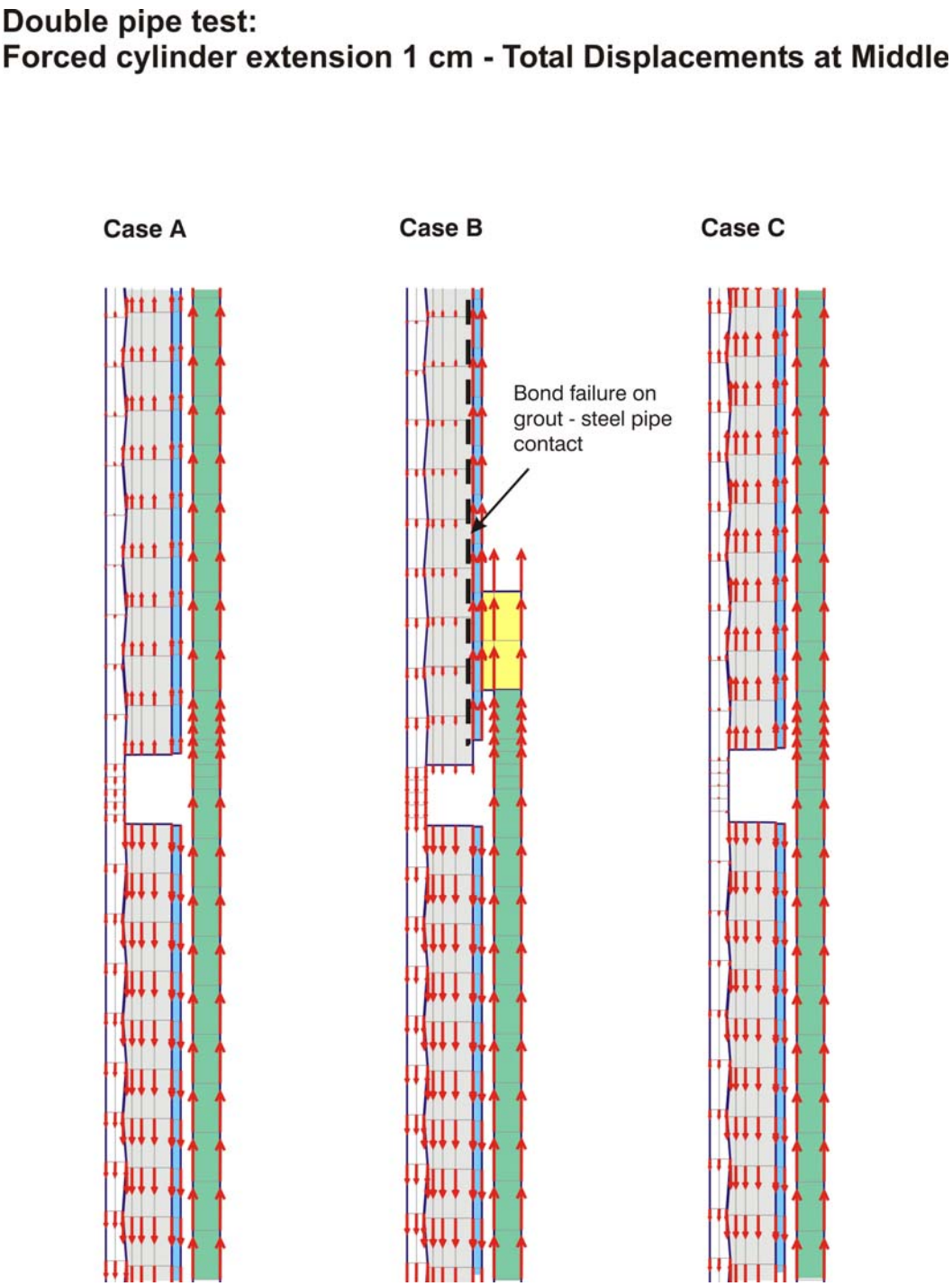

Figure D.3. Total displacements in the middle in cases A, B and C. Case B connection type induces unwanted bond failure at grout-steel pipe contact (Hakala, unpubl.).

APPENDIX D

DOUBLE PIPE TEST SYSTEM. FLAC 3.3 SIMULATIONS

Case C

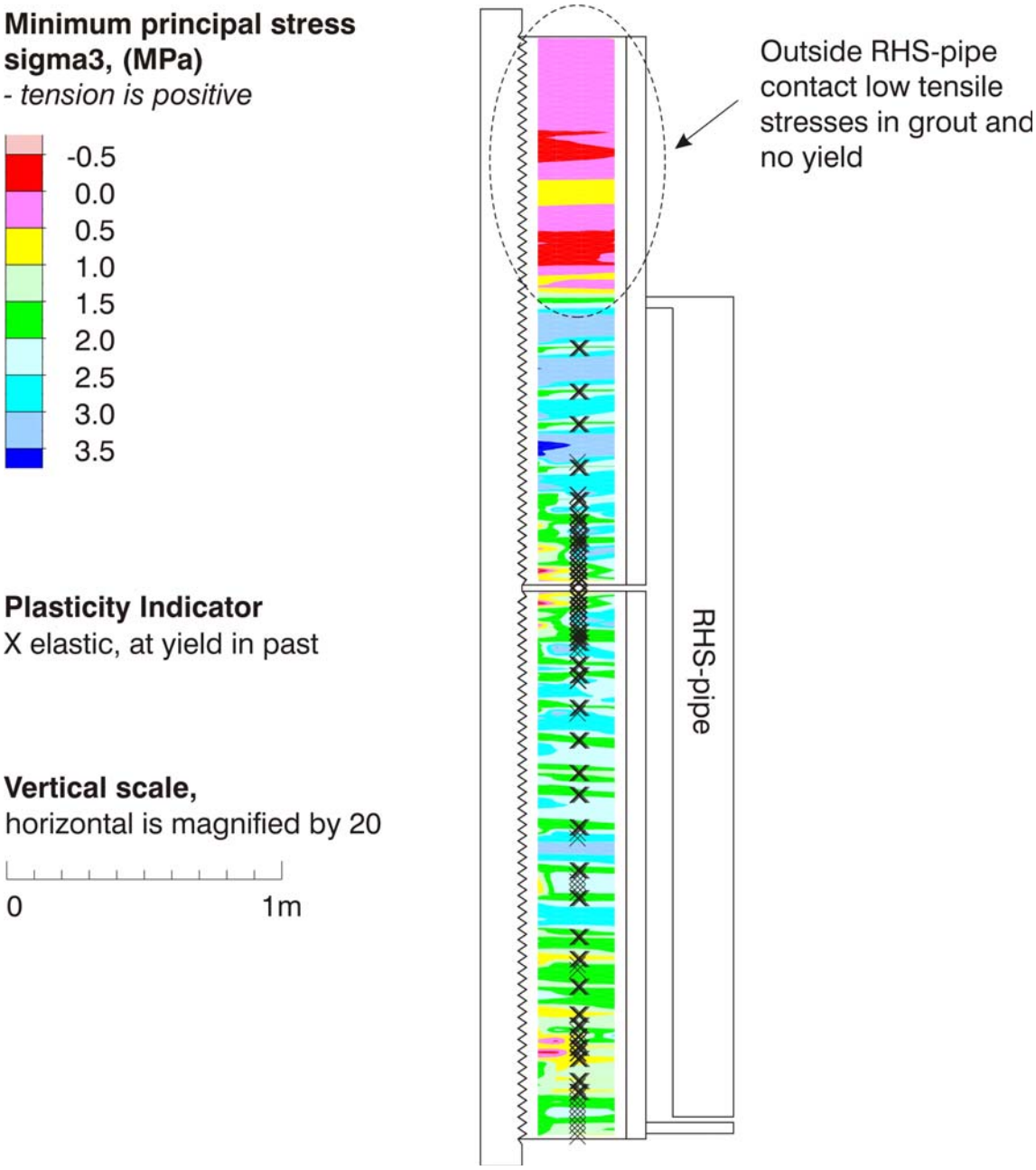

Figure D.4. In case C the grouting outside the RHS-pipe is subjected to less tension in the beginning of loading and therefore the grouting inside the RHS-pipe fails and major strains are taking place in that section. Case C is not recommended because of the length of efficiently working grouting is hard to predict and the overall mechanical behaviour is two-parted (Hakala, unpubl.).

ISBN 978-951-22-8972-1
ISBN 978-951-22-8973-8 (PDF)
ISSN 1795-2239
ISSN 1795-4584 (PDF)